FINITE ELEMENT MODELING OF NON-LINEAR STRUCTURAL RESPONSE OF TRANSMISSION TOWERS INCLUDING BOLTED JOINT SLIPPAGE

By

Khaled I. E. Ahmed

B.A.Sc., Ain Shams University, Cairo, Egypt

M.A.Sc., Assiut University, Assiut, Egypt

A THESIS SUBMITTED IN PARTIAL FULFILLMENT OF
THE REQUIREMENTS FOR THE DEGREE OF
MASTER OF APPLIED SCIENCE

in

THE FACULTY OF GRADUATE STUDIES

(Mechanical Engineering)

THE UNIVERSITY OF BRITISH COLUMBIA

September 2007

ABSTRACT

Slippage of bolted joints plays an important role in the behavior of transmission tower structures under various loading. Two main types of bolted joints are commonly used in towers; column-to-column and beam-to-column joints. The effect of slippage of the bolted joints on the behavior of transmission towers was previously analyzed using two approximate models; instantaneous and continuous joint slippage models. The previously proposed models of joint slippage implied that joint slippage has little effect on a transmission tower load carrying capacity. These models have also shown that deflections of towers due to slippage are very small compared to the overall deformation. These studies have considered only beam-to-column joints, ignoring column-to-column joints. The previous models based on the above assumptions and models based on rigid joint behavior were not able to capture the response of transmission towers under considerable differential settlements caused by frost heave.

In this thesis, two common bolted joint types used in transmission tower structure are analyzed and discussed based on a series of full-size tower joint experiments conducted at the University of Manitoba. It is observed that joints stiffness properties such as equivalent modulus of elasticity, yield strength and fracture strength are much lower than that of the connected members. The experimental results also show that previously reported instantaneous and continuous joint slippage models do not accurately simulate the behavior of bolted joints.

Two finite element models are proposed in this thesis to simulate the slippage of the two main joint types; column-to-column (type-A joints) and beam-to-column (type-C joints). Stiffness matrices of the new joint finite elements are established with the aid of the experimental data. An elastic geometrically nonlinear finite element code is developed using Fortran 90 to analyze the 3-D response of transmission tower structures taking into account the effect of joint slippage. A graphical user interface based on Visual Basic is attached to the finite element code to allow practicing engineers to input all data, build the tower finite element model and display the tower response in an efficient and convenient manner.

The response of a 2-D tower substructure and a 3-D full-scale tower used by Manitoba Hydro is analyzed by using the finite element code. The numerical study shows that slippage of beam-to-column and column-to-column joints have significant effects on the tower load carrying capacity. Column-to-column joint slippage shows the most significant impact on the transmission tower behavior by either reducing the tower load carrying capacity or significantly increasing the tower deflection under working loads. On the other hand, joint slippage has a positive effect on the tower response under frost heave induced displacements as substantial redistribution of tower member forces takes place due to joint slippage and actual member forces are much lower than those predicted by standard structural analysis software based on the rigid joint assumption or simplified slippage models.

TABLE OF CONTENTS

ABSTRACT ii

TABLE OF CONTENTS iv

LIST OF TABLES vi

LIST OF FIGURES vii

ACKNOWLEDGEMENTS x

Chapter 1: INTRODUCTION

1.1 General 1

1.2 Problem Statement 5

1.3 Literature Review 7

1.4 Objectives and Scope 13

Chapter 2: FINITE ELEMENT ANALYSIS OF TRANSMISSION TOWERS

2.1 General 15

2.2 Non-linear Finite Element Model For Beams 16

2.3 Bolted Joint Behavior 24

2.4 Bolted-Joint Finite Element Model 34

2.4.1 Column-to-Column Joint (Type-A) 35

2.4.2 Beam-to-Column Joint (Type-C) 37

2.4.3 Joint Stiffness Calculations 39

2.5 Tower Boundary Conditions 41

2.6 Updating Geometry and Solution Scheme 44

Chapter 3: JOINT SLIPPAGE ANALYSIS PROGRAM

3.1 General 46
3.2 The FE Program Structure 46
3.2.1 Input Data 47
3.2.2 Assembly of the Global Stiffness Matrix 49
3.2.3 Solution of the System of Equations 50
3.2.4 The FE Program Output Results 51
3.3 The User Interface 53
3.3.1 The Pre-Processing Phase 54
3.3.2 The Solution Phase 62
3.3.3 The Post-Processing Phase 65

Chapter 4: TRANSMISSION TOWER ANALYSIS

4.1 General 69
4.2 Program verification 69
4.2.1 Simple Cantilever 69
4.2.2 Double Diagonal Plane Truss 73
4.2.3 Simple Transmission Tower 75
4.3 Effect of Slippage on the Response of Towers 77
4.3.1 2-D Tower Case 77
4.3.2 Full-Scale Tower 81

Chapter 5: CONCLUSIONS

5.1 Summary and Conclusions 94
5.2 Future Work 95

REFERENCES 97

LIST OF TABLES

Chapter 4: TRANSMISSION TOWER ANALYSIS

Table 4-1: Comparison of deflection of Node 2 (F=3.145 kN). 74

Table 4-2: Comparison of transverse deflection (U_Z) of point A for (F_Z, F_Y, F_X) = 27.9 * (5, 15, 1) kN 76

Table 4-3: Comparison between the yield loads of the structure different members . . . 79

Table 4-4: Comparison of tower deflections (UX, UY, and UZ) at point A 82

LIST OF FIGURES

Chapter 1: INTRODUCTION

Figure 1.1: Transmission tower. 1

Figure 1.2: Different types of transmission towers. 3

Figure 1.3: Ice accumulations in conductor wires. 4

Figure 1.4: Transmission tower failure due to Ice storm, Quebec, 1998. 4

Figure 1.5: Foundation movement due to frost heave. 5

Figure 1.6: Tower foundation movement due to frost heave in North Dakota, (1997). . . 5

Figure 1.7: Effect of joint rotational stiffness on the structure response for different joint types, Al-Bermani et al., (1992). 8

Figure 1.8: Simple bolted Joint. 10

Figure 1.9: Different clearance configurations of a bolted joint. 10

Chapter 2: FINITE ELEMENT ANALYSIS OF TRANSMISSION TOWERS

Figure 2.1: Beam under large rotation and deformation. 17

Figure 2.2: Three dimensional beam element. 20

Figure 2.3: Instantaneous and continuous slippage approaches. 24

Figure 2.4: The test specimens of the column-to-column and beam-to-column joints . . 27

Figure 2.5: Typical test results of the three configurations of the type-A joints reported by Ungkurapinan (2000). 28

Figure 2.6: Idealized load-deformations relations of the three configurations of the type-A joints reported by Ungkurapinan (2000). 29

Figure 2.7: Typical test results of the three configurations of the type-C joints reported by Ungkurapinan (2000). 31

Figure 2.8: Idealized load-deformations relations of the three configurations of the type-C joints reported by Ungkurapinan (2000). 32

Figure 2.9: Deformation regions of a bolted joint. 34

Figure 2.10: A Column-to-Column, Type-A, Joint and the finite element model. 35

Figure 2.11: A Beam-to-Column joint, and the finite element model. 38

Figure 2.12: Stiffness of type-A joint obtained from experimental results 40

Figure 2.13: Generated stiffness for type-C joint. 41
Figure 2.14: Beam under large rotation and deformation. 44
Figure 2.15: Iterative solution of nonlinear system equations. 45

Chapter 3: JOINT SLIPPAGE ANALYSIS PROGRAM

Figure 3.1: Flow chart of the nonlinear finite element code. 52
Figure 3.2: Starting screen of the user interface of the program. 54
Figure 3.3: Main screen of the user interface. 55
Figure 3.4: Preview of the tower front view in the geometry tab in the pre-processing phase. 56
Figure 3.5: Different views and zooming of the tower sections in the pre-processing phase. a- Side full view, b- Isometric full view c- Isometric zooming for section -1-, c- Isometric zooming for section -3-. 57
Figure 3.6: "Meshing" tab contents in the pre-processing phase. 59
Figure 3.7: "Elements Properties" tab contents in the pre-processing phase. 60
Figure 3.8: "Elements Properties" tab contents in the pre-processing phase. 61
Figure 3.9: "Loads and Boundary Conditions" tab contents in the Solution phase. 63
Figure 3.10: "Solution Properties" tab contents in the Solution phase. 64
Figure 3.11: Post-Processing phase showing tower geometry. 66
Figure 3.12: Post-Processor display if result file is not available. 67
Figure 3.13: Post-Processor display showing the results for element 77 at load step number 2 and last sub-step. 68

Chapter 4: TRANSMISSION TOWER ANALYSIS

Figure 4.1: 3-D beam model used in FE code verification 70
Figure 4.2: Comparison of deformations obtained from ANSYS and the current FE code for one-element model 71
Figure 4.3: Comparison of deformations obtained from ANSYS and the current FE code for four-element model. 71
Figure 4.4: Comparison of deformations obtained from ANSYS and the current FE code for 50-element model 72
Figure 4.5: Double-diagonal plane truss. 73
Figure 4.6: Simple transmission tower model. 75

Figure 4.7: Finite element model of the transmission tower substructure. 77
Figure 4.8: Effect of joint slippage on load carrying capacity for various load ratios and joint types 79
Figure 4.9: Tower tip deflections in x- and y- directions for a tower with different types of joints. 80
Figure 4.10: Full-scale transmission tower used by Manitoba Hydro. 81
Figure 4.11: Finite element model of full-scale tower with the six locations of the type-A joints 83
Figure 4.12: Normalized axial loads of tower columns under self weight and working loads without joint slippage. 85
Figure 4.13: Normalized axial loads of tower columns under self weight and working loads with joint slippage 85
Figure 4.14: Normalized axial loads of tower beams under self weight and working loads without joint slippage 86
Figure 4.15: Normalized axial loads of tower beams under self weight and working loads with joint slippage. 86
Figure 4.16: Increase of normalized axial load of tower columns due to a frost-heave displacement of 100 mm (without joint slippage). 87
Figure 4.17: Increase of normalized axial load of tower beams due to a frost-heave displacement of 100 mm (without joint slippage). 88
Figure 4.18: Increase of normalized axial load of tower columns due to a frost-heave displacement of 100 mm (with joint slippage). 88
Figure 4.19: Increase of normalized axial load of tower beams due to a frost-heave displacement of 100 mm (with joint slippage). 89
Figure 4.20: Increase of normalized axial load of tower columns due to a frost-heave displacement of 100 mm of two adjacent legs (without joint slippage). . . . 90
Figure 4.21: Increase of normalized axial load of tower beams due to a frost-heave displacement100 mm of two adjacent legs (without joint slippage) 90
Figure 4.22: Increase of normalized axial load of tower columns due to a frost-heave displacement of 100 mm of two adjacent legs (with joint slippage). 91
Figure 4.23: Increase of normalized axial load of tower beams due to a frost-heave displacement of 100 mm of two adjacent legs (with joint slippage). 91
Figure 4.24: Increase of normalized axial load of tower columns due to different frost heave displacements (with joint slippage). 92
Figure 4.25: Increase of normalized axial load of tower beams due to different frost heave displacements (with joint slippage). 93

ACKNOWLEDGEMENTS

First of all, my sincere gratitude and full thanks are to ALLAH, The Creator, The Most Gracious and The Most Merciful. All praises are to HIM for HIS continuous support and guidance without which I would not have been able to reach this goal.

I would like to express my gratitude to Professor Nimal Rajapakse, my major supervisor, for his kind supervision, valuable discussions, and suggestions, which helped me with the work of this thesis. The financial support in terms of a research assistantship is greatly appreciated.

I would also like to express my gratitude to Professor Mohamed Gadala, my co-supervisor, for his kind supervision, valuable discussions, and suggestions, which helped me to complete this thesis.

I would also like to thank all the members of the FEA lab for their help during my study at UBC.

Finally, I wish to thank everyone in my family for their encouragement and support.

Chapter 1

INTRODUCTION

1.1 General

Transmission towers are the main structural component of a power transmission line. In a typical transmission line, high voltage conducting wires are supported by transmission towers of 30-50 meters height placed at intervals of 200 – 600 meters. Their structural stability and integrity are the most important factors in safe and reliable electric power transmission and distribution from generating stations to distant cities. Transmission towers, Figure 1.1, are often three-dimensional latticed structures made of steel members with bolted connections. Towers made of tubular steel columns and polymer composite materials are becoming popular in recent years.

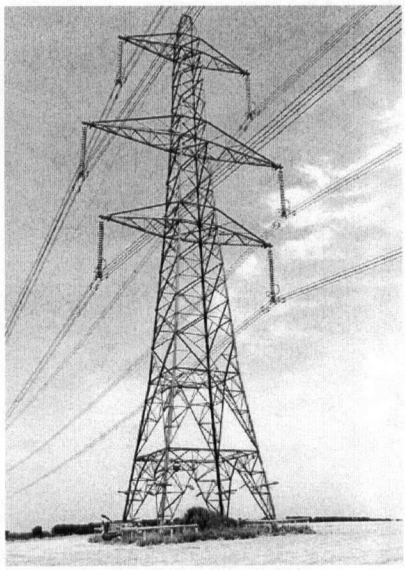

Figure 1.1: Transmission tower.

Latticed structures are relatively light in comparison to other conventional types of structures. They are considered highly efficient in terms of their load carrying capacity to weight ratio. In addition, they are easy to fabricate and construct. Transmission tower structures are normally composed of several hundreds of galvanized steel asymmetric thin-walled angle sections eccentrically connected by bolted joints. Typical towers have a square body configuration with identical bracing in all faces. The configuration design of a transmission tower largely depends on its uses. There are several types of transmission towers as shown in Figure 1.2. Some of the parameters that determine the most suitable tower configuration include the amount of transmitted power, type of the transmission circuit, environmental factors (e.g., temperature, wind, and potential for ice accumulation) and geography of the region (e.g., mountains, rivers, cities, etc.).

Most electric utilities prefer to limit the variety of transmission towers in their transmission systems for ease of maintenance and economical reasons while this may not result in the ideal tower design for a particular location. A utility typically has six to ten tower types depending on the peculiarities of the geography of the region. A thorough understanding of the structural behavior is very important to the design, construction and maintenance of a reliable and economically efficient power transmission system. Structural analysis of transmission towers is therefore an important area of research for electric utilities. Significant advances in structural analysis of latticed structures have occurred in the past decades. Today, computer-aided software based on the finite element method is available for both linear and non-linear analysis of transmission towers.

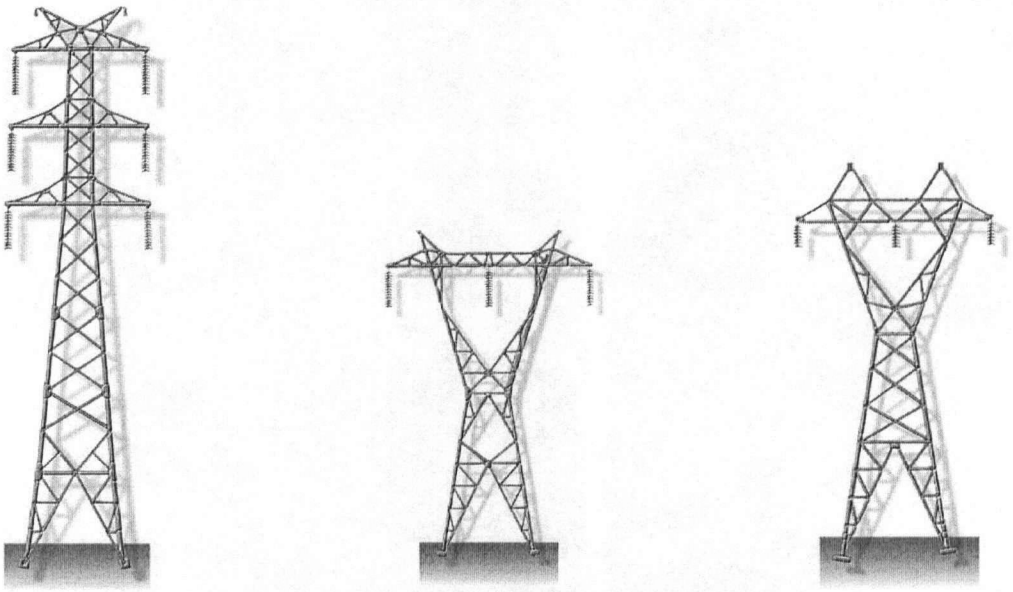

220,000 volt double circuit transmission tower

110,000 volt single circuit transmission tower

220,000 volt single circuit transmission tower

Figure 1.2: Different types of transmission towers.

In order to understand the structural behavior of a transmission tower it is important to look at factors that govern the overall response such as the tower loads, tower foundations, member types and connections, tower geometry, etc. A major component of the tower design load is related to the heavy conductor wire loads representing the self-weight of the conductor wires that run between the towers. Needless to say, the tower self-weight is another significant dead load.

Towers are also subjected to a variety of environmental loads such as wind, earthquake, ice and frost heave related loads. Ice accumulation in tower members and conducting wires, as shown in figure 1.3, increases the dead weight significantly during ice storms such as the 1998 Quebec ice storm and leads to catastrophic failures. Figure 1.4 shows a failed transmission tower following the 1998 ice storm in Quebec.

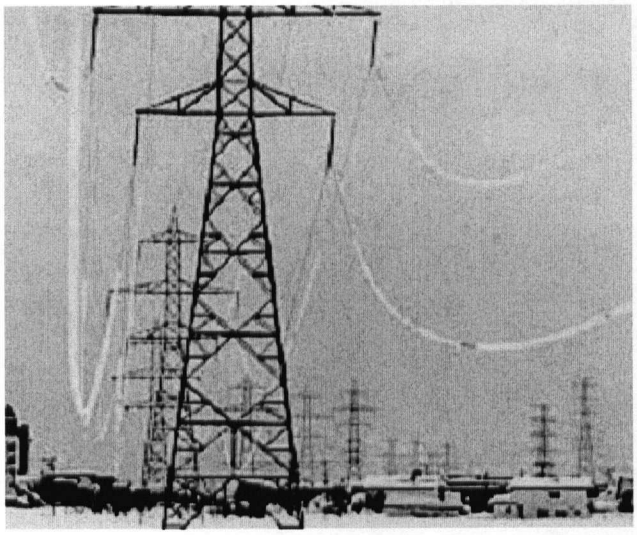

Figure 1.3: Ice accumulations in conductor wires

Figure 1.4: Transmission tower failure due to Ice storm, Quebec, 1998.

Another important loading on tower structures is galloping induced loads. Galloping is low frequency (from 0.1 to 1 Hz), large amplitude (from 0.1 to 1 times the sag of a transmission line between two towers), wind induced vibrations of both single and bundle conductors, with a single or a few loops of standing waves per span. This is caused by moderately strong, steady crosswind acting upon an asymmetrically iced conductor surface. In cold regions such as Northern parts of Canada, frost heave is an important factor in tower design. Frost heave is a seasonal loading condition that depends on the ground temperature, and the amount of water pockets in soil layers. In the winter time, freezing of underground water pockets under a foundation pushes the tower legs upward causing differential settlements (Figure 1.5) and a significant upward loading at the legs. Figure 1.6 shows a typical tower leg movement due to frost heave in North Dakota. Marthaller (1997) has reported that in a North Dakota case, the elevation difference between the tower legs was as large as 325mm.

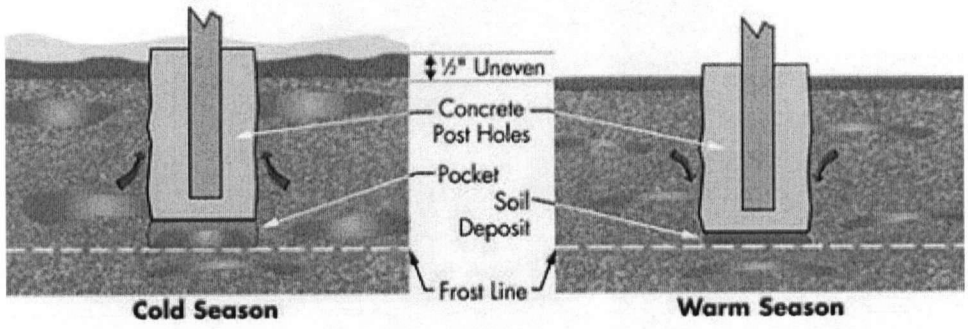

Figure 1.5: Foundation movement due to frost heave.

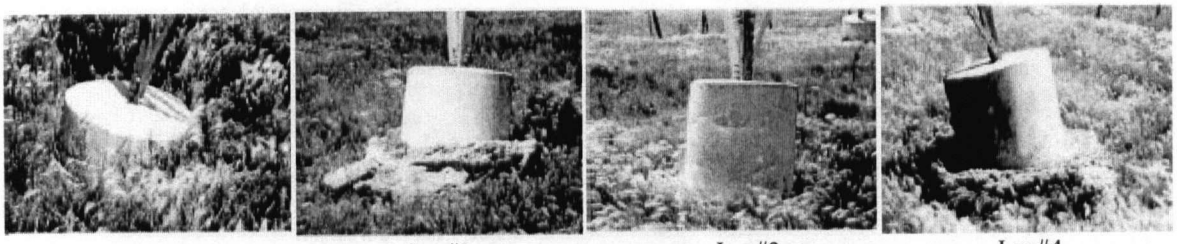

Figure 1.6: Tower foundation movement due to frost heave in North Dakota, (1997).

1.2 Problem Statement

An important consideration in the design and construction of transmission towers in the Northern regions of Canada is frost heave. This study is motivated by discussion with Manitoba Hydro engineers who indicated the need for better understanding of the response of a tower under loading caused by frost heave. Frost heave induces differential upward movement of tower legs causing significant redistribution of tower member forces. Site inspections have shown differential displacements amounting to over 300mm at the tower leg bases and local buckling of tower legs. The conventional structural analysis software currently used by design engineers for

latticed tower analysis is based on the assumption of either pin-ended trusses or 3-D frames with rigid joints. Design engineers have found that tower leg members are subjected to loads exceeding their ultimate design load when a tower is analyzed under typical frost heave displacements by using the standard structural analysis software. However, site inspections show that towers are stable and sound and show no evidence of member failure except for local buckling of tower legs under a few cases of extreme frost heave induced displacements.

A possible explanation of the discrepancy between member forces predicted by standard software and actual tower behavior is the rigid joint assumption used in standard tower analysis software. The software packages do not account for slippage at bolted joints of the tower and bending stiffness of main legs. In addition, it is believed that non-linear geometric stiffness also has an effect on the overall deformations of a tower. Tower design engineers believe that bolted joints allows for significant slippage at tower member joints and thereby allow substantial redistribution of member forces when subjected to frost heave. This together with additional bending stiffness of leg members and geometric stiffness results in a tower being capable of withstanding significant frost heave induced displacements. It is therefore necessary to verify the observations of design engineers by a refined structural analysis that accounts for joint slippage, tower leg bending stiffness and geometric stiffness of leg members. Findings of such a study would be useful to the design engineers to estimate the actual member forces due to frost heave and to improve the current design practices. In addition, current tower maintenance practices can also benefit from a better understanding of the tower member forces and deformations due to frost heave.

1.3 Literature Review

Many attempts have been made to analyze transmission towers over the past decades. Before the era of digital computers, statically indeterminate transmission towers were analyzed by approximating them into statically determinate planer trusses (Bergstrom, 1960). With the introduction of computers in the analysis and design process, many software packages have been developed to analyze transmission towers as three-dimensional truss or frame structures. These programs, based on linear elastic properties of the members, are capable of calculating the joint displacements and members internal forces using the stiffness method of structural analysis (Marjerrison, 1968). Early studies modeled the towers angle members as truss elements, pin-connected at the joints that do not carry bending stresses. This model required extra redundant members or springs to eliminate the singularity of the stiffness matrix without altering the characteristic of the structure (Lo, 1975). This approach was further enhanced by utilizing beam elements and considering the bending stiffness of the joints. The bracing members were still modeled as tension or compression only members with buckling consideration. The analysis requires an iterative process to find which members have exceeded their buckling load and to remove them from the analysis. Another enhancement was added by utilizing a technique called "formex formulation". This formulation utilizes the repeated patterns in a tower and its symmetry to reduce the effort involved in generating the nodes and elements of a tower analysis model (Haristchian and Maalek, 1984). Linear elastic models were later improved by introducing geometric nonlinear or second order elastic analysis (ASCE 1988; Roy 1984). The second order deformation analysis considers the force equilibrium of the structure in the deformed configuration rather than the original configuration and a nonlinear strain displacement relation. This type of analysis is significant when the displacement of the structure is large.

A latticed transmission tower consists of columns, which are the main legs, and bracings that connect the legs together either horizontally or diagonally. The members are connected by different kinds of bolted joints. The behavior of bolted joints plays an important role in tower behavior. Figure 1.7, shows the in-plane behavior of beam-to-column connections based on experimental studies by Jones et al. (1980) and Chen and Zhou (1987). Incorporation of bolted joint behavior in tower analysis is an important consideration based on the observations made by design engineers. For simplicity, most of transmission tower analyses model the beam-to-column connection as a pure hinge connection, which is similar to the behavior of the single web-angle connection shown in Figure 1.7.

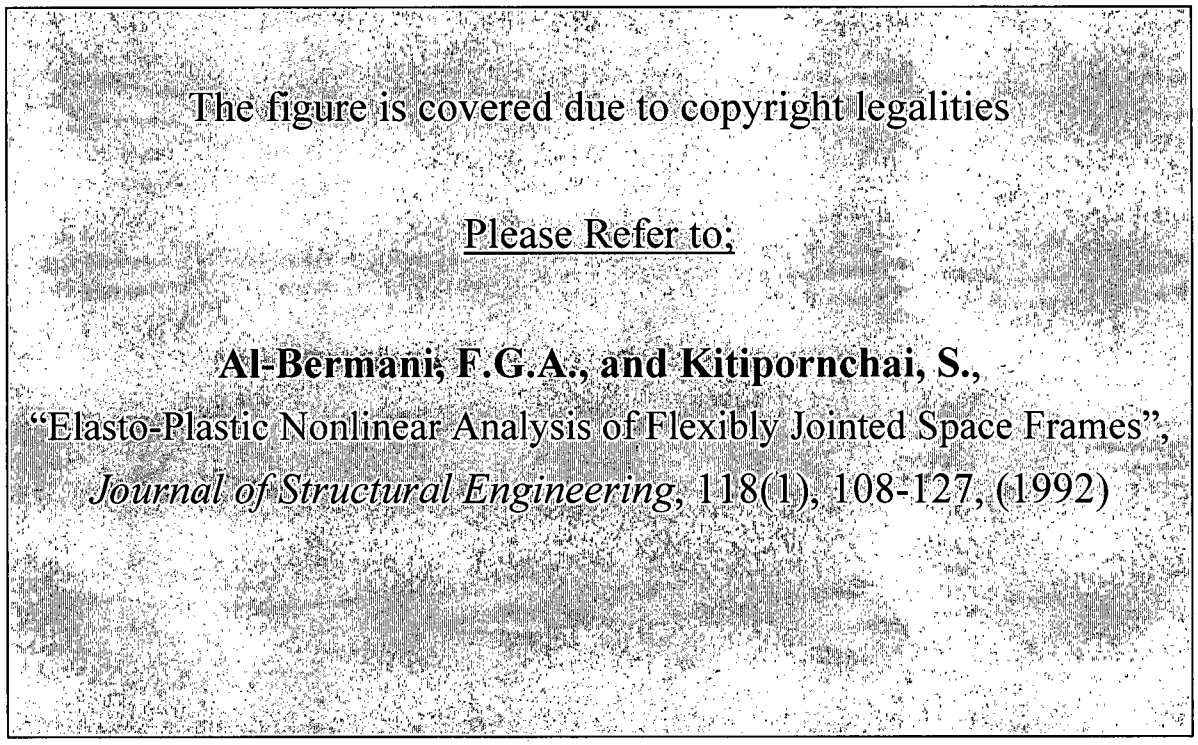

Figure 1.7: Effect of joint rotational stiffness on the structure response for different joint types, Al-Bermani et al., (1992).

Many studies have been done to understand the behavior of bolted joints under different loading conditions. These studies concluded that slippage at a bolted joint plays a very important role in defining the stiffness of a joint and the global stiffness of a structure. A simple bolted joint, as shown in Figure 1.8, consists of two members and a bolt. The diameter of the hole in each member is normally slightly larger than the bolt diameter leaving some clearance between the bolt and members. A bolted joint has three configurations as shown in Figure 1.9; minimum clearance, normal clearance, and maximum clearance. A typical test, for this simple joint, shows that the behavior of the joint under uni-axial tension is very different from the behavior of an individual member. Due to the clearance between the hole and the bolt, the two members start to slip over each other after reaching the threshold slippage load. The stiffness of the joint before slippage is almost similar to the stiffness of the members. After slippage starts, the joint stiffness reduces dramatically until the joint reaches a bearing status. The stiffness then starts to increase slightly until it reaches the yielding point. The maximum, normal, and minimum clearance arrangements reach the same yielding point. This means that the slippage amount does not affect the failure point of a structure but rather affects the deformation pattern of a structure. In other words, the amount of clearance has a significant effect on the generated internal forces in the joint under certain displacement. This observation could explain the discrepancy between the standard structural analysis results and the real field behavior of transmission towers under frost heave loading.

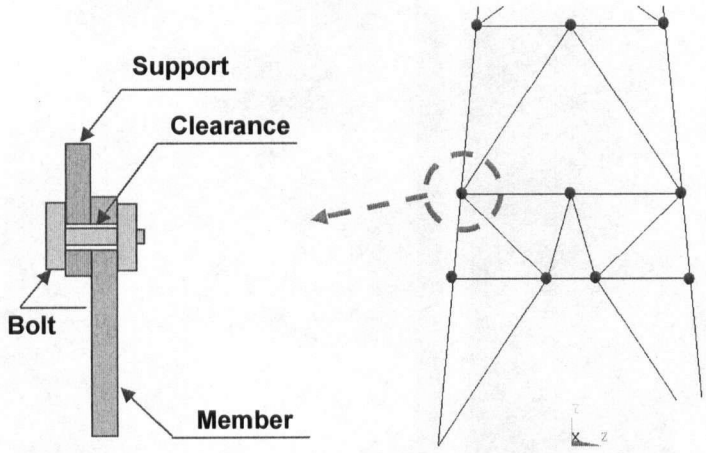

Figure 1.8: Simple bolted Joint.

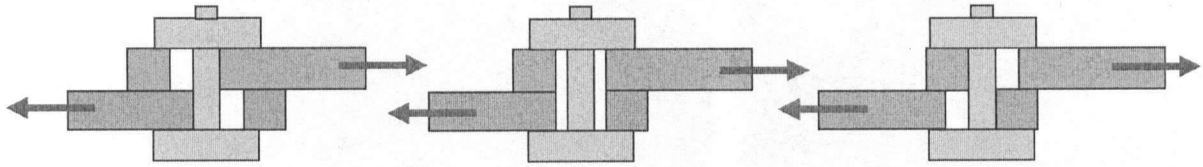

Figure 1.9: Different clearance configurations of a bolted joint.

There are three types of joints in a typical transmission tower structure. These are the column-to-column, beam-to-column, and beam-to-beam joints. The column-to-column joint is normally simulated as a rigid joint, whereas the other two, beam-to-column and beam-to-beam joints are simulated as pinned joints. It means that these joints have zero rotational stiffness. In reality, the joints are neither fully rigid nor fully pinned. The stiffness of a joint lies somewhere between the two limiting cases of rigid and pinned joints and depends on the details of the type of connection. Chen and Lui (1987) modified a beam-column joint to include a flexible connection spring. A two-node zero length non-linear rotational spring element is proposed to model the rotational stiffness of a joint. The connection element is attached to the end of a

beam-to-column element via kinetic transformation and the stiffness is then reduced using static condensation. Al-Bermani and Kitipornchai (1992) extended this procedure to a three-dimensional beam-column element. Both studies showed that the response of a structure is highly sensitive to the magnitude of the joint rotational stiffness. Al-Bermani and Kitipornchai (1992) enhanced the modeling of transmission towers by considering different kinds of nonlinearities. In addition to the second order deformation analysis, they considered the effects of joint rotational flexibility, torsional deformations and elastic-plastic behavior of the tower members.

As mentioned previously bolt slippage is recognized as a significant factor in the behavior of transmission towers. Only a few studies have addressed this issue primarily due to lack of experimental data. Peterson (1962) concluded that up to one-half of the measured deflections of transmission towers could be due to bolt slippage while the remainder was due to elastic deformation. Marjerrison (1968) concluded that the deformations of holes and bolts of the tower joints are responsible for increasing the theoretical deflections of a tower by three times. The first attempt to simulate bolt slippage in towers is due to Williams and Brightwell (1987). They presented a stochastic model to assess the effect of joint slippage on bolted lattice structures. They included the joint axial movement in axial strain of bracing or leg members. They concluded that there was no deterministic way in which the amount of joint deformation can be specified for each member of a structure. Devlecchio and Soom (1991) studied the effect of statistical tolerances of location on the amount of available slippage or movements that can occur in bolted assemblies. They showed that the increase in average hole-to-hole distance reduces the available rotational displacements but not the translational displacements. They have also shown that increasing the number of holes decreases the movement available at joints.

Dutson and Folkman (1996) reported that clearance in joints was found to significantly change the dynamic behavior by altering the damping characteristics of a structure.

Kitipornchai et al. (1994) developed two idealized slippage models, namely instantaneous and continuous slippage models, to study the effect of bolt slippage on the ultimate strength and deformations of a transmission tower. Bolted joints, in both models, behave rigidly until the slippage load. After the slippage load, the continuous slippage model assumes that a joint slips incrementally as the load increases until the maximum allowed slippage. The instantaneous slippage model assumes that a joint experiences the full allowable slippage just at the onset of slippage and then behaves rigidly. They concluded that, bolt slippage has no effect on tower load carrying capacity. However, it significantly affects the deformation of a tower under working loads. This conclusion was drawn based on the response of a transmission tower under force boundary conditions. Kroeker (2000) analyzed a full-scale transmission tower with joint slippage under both force and displacement boundary conditions using a continuous slippage model. He showed that axial stresses in the critical members were greatly reduced when slippage was considered. Pai and Hess (1998) experimentally showed that bolt slippage under dynamic loads loosens the fastener, and changes the stiffness of a joint. Pai and Hess (2002) also studied a fastener using a 3-D finite element model. The results showed that loosening could occur at relatively low shear loads due to localized slip.

Ungkurapinan (2000) and Ungkurapinan et al. (2003) performed an extensive experimental study on the stiffness of three types of joints that are commonly used in transmission towers. One type of joint corresponds to a column-to-column joint and the other two are beam-to-column joints. They studied the behavior of bolted joints at the three different clearance configurations, i.e., full clearance, normal clearance, and zero clearance. The stiffness behavior of the joints was

obtained for tension forces. The experimental data is a good resource for numerical simulation of bolted joint behavior. Ungkurapinan (2000) fitted the continuous slippage model proposed by Kitipornchai, et al (1994) to his data and gave explicit load-deformation relationships for different bolted joint configurations. The load-displacement relations obtained by Ungkurupanian (2000) for the transmission tower bolted joints are useful for future studies dealing with transmission towers.

1.4 Objectives and Scope

Current structural analysis packages and finite element models require further improvement to account for joint slippage when applied to analyze transmission towers. Joint slippage modeling should be based on reliable experimental data. The recent study by Ungkurapinan (2000) provides a sound experimental basis for the behavior of bolted joints in transmission towers. In an effort to provide practicing engineers with a tool to better understand the behavior of latticed transmission towers, this study presents a finite element based software package to analyze transmission towers that incorporates joint slippage, bending stiffness of leg members and geometric stiffness. In the current study, the experimental data obtained by Ungkurapinan (2000) are analyzed for two joint types; column-to-column and beam-to-column. The behavior of the joints is discussed and equivalent joint parameters such as modulus of elasticity, yielding strength, and hardening conditions are obtained from the experimental data. Based on the joint parameters, a nonlinear finite element formulation for the two types of joint is developed. The behavior of selected tower structures under force and displacement boundary conditions is investigated by considering joint slippage. The thesis is arranged into five chapters including this first chapter.

Chapter 2 describes the finite element formulation of a transmission tower structure. It includes a discussion of the nonlinear finite element analysis of a 2-D beam element and its generalization to 3-D beams that are used to model transmission towers. Next, a discussion of the behavior of bolted joints of transmission towers and related experimental results is presented. Thereafter, the finite element formulation of joint elements is presented. Last, a discussion of the application of boundary conditions and non-linear solution algorithms is presented.

Chapter 3, describes the in-house FE program developed to analyze transmission towers. The program structure, input file format, main program subroutines, element types available, solution scheme, and the output results are discussed. Thereafter, the user interface program and the main interface components are described.

Chapter 4 shows selected results from the FE program. The FE program is first verified by comparing its results for different structures against the commercial FE code "ANSYS", Kitipornchai, et al (1994) and Kroeker (2000). Thereafter the study of a 2-D frame structure is engaged to examine the influence of different joint types on the behavior of a structure. Finally, a full scale tower under dead and working loads and different frost heave conditions is analyzed to examine tower responses under different loading modes and the influence of joint slippage.

The Chapter 5 presents conclusions and recommendations for future work.

Chapter 2

FINITE ELEMENT ANALYSIS OF TRANSMISSION TOWERS

2.1 General

Latticed transmission towers have several hundreds of elements and joints, three-dimensional geometry and complex loading. Their structural analysis is performed by using computer-based techniques, primarily the finite element method. Linear analysis of transmission towers as 3-D truss or framed structures is now a relatively straight forward task considering the current state-of-the-art of the finite element method. Non-linear behavior of transmission towers is portly associated with large deflections of the tower and/or plastic deformation of members due to external loads. The consideration of large deflections and elasto-plastic material behavior in finite element analysis is also now well established. As mentioned in Chapter 1, another important source of nonlinearity in transmission towers is the non-linear joint behavior. Practically all joints in transmission towers are bolted joints and significant slippage exists at these joints (Ungkurupinan 2000). Currently available struructral analysis software packages do not provide tools to simulate the non-linear bolted joint behavior based on experimental observations. In this Chapter, the development of a non-linear finite element model for transmission towers that accounts for experimentally observed nonlinear bolted joint behavior and geometric stiffness effects is presented.

The first section of this chapter discusses the nonlinear finite element analysis of a 2-D beam element and its generalization to 3-D beams that are used to model transmission towers. The next section discusses the behavior of bolted joints of transmission towers. Thereafter, the finite element formulation of joint elements is presented. The last section discusses the application of boundary conditions and non-linear solution algorithms.

2.2 Non-linear Finite Element Model For Beams

A member of a transmission tower can be modeled either as a 3-D beam element with axial forces or a 3-D truss element. The tower leg elements and horizontal bracing elements are usually modeled as 3-D beam elements while diagonal bracing elements are modeled using 3-D truss elements. The beam elements in transmission towers are long and made of angle sections. Therefore, Bernoulli-Euler beam theory, in which the shear deformations are ignored, is used. Material non-linearity is not considered in the present analysis as towers are not designed to undergo plastic deformations. However, large deformations and rotations are considered.

Figure 2.1 shows a beam element before and after deformation, and the following relationships can be developed by considering the deformation of an element along the neutral axis.

$$\varepsilon_x = \frac{ds - dx}{dx} = \frac{ds}{dx} - 1 \tag{2-1}$$

$$ds^2 = (dw)^2 + (dx + du)^2;\ \frac{ds}{dx} = \sqrt{\left(1 + \frac{du}{dx}\right)^2 + \left(\frac{dw}{dx}\right)^2}$$

$$\varepsilon_x = \left(\sqrt{\left(1 + \frac{du}{dx}\right)^2 + \left(\frac{dw}{dx}\right)^2}\right) - 1 \ \cong\ \frac{du}{dx} + \frac{1}{2}\cdot\left(\frac{dw}{dx}\right)^2 \tag{2-2}$$

where

dx: is the element length before deformation.

ds: is the element length after deformation.

du: is the deformation component in x-direction.

dw: is the deformation component in y-direction.

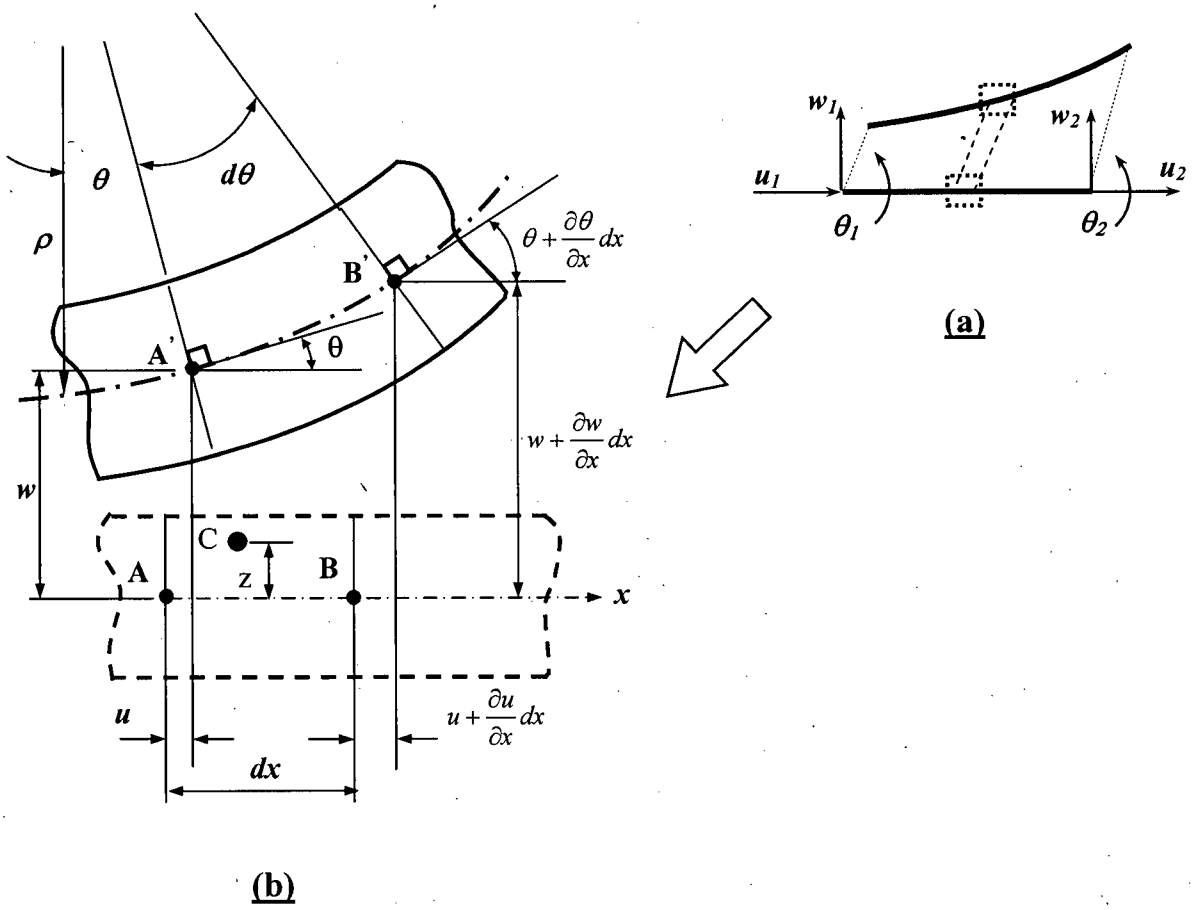

Figure 2.1: Beam under large rotation and deformation
(a) Beam element with degrees of freedom (b) Detailed view of an incremental element

For a general point "C" at a distance z from the neutral axis, the strain can be expressed by,

$$\varepsilon_x(z) = \frac{du}{dx} + \frac{1}{2}\cdot\left(\frac{dw}{dx}\right)^2 - z\cdot\frac{d^2w}{dx^2} \tag{2-3}$$

To develop the finite element equations based on energy methods, assume that a beam element has a uniform cross sectional area A, length L, moment of inertia about the z-axis I_z and Young's modulus, E. The strain energy of the element is:

$$U = \int_V \frac{1}{2} E\varepsilon^2 dV = \int_0^L \int_A \frac{1}{2} E\left(\frac{du}{dx} + \frac{1}{2}\cdot\left(\frac{dw}{dx}\right)^2 - z\cdot\frac{d^2w}{dx^2}\right)^2 dA\cdot dx \tag{2-4}$$

Expansion of Equation (2-4) yields,

$$U = \int_0^L \int_A \frac{1}{2} E\left(\begin{array}{l}\left(\frac{du}{dx}\right)^2 + \left(\frac{du}{dx}\right)\left(\frac{dw}{dx}\right)^2 + \frac{1}{4}\left(\frac{dw}{dx}\right)^4 \\ \qquad -2\,z\cdot\left(\frac{d^2w}{dx^2}\right)\left(\left(\frac{du}{dx}\right) + \frac{1}{2}\left(\frac{dw}{dx}\right)^2\right) + z^2\left(\frac{d^2w}{dx^2}\right)^2\end{array}\right) dA\cdot dx \tag{2-5}$$

Equation (2-5) can be further simplified by neglecting the higher order term, $(dw/dx)^4$, and noting that (du/dx) is constant along the length to obtain:

$$\begin{aligned} U = &\left[\int_0^L \tfrac{1}{2} E\left(\frac{du}{dx}\right)^2 dx\cdot\int_A dA\right] + \left[\int_0^L \tfrac{1}{2}\left(\frac{dw}{dx}\right)^2 dx\cdot\int_A \mathrm{E}\left(\frac{du}{dx}\right) dA\right] \\ &- \left[\int_0^L E\left(\frac{d^2w}{dx^2}\right)\left(\left(\frac{du}{dx}\right) + \frac{1}{2}\left(\frac{dw}{dx}\right)^2\right) dx\cdot\int_A z dA\right] + \left[\int_0^L \tfrac{1}{2} E\left(\frac{d^2w}{dx^2}\right)^2 dx\cdot\int_A z^2 dA\right] \end{aligned} \tag{2-6}$$

In Equation (2-6), the first term corresponds to the standard truss element stiffness matrix $[\mathbf{K}^{(t)}]$, the second term corresponds to the stress-stiffening matrix $[\mathbf{K}^{(\sigma)}]$, the third term vanishes, and the final term corresponds to the standard beam stiffness matrix $[\mathbf{K}^{(b)}]$.

To derive the stiffness matrices of a beam element (Figure 2.1a), the following

displacement interpolations are used.

$$u(x) = \{N_1 \quad N_2\} \begin{Bmatrix} u_1 \\ u_2 \end{Bmatrix} \tag{2-7}$$

where

$$N_1 = 1 - \frac{x}{L} \quad ; \; N_2 = \frac{x}{L} \tag{2-7}$$

and

$$w(x) = \{H_1 \quad H_2 \quad H_3 \quad H_4\} \begin{Bmatrix} w_1 \\ \theta_1 \\ w_2 \\ \theta_2 \end{Bmatrix} \tag{2-8}$$

where

$$H_1 = \frac{1}{L^3}\left(1 - 3Lx^2 + 2x^3\right) \quad ; \qquad H_2 = \frac{1}{L^2}\left(L^2 x - 2Lx^2 + x^3\right) \tag{2-8a}$$

$$H_3 = \frac{1}{L^3}\left(3Lx^2 - 2x^3\right) \quad ; \; H_4 = \frac{1}{L^2}\left(-Lx^2 + x^3\right) \tag{2-8b}$$

Utilizing the shape functions described above and applying the standard energy based finite element formulation, the following element stiffness matrices corresponding to different modes of deformations can be derived.

$$\left[\mathbf{K}^{(l)}\right] = \frac{EA}{L}\begin{bmatrix} 1 & -1 \\ -1 & 1 \end{bmatrix} \tag{2-9}$$

$$\left[\mathbf{K}^{(b)}\right] = \frac{EI_z}{L^3}\begin{bmatrix} 12 & 6L & -12 & 6L \\ 6L & 4L^2 & -6L & 2L^2 \\ -12 & -6L & 12 & -6L \\ 6L & 2L^2 & -6L & 4L^2 \end{bmatrix} \tag{2-10}$$

$$\left[\mathbf{K}^{(\sigma)}\right] = \frac{P}{30L}\begin{bmatrix} 36 & 3L & -36 & 3L \\ 3L & 4L^2 & -3L & -L^2 \\ -36 & -3L & 36 & -3L \\ 3L & -L^2 & -3L & 4L^2 \end{bmatrix} \tag{2-11}$$

Next, the 2-D beam element formulation is generalized to analyze a 3-D beam element.

Figure 2.2 shows a three dimensional beam element with local axes, *x, y* and *z,* and global axes, *X, Y* and *Z.* For a node *i*, the degrees of freedom in the local coordinates are denoted by u_{xi}, v_{yi}, w_{zi}, θ_{xi} , θ_{yi} , and θ_{zi} whereas the degrees of freedom in the global coordinates are identified by u_{Xi} , u_{Yi} , u_{Zi} , θ_{Xi} , θ_{Yi} , θ_{Zi} . For clarity, the DOFs in the local coordinates are shown at node-i whereas the DOFs in the global coordinates are shown at node-j. The axial and torsional deformations are assumed decoupled from the bending deformations. In addition, the bending deformations in xz-plane and xy-plane are also assumed decoupled.

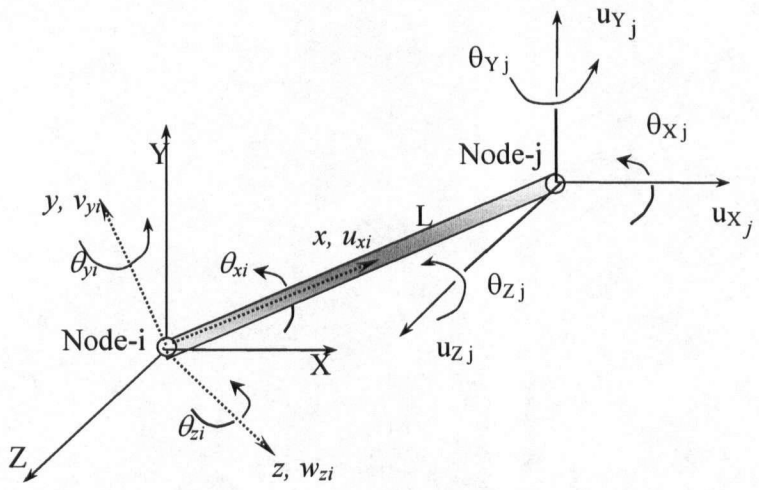

Figure 2.2: Three dimensional beam element

The beam element shown in Figure 2.2 can be subjected to bending deformations in the *xy* and *xz* planes. The stiffness matrices given by Equations (2-9, 2-10, and 2-11) can be applied separately to both planes to obtain the following stiffness matrices for a 3-D beam element in the local coordinates.

$$\left[\mathbf{K}^{(l,b)}\right]_{xyz} = \begin{bmatrix}
\frac{EA}{L} & & & & & & & & & & & \\
0 & \frac{12EI_z}{L^3} & & & & & & & & & & \\
0 & 0 & \frac{12EI_y}{L^3} & & & & & & & & & \\
0 & 0 & 0 & \frac{GJ}{L} & & & & & & & & \\
0 & 0 & -\frac{6EI_y}{L^2} & 0 & \frac{4EI_y}{L} & & & & & & & \\
0 & \frac{6EI_z}{L^2} & 0 & 0 & 0 & \frac{4EI_z}{L} & & & & & & \\
-\frac{EA}{L} & 0 & 0 & 0 & 0 & 0 & \frac{EA}{L} & & & & & \\
0 & -\frac{12EI_z}{L^3} & 0 & 0 & 0 & -\frac{6EI_z}{L^2} & 0 & \frac{12EI_z}{L^3} & & & & \\
0 & 0 & -\frac{12EI_y}{L^3} & 0 & \frac{6EI_y}{L^2} & 0 & 0 & 0 & \frac{12EI_y}{L^3} & & & \\
0 & 0 & 0 & -\frac{GJ}{L} & 0 & 0 & 0 & 0 & 0 & \frac{GJ}{L} & & \\
0 & 0 & -\frac{6EI_y}{L^2} & 0 & \frac{2EI_y}{L} & 0 & 0 & 0 & \frac{6EI_y}{L^2} & 0 & \frac{4EI_y}{L} & \\
0 & \frac{6EI_z}{L^2} & 0 & 0 & 0 & \frac{2EI_z}{L} & 0 & -\frac{6EI_z}{L^2} & 0 & 0 & 0 & \frac{4EI_z}{L}
\end{bmatrix} \quad \text{Symm} \tag{2-12}$$

The stress stiffening stiffness matrix in local coordinates is given by:

$$\left[\mathbf{K}^{(\sigma)}\right]_{xyz} = \frac{P}{30L}\begin{bmatrix}
0 & 0 & 0 & 0 & 0 & 0 & 0 & 0 & 0 & 0 & 0 & 0 \\
 & 36 & 0 & 0 & 0 & 3L & 0 & -36 & 0 & 0 & 0 & 3L \\
 & & 36 & 0 & -3L & 0 & 0 & 0 & -36 & 0 & -3L & 0 \\
 & & & 0 & 0 & 0 & 0 & 0 & 0 & 0 & 0 & 0 \\
 & & & & 4L^2 & 0 & 0 & 0 & -3L & 0 & -L^2 & 0 \\
 & & & & & 4L^2 & 0 & 3L & 0 & 0 & 0 & -L^2 \\
 & & & & & & 0 & 0 & 0 & 0 & 0 & 0 \\
 & & & \text{Symm} & & & & 36 & 0 & 0 & 0 & -3L \\
 & & & & & & & & 36 & 0 & 3L & 0 \\
 & & & & & & & & & 0 & 0 & 0 \\
 & & & & & & & & & & 4L^2 & 0 \\
 & & & & & & & & & & & 4L^2
\end{bmatrix} \tag{2-13}$$

The nodal DOF and force vectors corresponding to the above stiffness matrices are:

$$\begin{aligned}\{u\}_{xyz} &= \begin{bmatrix} u_{ix} & u_{iy} & u_{iz} & \theta_{ix} & \theta_{iy} & \theta_{iz} & u_{jx} & u_{jy} & u_{jz} & \theta_{jx} & \theta_{jy} & \theta_{jz} \end{bmatrix}^T, \\ \{F\}_{xyz} &= \begin{bmatrix} F_{ix} & F_{iy} & F_{iz} & M_{ix} & M_{iy} & M_{iz} & F_{jx} & F_{jy} & F_{jz} & M_{jx} & M_{jy} & M_{jz} \end{bmatrix}^T \end{aligned} \tag{2-14}$$

where M_x, M_y, and M_z are the bending moments about x-axis, y-axis, and z-axis, respectively; I_x, I_y, and I_z are the moments of inertia about the centroidal x-axis, y-axis and *z-axis* respectively; subscript "*xyz*" represents the local coordinates; superscript (t,b) means that the stiffness matrix is combined for truss and beam; and superscript "σ" denotes the geometric nonlinear stiffness.

The total stiffness matrix of a 3-D beam element is the sum of the linear and stress stiffness matrices and,

$$[\mathbf{K}]_{xyz} = \left[\mathbf{K}^{(t,b)}\right]_{xyz} + \left[\mathbf{K}^{(\sigma)}\right]_{xyz} \tag{2-15}$$

The stiffness matrix in the global coordinates is given by,

$$[K]_{XYZ} = \begin{bmatrix} [T] & [0] & [0] & [0] \\ [0] & [T] & [0] & [0] \\ [0] & [0] & [T] & [0] \\ [0] & [0] & [0] & [T] \end{bmatrix}^T [K]_{xyz} \begin{bmatrix} [T] & [0] & [0] & [0] \\ [0] & [T] & [0] & [0] \\ [0] & [0] & [T] & [0] \\ [0] & [0] & [0] & [T] \end{bmatrix} \tag{2-16}$$

where $[K]_{XYZ}$ is the stiffness matrix in the global coordinates and [T] is the transformation matrix.

The elements of the transformation matrix are calculated from the nodal coordinates of a beam element and [T] has to be updated based on the current position coordinates and definition of the centroidal principal local axes of the beam cross section. For beam elements, the two nodal

coordinates of an element cannot uniquely define the orientation of its local coordinates. Thus, an extra node, located on the local x- and z- axes, is required. This node defines an orientation angle, β, of the element local y-axis to the global X-Y plane. Thus, for an element with the nodal coordinates (x_1, y_1, z_1) and (x_2, y_2, z_2), a third node at coordinates (x_3, y_3, z_3) defines the angle (β) according to the following relation (ANSYS Theoretical Manual, 2005).

$$\cos(\beta) = \frac{(\mathbf{V}_1 \times \mathbf{e}) \cdot (\mathbf{V}_1 \times \mathbf{V}_2)}{|(\mathbf{V}_1 \times \mathbf{e})| \cdot |(\mathbf{V}_1 \times \mathbf{V}_2)|} \quad \textit{and} \quad \sin(\beta) = \frac{\mathbf{V}_1 \cdot ((\mathbf{V}_1 \times \mathbf{e}) \times (\mathbf{V}_1 \times \mathbf{V}_2))}{|(\mathbf{V}_1)| \cdot |(\mathbf{V}_1 \times \mathbf{e})| \cdot |(\mathbf{V}_1 \times \mathbf{V}_2)|} \tag{2-17}$$

where

$\mathbf{V}_1$ is a vector along the element x-axis between nodes 1 and 2

$\mathbf{V}_2$ is a vector in the element x-z-plane between nodes 1 and 3

e is a unit vector parallel to global Z-axis unless $\mathbf{V}_1$ is parallel to Z-axis, in which case **e** is taken to be parallel to the X-axis.

With this definition of β, it can be shown that

$$[T] = \begin{bmatrix} \frac{\Delta x}{L} & \frac{\Delta y}{L} & \frac{\Delta z}{L} \\ \frac{(\Delta x)(\Delta z)(S/L) - (\Delta y)C}{\sqrt{(\Delta x)^2 + (\Delta y)^2}} & \frac{(\Delta x)C - (\Delta y)(\Delta z)(S/L)}{\sqrt{(\Delta x)^2 + (\Delta y)^2}} & \frac{LS}{\sqrt{(\Delta x)^2 + (\Delta y)^2}} \\ -\frac{(\Delta x)(\Delta z)(C/L) + (\Delta y)S}{\sqrt{(\Delta x)^2 + (\Delta y)^2}} & -\frac{(\Delta y)(\Delta z)(C/L) + (\Delta x)S}{\sqrt{(\Delta x)^2 + (\Delta y)^2}} & \frac{LC}{\sqrt{(\Delta x)^2 + (\Delta y)^2}} \end{bmatrix} \tag{2-18}$$

where C=cos(β), S=sin(β) and

$$\Delta x = x_2 - x_1, \quad \Delta y = y_2 - y_1, \quad \Delta z = z_2 - z_1 \quad \textit{and} \quad L = \sqrt{(\Delta x)^2 + (\Delta y)^2 + (\Delta z)^2}$$

2.3 Bolted Joint Behavior

The members of a transmission tower are normally connected by one of the three types of bolted joints, namely, column-to-column, beam-to-column, and beam-to-beam joints. The joints provide a higher level of flexibility to a tower because of the loosening of bolts or slippage. The numerical simulation of bolted joints is based on an instantaneous or a continuous slippage model (Kitipornchai et al., 1994). In the instantaneous slippage model, a joint is assumed to start slipping at an axial load, P_s. Then the joint continues to slip while P_s is constant until the joint clearance is fully accumulated (Figure 2.3). The final amount of slippage Δ_s is added to the element length L in the case of tension members and subtracted from the member length in compression members. The main problem of this model is the stiffness singularity at the onset of slippage. This singularity requires a special numerical treatment and may cause convergence problems in the analysis. It is noted that joint behavior represented by this model does not favorably match the experimental results reported by Ungkurapinan (2000).

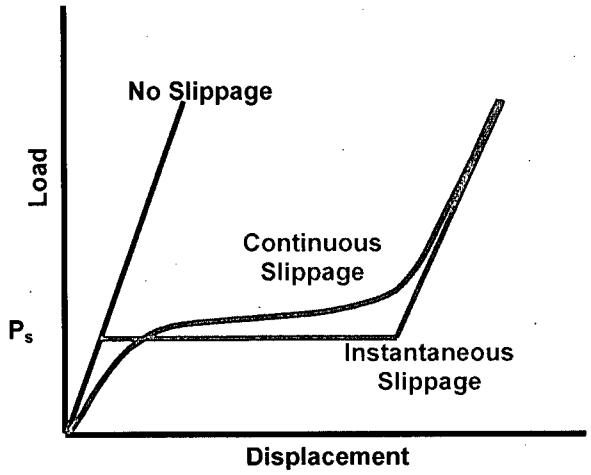

Figure 2.3: Instantaneous and continuous slippage models.

In the continuous slippage model, it is assumed that slippage takes continuously and can be represented by a Ramberg-Osgood type function. In this model the incremental slip in the member is expressed by:

$$\Delta_s = \Delta\left(v - v^m\right); \qquad v = \left(P/P_S\right) \Big/ \left(1 + \left(P/P_S\right)^n\right)^{\frac{1}{n}} \tag{2-19}$$

where P is the axial force in the member, P_s is the slippage load, Δ is the elastic displacement of the member, and m and n are parameters that control the slip–load relation.

The model behavior is highly sensitive to the values of m and n, which affects the shape of the load-deformation relation. The continuous slippage model assumes that internal axial loads are not affected by joint slippage. The stiffness of a member undergoing slippage is defined by (Kitipornchai et al., (1994)):

$$K_{slip} = \frac{AE}{L} \cdot \left(1 - \left(v - v^m\right)\right) \tag{2-20}$$

The above two models do not take into account the yielding of a joint, which depends on material and joint types (Ungkurapinan (2000)). Furthermore, the two models were developed and applied to study slippage of only beam-to-column joints. The experimental findings of Ungkurupinan (2000) show that different types of bolted joints(column-to-column, beam-to-column, beam-to-beam) have different stiffness characteristics and slippage behavior. In addition, slippage of a particular joint type depends on the arrangement of bolts and bolt clearances. Ignoring these factors in the finite element simulation probably led to the conclusion that joint slippage has no or little effect on the behavior and the load carrying capacity of transmission towers (Kitipornchai et al., (1994)).

In order to account for joint slippage in towers in a more complete manner, the present study aims to develop different joint elements based on the experimental work done by Ungkurapinan (2000) who obtained the axial stiffness of column-to-column and beam-to-column joints through a series of simple tension tests for each type of joint. The column-to-column joint was labeled by Ungkurupinan (2000) as "type-A joint" and the beam-to-column joint was labeled as "type-C joint". Each joint was tested with three different clearance configurations: maximum, normal, and minimum. Figure 2.4 shows the details of the joint types, their locations in a transmission towers, and the test specimens used by Ungkurapinan (2000).

For type-A joints, Ungkurapinan (2000) measured the deformations at the joint ends and at each of the joint bolts to figure out the contribution of each bolt in the joint behavior under loading. Since the current study focuses on the joint stiffness, only the deformations at the joint ends are considered. Figure 2.5 shows the measured behavior of the three configurations of type-A joint under loading. Ungkurapinan (2000) reported that narrowing the gap reduces the joint deformation and increases the stiffness from an early load, however, this gap has no significant influence on tensile load carrying capacity.

Ungkurapinan (2000) has idealized these results to simplify the modeling of joint stiffness (Figure 2.6). The joint behavior is described by 8-10 parameters as shown in Figure 2.6 for type-A joint. These joint parameters also facilitate the interpolation or extrapolation of the load-deformation relationship of similar joints with different number of rows of bolts.

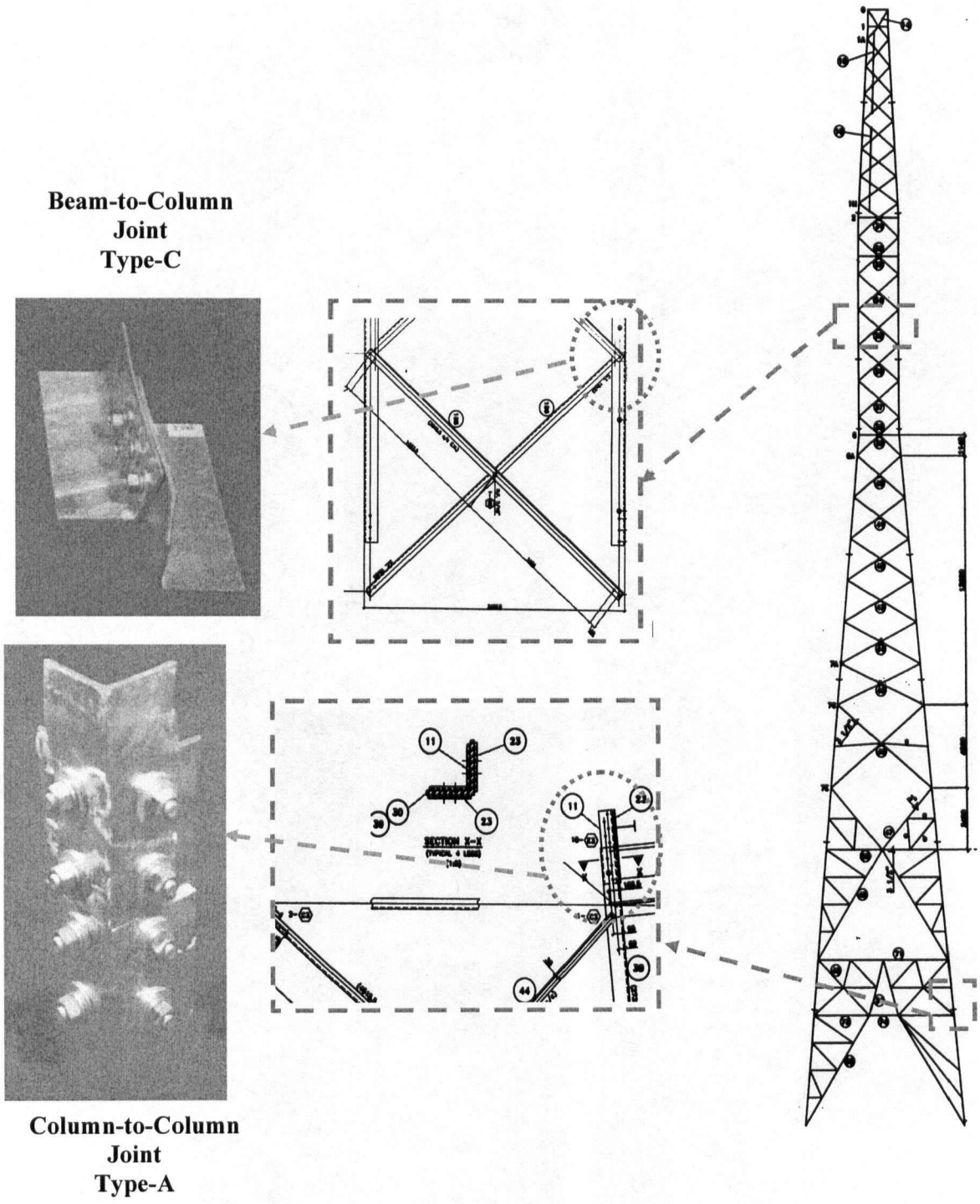

Figure 2.4: The test specimens and details of the column-to-column and beam-to-column joints.

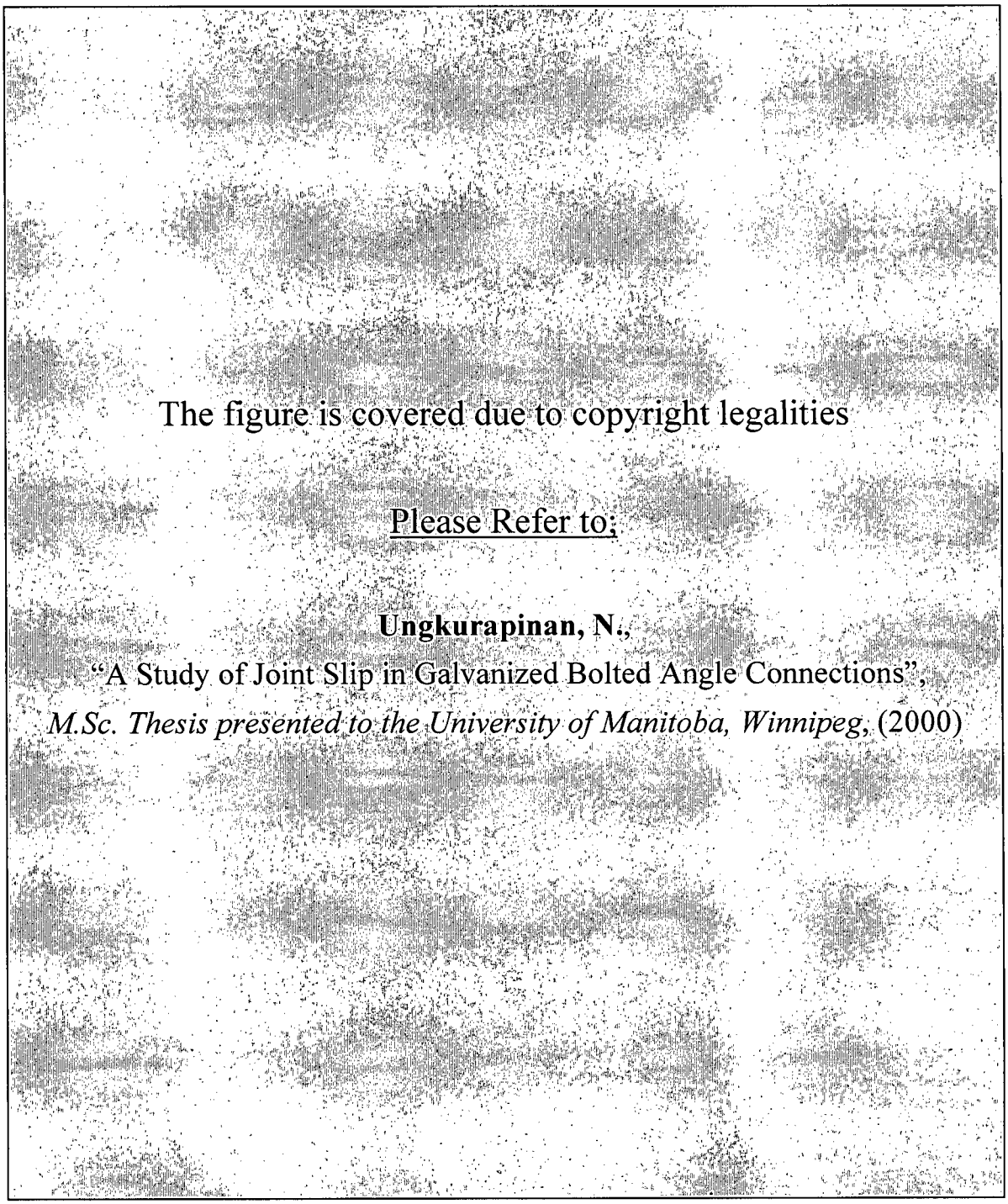

Figure 2.5: Typical test results for the three configurations of the type-A joints reported by Ungkurapinan (2000)

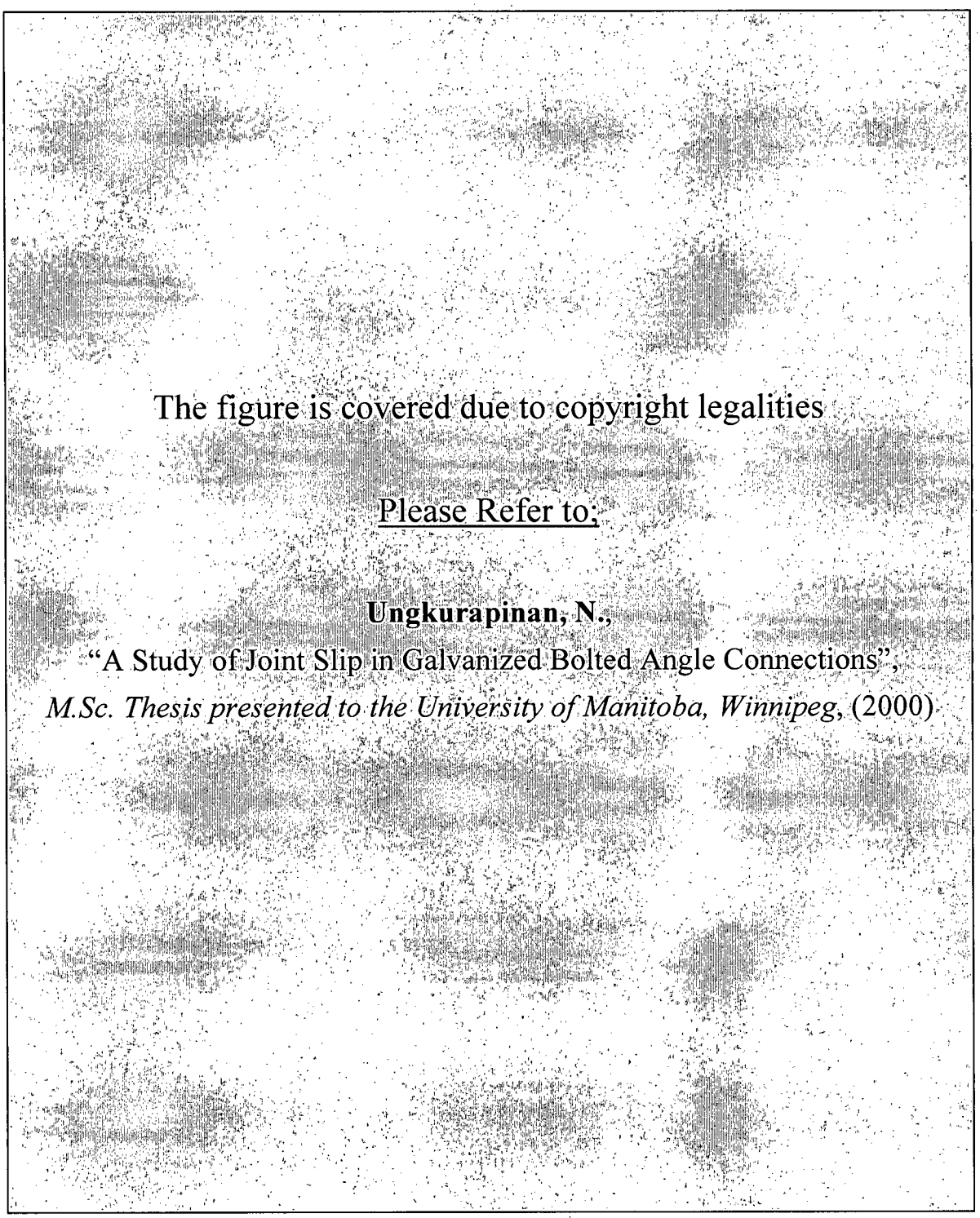

Figure 2.6: Idealized load-deformations relations and related parameters for the three configurations of the type-A joints reported by Ungkurapinan (2000)

For type-C joints (beam-to-column joints), Ungkurapinan (2000) measured the deformations at the joint ends and at each of the bolts to determine the contribution of each bolt to the joint behavior. Joints with one, two, three, and four bolts with the three clearance configurations were tested by Ungkurapinan (2000). Since the current study focuses on joints with one or two bolts, only the deformations at the joint ends with one or two bolts are considered. Figure 2.7 shows the behavior of the three configurations of type-C joints obtained from experiments. Ungkurapinan (2000) reported that type-C joints experience higher slippage than type-A joints. As in the case of type-A joints, Ungkurapinan (2000) idealized the experimental results to simplify the modeling of joint stiffness. The idealized curves are shown in Figure 2.8 for the three configurations of the type-C joint.

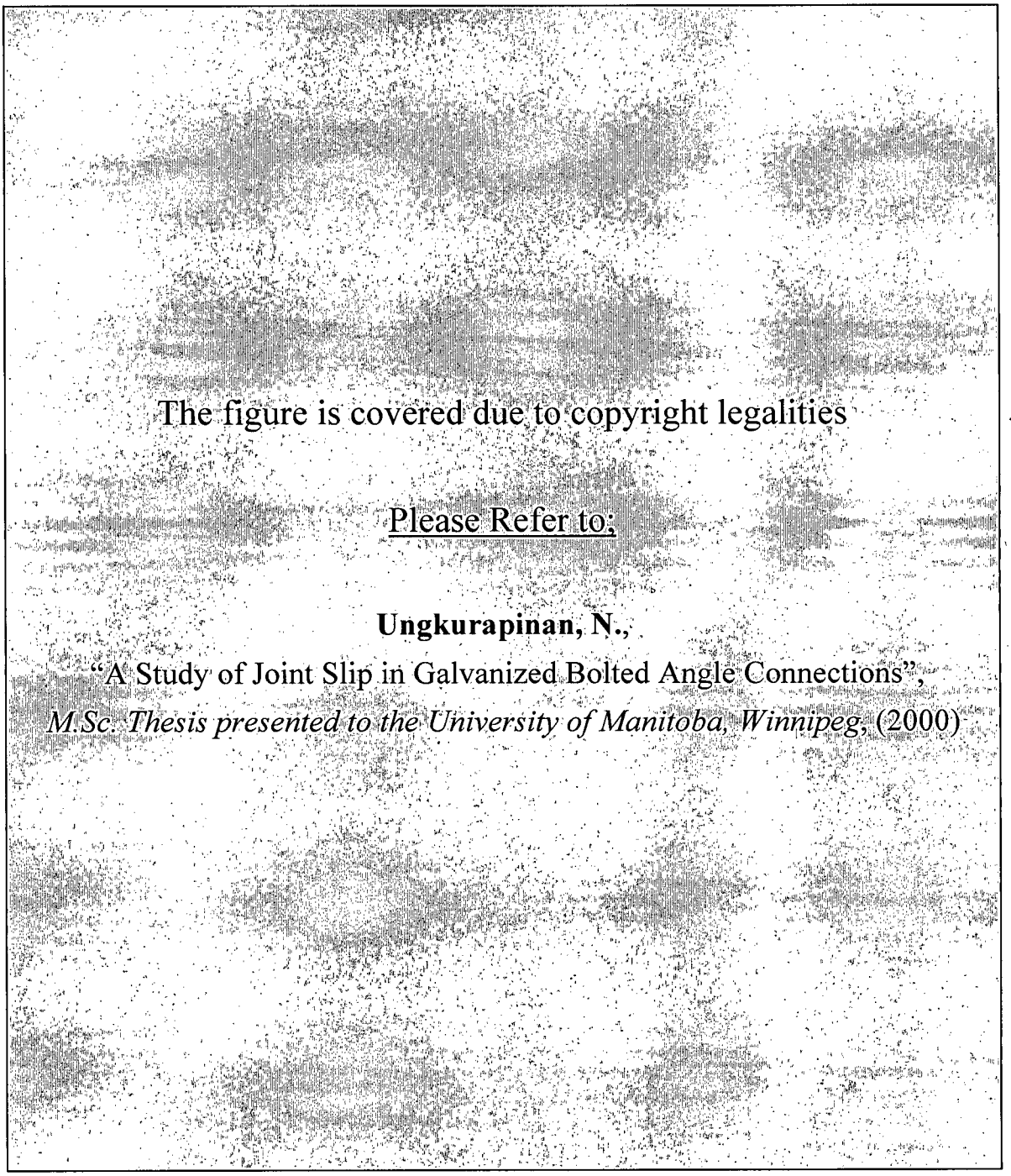

Figure 2.7: Typical test results for the three configurations of the type-C joints reported by Ungkurapinan (2000)

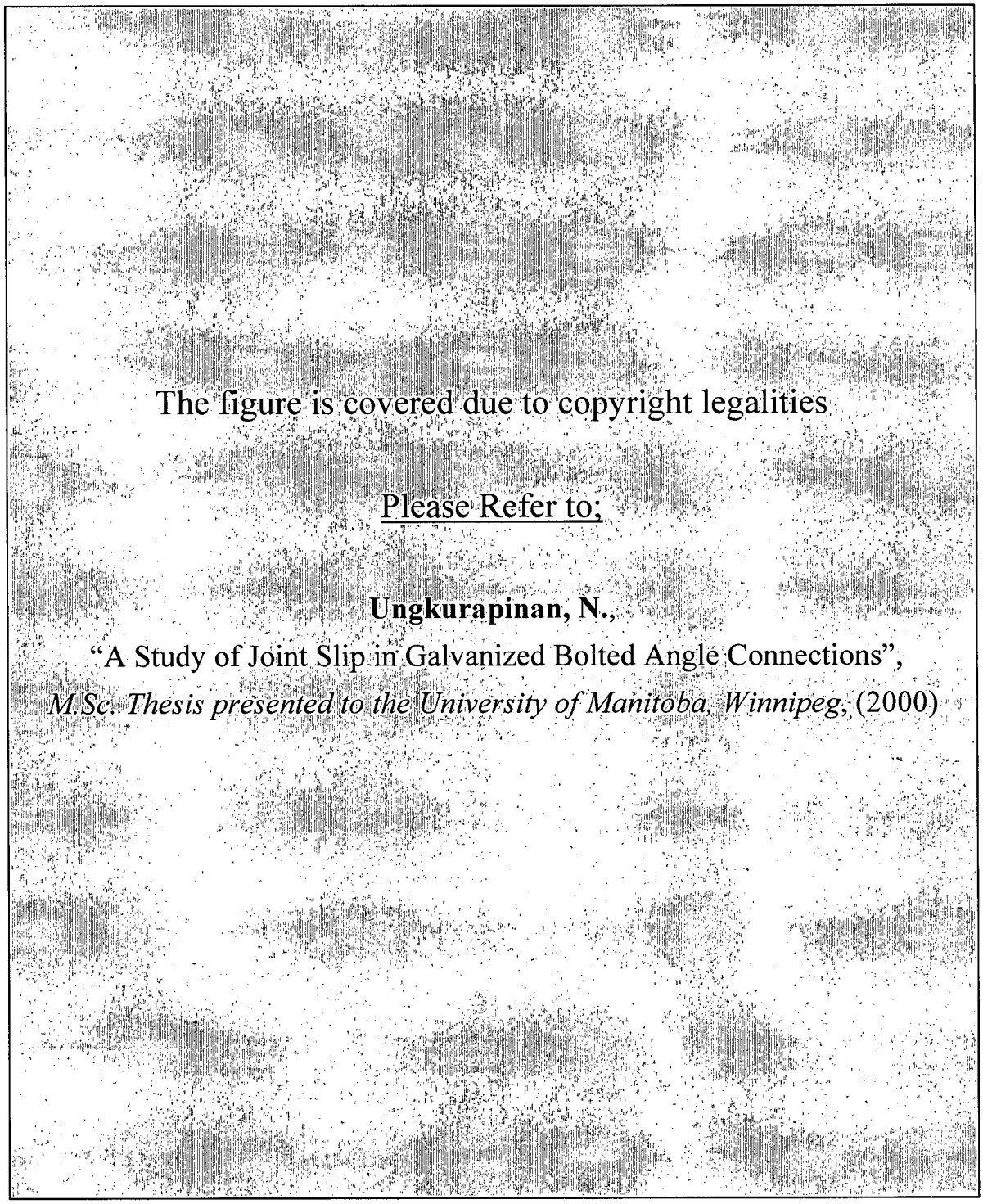

Figure 2.8: Idealized load-deformation relations and related parameters of the three configurations of the type-C joints reported by Ungkurapinan (2000)

The experimentally obtained load-deformation curves can be divided into four regions corresponding to different joint behavior mechanisms as shown in Figure 2.9. The first region is the micro-slip region in which the two connected elements are overcoming their asperities. The joint stiffness in this region is much weaker than the stiffness of each element. After the asperities are shaved off, the two elements start to slip over each other giving rise to a macro slip region which identifies the lowest level of stiffness for the joint (stiffness may become singular in this region). The end of the second region is identified by the maximum clearance of the joint and the joint response enters a third region representing a bearing state in which the load is transformed by shearing of the bolts. In the third region, the joint stiffness is slightly increased due to the addition of the bolt shear stiffness to the global stiffness. Further loading eventually gets the joint into plastic deformation when members or bolts start to yield. Investigation of the experimental results corresponding to the fourth stage shows that yielding of the joint occurs at a load level much lower than the yield load of the connecting members. The joint load carrying capacity is therefore much lower than that of the individual members. This important observation was not considered in the slip models proposed by Kitipornchai, et al (1994) and Kroeker (2000).

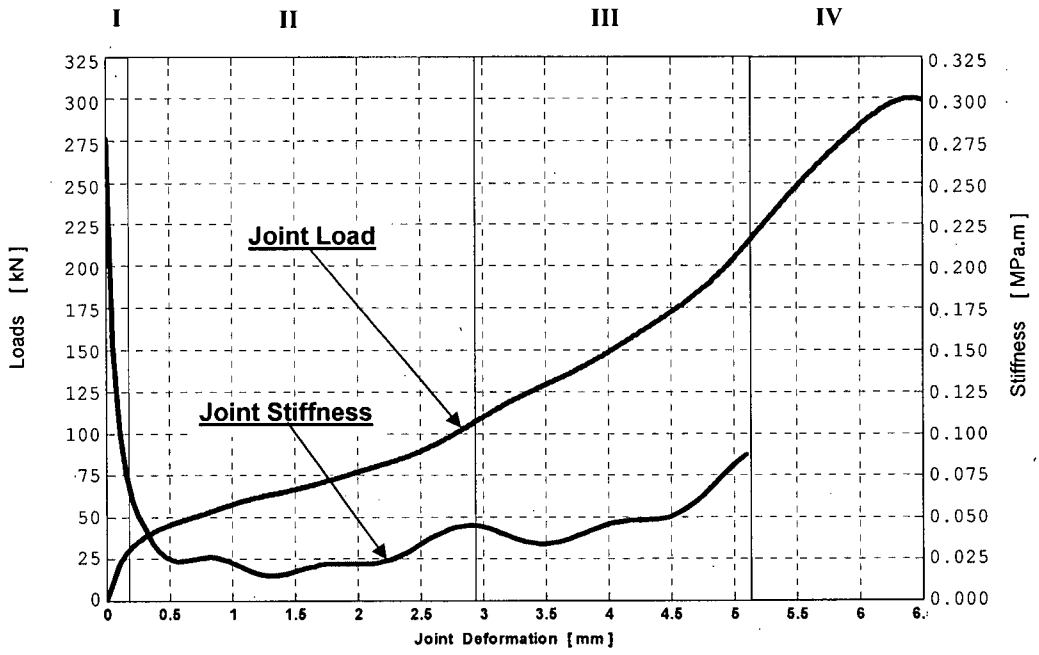

Figure 2.9: Deformation regions of a bolted joint
I-Micro-Slipping II-Macro-Slipping III-Bearing VI-Plastic zone

2.4 Bolted-Joint Finite Element Model

In the present study, beam-to-beam type joints are assumed to have negligible effect on the overall response of a tower as such types of joints do not involve major load-bearing members. Primary tower joints are either column-to-column or beam-to-column type. The finite element modeling of these two joint types are presented in the ensuing sections.

2.4.1 Column-to-Column Joint (Type-A) FE model

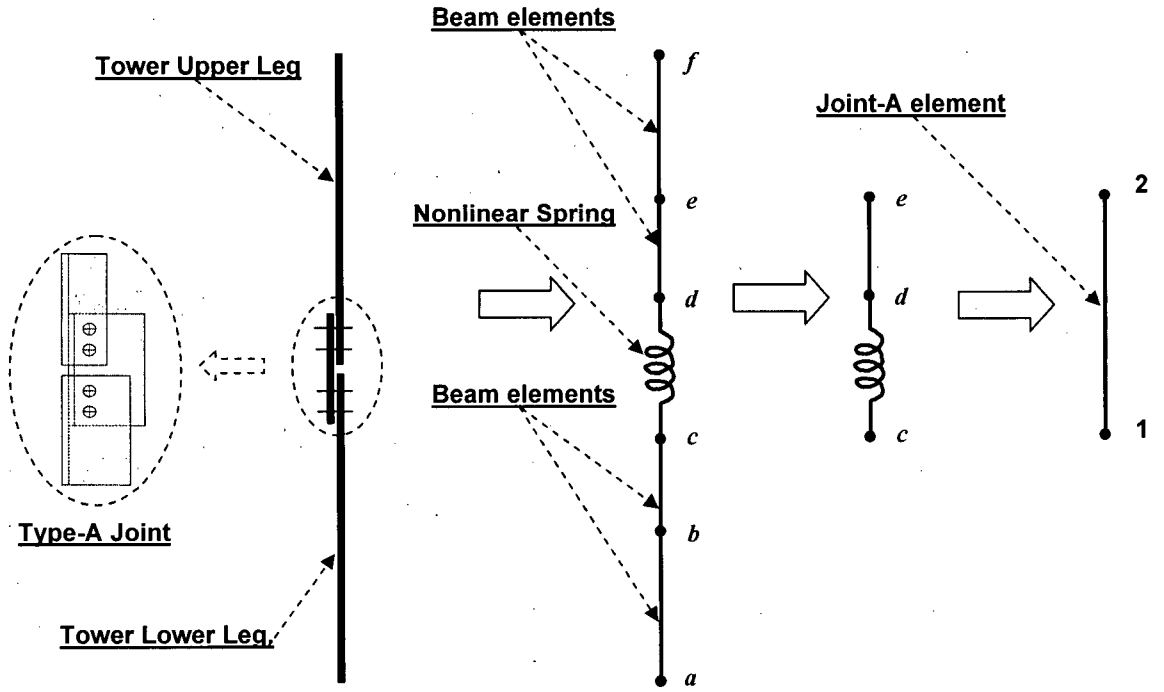

Figure 2.10: A Column-to-Column, Type-A, Joint and the finite element model

Figure 2.10 shows a detailed configuration of a type-A joint. Each tower leg is composed of segments of angle sections connected with column-to-column (Type-A) joints. This type of joints normally transfers axial and bending loads between the two column elements. Experimental results are only available for axial loading. No experimental data is available for transverse or torsional loading. However, a close examination of the joint geometry and its load carrying capacity behavior may justify the assumption of rigid behavior in these two directions.

The finite element modeling of the type-A joint sets through simple steps. Tower upper leg is modeled as beam elements with nodes "***f***", "***e***", and "***d***" and tower lower leg is modeled beam elements with nodes "***a***", "***b***", and "***c***". The type-A joint element is simply the series connection

between the beam element ("***e***"-"***d***") and the nonlinear spring ("***c***"-"***d***") which in the final configuration is represented by a single element with nodes "***1***" and "***2***". The equivalent type-A joint axial stiffness can be calculated as;

$$K_A = K_{J_A}\left(\frac{EA}{L}\right)\Big/\left[K_{J_A}+\left(\frac{EA}{L}\right)\right] \tag{2-21}$$

Where; L is the length between nodes ("***c***" - "***e***"), E is the modulus of elasticity, A is the cross sectional area, and K_{JA} is the extracted stiffness from the load-deformation curves of type-A joints reported by Ungkurapinan (2000). The joint is thereafter modeled as a 2-node beam element with a nonlinear axial stiffness given by Equation 2-21. This method has the advantage of not adding extra nodes to the FE model of the structure. The joint behavior for transverse, bending and torsional deformations is assumed to be the same as that of the beam element. Substituting equation 2-21 into equation 2-12 gives the type-A joint element stiffness as:

$$\left[\mathbf{K}^{(A)}\right]_{xyz} = \begin{bmatrix}
k_A & & & & & & & & & & & \\
0 & \frac{12EI_z}{L^3} & & & & & & & & & & \\
0 & 0 & \frac{12EI_y}{L^3} & & & & & & & & & \\
0 & 0 & 0 & \frac{GJ}{L} & & & & & \textit{Symm} & & & \\
0 & 0 & -\frac{6EI_y}{L^2} & 0 & \frac{4EI_y}{L} & & & & & & & \\
0 & \frac{6EI_z}{L^2} & 0 & 0 & 0 & \frac{4EI_z}{L} & & & & & & \\
-k_A & 0 & 0 & 0 & 0 & 0 & k_A & & & & & \\
0 & -\frac{12EI_z}{L^3} & 0 & 0 & 0 & -\frac{6EI_z}{L^2} & 0 & \frac{12EI_z}{L^3} & & & & \\
0 & 0 & -\frac{12EI_y}{L^3} & 0 & \frac{6EI_y}{L^2} & 0 & 0 & 0 & \frac{12EI_y}{L^3} & & & \\
0 & 0 & 0 & -\frac{GJ}{L} & 0 & 0 & 0 & 0 & 0 & \frac{GJ}{L} & & \\
0 & 0 & -\frac{6EI_y}{L^2} & 0 & \frac{2EI_y}{L} & 0 & 0 & 0 & \frac{6EI_y}{L^2} & 0 & \frac{4EI_y}{L} & \\
0 & \frac{6EI_z}{L^2} & 0 & 0 & 0 & \frac{2EI_z}{L} & 0 & -\frac{6EI_z}{L^2} & 0 & 0 & 0 & \frac{4EI_z}{L}
\end{bmatrix}$$

The corresponding nodal vectors of DOFs and forces are:

$$\{u\}_{xyz} = \begin{bmatrix} u_{ix} & u_{iy} & u_{iz} & \theta_{ix} & \theta_{iy} & \theta_{iz} & u_{jx} & u_{jy} & u_{jz} & \theta_{jx} & \theta_{jy} & \theta_{jz} \end{bmatrix}^T,$$
$$\{F\}_{xyz} = \begin{bmatrix} F_{ix} & F_{iy} & F_{iz} & M_{ix} & M_{iy} & M_{iz} & F_{jx} & F_{jy} & F_{jz} & M_{jx} & M_{jy} & M_{jz} \end{bmatrix}^T \quad (2\text{-}22)$$

Where;

u, v, w, θ_x, θ_y *and* θ_z are the displacements and rotations of a point on neutral axis in the local coordinates (x, y, and z),

E is Young's modulus of the beam material,

M_x, M_y, and M_z are the bending moments about x-axis, y-axis, and z-axis, respectively,

J, I_y, and I_z are the moments of inertia about the centroidal x-axis, y-axis and *z-axis.*

k_A is the equivalent local axial stiffness of a type-A joint which is obtained from:

2.4.2 Beam-to-Column Joint (Type-C)

Figure 2.11 shows the detailed configuration of a type-C joint. The four tower legs are supported together by diagonal and horizontal truss elements having angle sections. A truss element is usually connected directly to a main leg by one or two bolts. As in the case of type-A joints, experimental data is available only for loading in the axial direction.

A close examination of the joint geometry and its load carrying capacity reveals that the transverse and torsional stiffnesses of the joint are very small compared to the axial stiffness and thus may be ignored. Hence, the joint is modeled as a truss element connected in series with two nonlinear springs at its ends..

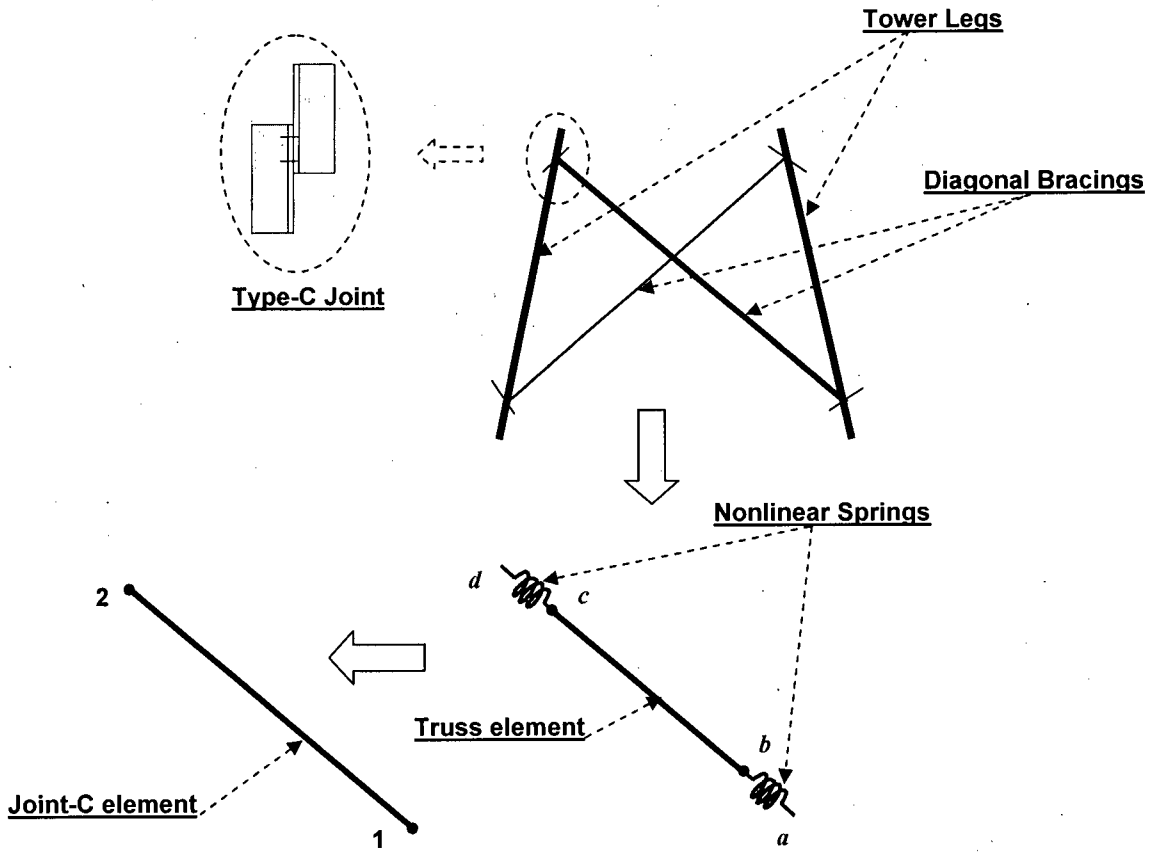

Figure 2.11: A Beam-to-Column joint, and the finite element model.

A type-C joint element is simply the series connection between a truss element ("***b***"-"***c***") and the two nonlinear springs ("***c***"-"***d***") and ("***a***"-"***b***") representing the connections at the end. Nodes ("***a***"-"***d***") become ("***1***"-"***2***") in the final reduction. Thereafter, the equivalent type-C joint axial stiffness can be calculated as;

$$K_C = K_{J_C}\left(\frac{EA}{L}\right)\Big/\left[K_{J_C} + 2\left(\frac{EA}{L}\right)\right] \tag{2-23}$$

Where; L is the length between the nodes "***a***" and "***d***", E is the modulus of elasticity, A is the

cross sectional area, and K_{JC} is the stiffness computed from the load-deformation curves of type-C joints reported by Ungkurapinan (2000).

The equilibrium of the type-C joint finite element can be expressed as,

$$\begin{bmatrix} k_C & 0 & 0 & -k_C & 0 & 0 \\ & 0 & 0 & 0 & 0 & 0 \\ & & 0 & 0 & 0 & 0 \\ & & & k_C & 0 & 0 \\ & & & & 0 & 0 \\ & & & & & 0 \end{bmatrix} \begin{Bmatrix} u_{x1} \\ u_{y1} \\ u_{z1} \\ u_{x2} \\ u_{y2} \\ u_{z2} \end{Bmatrix} = \begin{Bmatrix} F_{x1} \\ F_{y1} \\ F_{z1} \\ F_{x2} \\ F_{y2} \\ F_{z2} \end{Bmatrix} \tag{2-24}$$

2.4.3 Joint Stiffness Calculations

For the two types of joint elements discussed above the stiffness at a given load or displacement is obtained as the local tangent to the experimental load-deflection curve at a given point, i.e.,

$$k = dF / du \,. \tag{2-25}$$

The finite element program, developed in this thesis, has subroutines containing the joint load-deformation relations until the joint ultimate or fracture load. As discussed in Section 2.3, there are four stages in a joint load-deflection curve. The second stage of continuous slippage is identified by a rapid change in the slope of the curve. The third or the onset of yielding stage is, however, not easily identifiable and the following approximate equation is used for its definition (if it is not experimentally defined):

$$F_y = \frac{F_f}{S_f} \cdot S_y \tag{2-26}$$

where F_f is the fracture load of the joint, F_y is yield load of the joint, S_f is the fracture stress of the member, and S_y is the yield stress of the member.

The experimental load deflection response of a joint is then used to generate the joint stiffness as a function of the joint displacement using equation (2-25). Figures (2.12 and 2.13) show typical joint stiffness variations for type-A and type-C joints with various initial clearances.

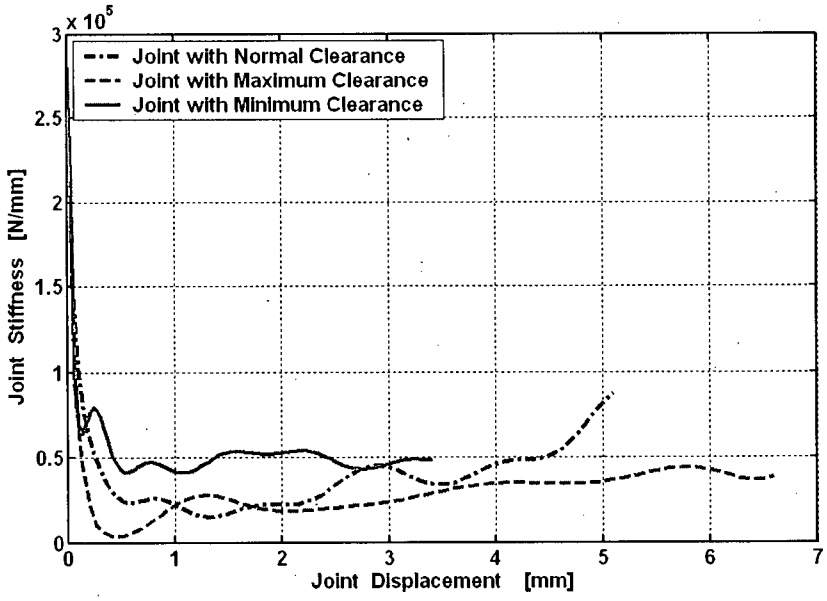

Figure 2.12: Stiffness of type-A joint obtained from experimental results.

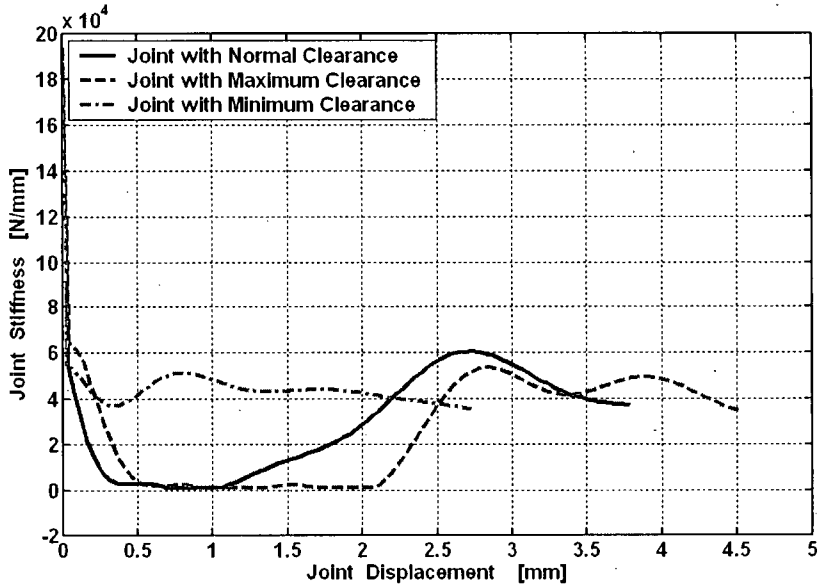

Figure 2.13: Stiffness of type-C joint obtained from experimental results.

2.5 Tower Boundary Conditions

The boundary conditions of a transmission tower are force and displacement boundary conditions. The force boundary conditions are related to external loads and self weight. The latter is applied on all tower nodes. The self weight load vector for an element is given by,

$$\left(\{F\}^b_{xyz}\right)_{Beam} = q\left[0 \quad \frac{L}{2} \quad 0 \quad 0 \quad 0 \quad \frac{L^2}{12} \quad 0 \quad \frac{L}{2} \quad 0 \quad 0 \quad 0 \quad -\frac{L^2}{12}\right]^T$$
$$\left(\{F\}^b_{xyz}\right)_{Truss} = q\left[0 \quad \frac{L}{2} \quad 0 \quad 0 \quad \frac{L}{2} \quad 0\right]^T \qquad (2\text{-}27)$$

where q is the weight per unit length of an element.

The external loads constitute all other working loads. One type is the conductor wire loads that act on the appropriate locations of the tower arms. The element load vectors are transformed

to the global coordinate system by the following relation.

$$\{F\}_{XYZ} = \begin{bmatrix} [T] & [0] & [0] & [0] \\ [0] & [T] & [0] & [0] \\ [0] & [0] & [T] & [0] \\ [0] & [0] & [0] & [T] \end{bmatrix} \{F\}_{xyz} \tag{2-28}$$

The conventional displacement boundary conditions are fixed ends at the foundation level of a tower. An important loading case to be considered in the present study is the frost heave induced displacements of the tower legs. This loading is modeled by prescribing a positive displacement in the y-direction for at the tower leg bases. As mentioned earlier, frost heave generally causes differential movement of tower foundations and the tower legs bases experience different displacements. The frost heave induced loading is normally analyzed by prescribing the vertical displacements at the tower leg base while fixing the other degrees of freedom. To solve the global matrix equation for prescribed kinematic boundary conditions, the elimination method is used for the constrained nodal degrees of freedom and the penalty method is used for the degrees of freedom contributing to the induced displacement. The elimination and penalty methods are summarized below.

(i) The Elimination Method

Consider a system of finite element equations with *n*-unknowns and a prescribed displacement boundary condition, $u_j=a$. The kinematic BC is imposed by first modifying the force vector by subtracting $K_{ij} * u_j$ from each element of the force vector as shown in Equation (2-29). Thereafter, the j^{th} row and j^{th} column of the stiffness matrix are eliminated together with the j^{th} element of the displacement and force vectors. The remaining system of (n-1) equations is

solved by using standard procedures.

$$\begin{bmatrix} K_{1,1} & \cdots & K_{1,j} & \cdots & K_{1,n} \\ \vdots & \vdots & \vdots & & \vdots \\ K_{j,1} & \cdots & K_{j,j} & \cdots & K_{j,n} \\ \vdots & & \vdots & & \vdots \\ K_{n,1} & \cdots & K_{n,j} & \cdots & K_{n,n} \end{bmatrix} \begin{Bmatrix} u_1 \\ \vdots \\ u_j \\ \vdots \\ u_n \end{Bmatrix} = \begin{Bmatrix} F_1 \\ \vdots \\ F_j \\ \vdots \\ F_n \end{Bmatrix} - \begin{Bmatrix} u_j * K_{1,j} \\ \vdots \\ F_j \\ \vdots \\ u_j * K_{n,j} \end{Bmatrix} \tag{2-29}$$

(ii) The Penalty Method

Consider the same system of equations and BC described above. To achieve the same result using the Penalty method, a very large number; *penalty number α,* is added to the stiffness $K_{j,j}$. There are different ways of assigning the penalty number but in the present study a value equal to $10^5 * K_{j,j}$ is used. The force F_j is then replaced by the prescribed displacement u_j multiplied by the penalty number. Thereafter, the following system of equations is solved for the unknown displacements, including u_j.

$$\begin{bmatrix} K_{1,1} & \cdots & K_{1,j} & \cdots & K_{1,n} \\ \vdots & \vdots & \vdots & & \vdots \\ K_{j,1} & \cdots & \alpha + K_{j,j} & \cdots & K_{j,n} \\ \vdots & & \vdots & & \vdots \\ K_{n,1} & \cdots & K_{n,j} & \cdots & K_{n,n} \end{bmatrix} \begin{Bmatrix} u_1 \\ \vdots \\ u_j \\ \vdots \\ u_n \end{Bmatrix} = \begin{Bmatrix} F_1 \\ \vdots \\ F_j \\ \vdots \\ F_n \end{Bmatrix} = \begin{Bmatrix} F_1 \\ \vdots \\ \alpha * u_j \\ \vdots \\ F_n \end{Bmatrix} \tag{2-30}$$

Where; $\alpha = 10^5 * K_{j,j}$ *and* $u_j = a$

The penalty method is typically used with the linear and nonlinear analyses for the displacement boundary conditions due to frost heave settlements. On the other hand, the elimination method is used for the fixed nodes.

2.6 Updating Geometry and Solution Scheme

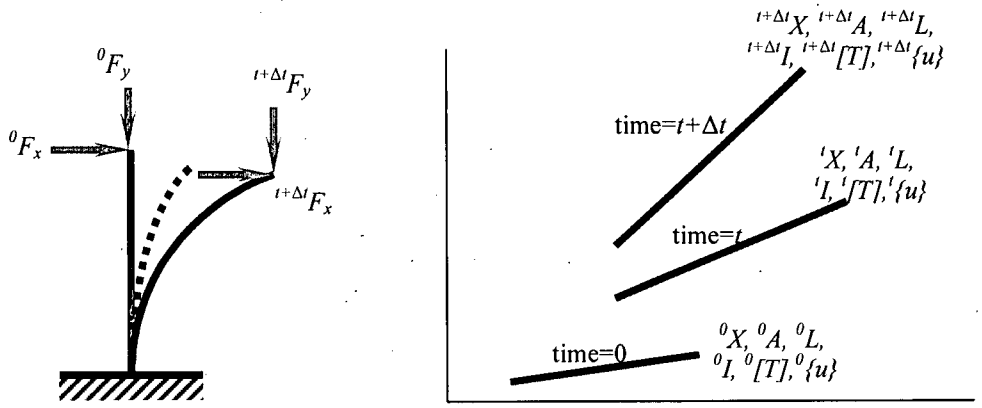

Figure 2.14 Beam under large rotation and deformation

For large deformations, as shown in Figure 2.14, the loads and specified nonzero BC conditions are applied incrementally and the initial stress-free configuration must be updated at each load increment to account for the deformed configuration. The finite element procedure is summarized below (see Figure 2.15):

It is assumed that the solution is known at a given time t and the aim is to find the solution for time $t+\Delta t$.

1- Update the geometry; $^{t}\mathbf{X} = {}^{t-\Delta t}\mathbf{X} + {}^{t}\Delta\mathbf{u}$

2- Update the element's dimensions; $^{t}L = \sqrt{\left(^{t}\Delta x\right)^2 + \left(^{t}\Delta y\right)^2 + \left(^{t}\Delta z\right)^2}$

3- Update the transformation matrix $^{t}[T] = f\left(^{t}\mathbf{X}\right)$

4- Obtain the current stiffness matrix $^{t}K = {}^{t}K_{linear} + {}^{t}K_{\sigma}$ using the updated geometry and loads.

5- Solve the system equation $^{t}K \cdot \left(^{t+\Delta t}\Delta u\right)_1 = {}^{t+\Delta t}\Delta F$ where $^{t+\Delta t}\Delta F$ is the load increment and $(^{t+dt}\Delta u)_1$ is the unknown displacement to be solved for the first iteration. The stiffness matrix in step 4 and the displacement in step 5 are considered as first iteration values of the load increment $t+\Delta t$

6- Update the geometry; $\left({}^{t+\Delta t}\mathbf{X}\right)_i = {}^{t}\mathbf{X} + \left({}^{t+\Delta t}\Delta\mathbf{u}\right)_i$ where i is the iteration number

7- Update the element's dimensions; $\left({}^{t+\Delta t}L\right)_i = \sqrt{\left({}^{t+\Delta t}\Delta x\right)_i^2 + \left({}^{t+\Delta t}\Delta y\right)_i^2 + \left({}^{t+\Delta t}\Delta z\right)_i^2}$

8- Update the transformation matrix $\left({}^{t+\Delta t}[T]\right)_i = \left(f\left({}^{t+\Delta t}\mathbf{X}\right)\right)_i$

9- Obtain the current stiffness matrix $\left({}^{t+\Delta t}K\right)_i = \left({}^{t+\Delta t}K_{linear}\right)_i + \left({}^{t+\Delta t}K_{\sigma}\right)_i$ using the updated geometry and loads.

10- Solve the system equation $\left({}^{t+\Delta t}K\right)_i \cdot \left({}^{t+\Delta t}\Delta u\right)_{i+1} = {}^{t+\Delta t}\Delta F$ for the unknown displacements $({}^{t+dt}\Delta u)_{i+1}$

Repeat Steps 6 to 10 to get the displacement values of the next iteration (i+1). Continue until iteration limit is reached or until convergence is achieved. In the current analysis the convergence criterion is : $({}^{t+\Delta t}\Delta u)_i - ({}^{t+\Delta t}\Delta u)_{i-1} < 1E\text{-}7$.

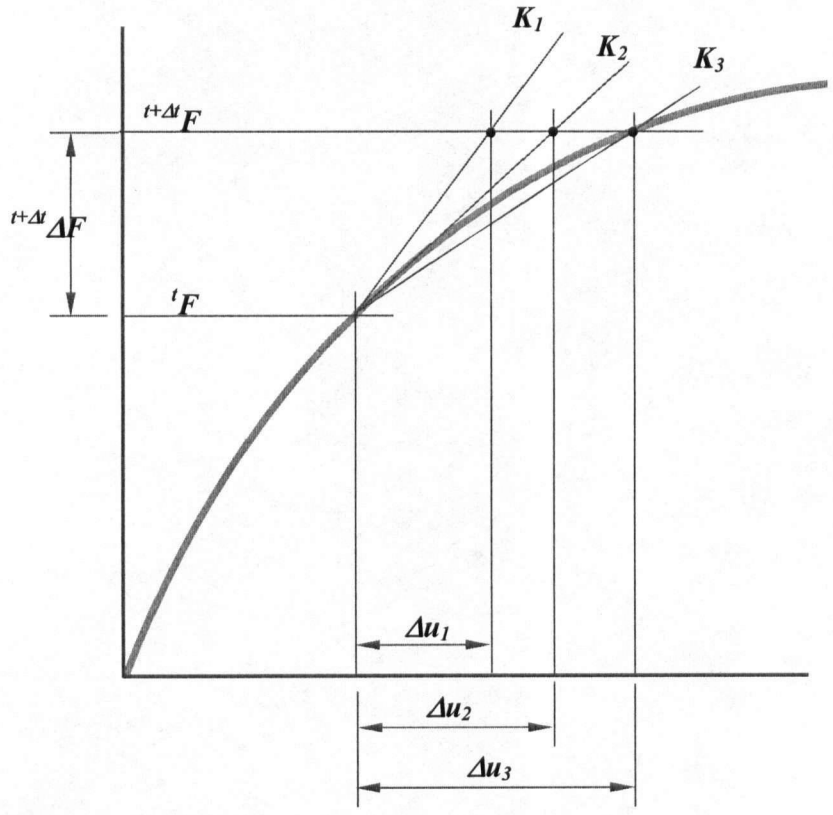

Figure 2.15 Iterative solution of nonlinear system equations

Chapter 3

JOINT SLIPPAGE ANALYSIS PROGRAM

3.1 General

This chapter presents the details of the finite element program developed in this thesis. The program structure, input file format, main program subroutines, element types available, solution schemes, and sample output results are discussed. Then the chapter presents the user interface program and the main components of the interface. The finite element program was written using Compaq virtual FORTRAN version 6.1 professional edition that facilitates programming using FORTRAN 90, (Compaq, 2001). The version 6.1 has the latest Microsoft integrated visual development environment with full FORTRAN-90/95 language features. In addition, it has an advanced compiler optimizer to optimize the running time. Furthermore, Compaq has amended an extended math library, in addition to the standard built-in ISML math library (Compaq, 2001), for advanced scientific applications. Fortran 90 has many features that enhances the programming of the finite element method (Smith, 2001).

3.2 The FE Program Structure

The finite element program has the following modules:

- Read and process the model data, control parameters and the boundary and the loading conditions.
- Evaluate the individual element stiffness in local and global coordinate system.
- Assemble the global stiffness matrix

- Solve the system of equations and obtain the nodal deformations due to prescribed loads.
- Calculate the reactions, stresses and strains of the structural elements (Post processing phase).

In the following a brief description of each module is given.

3.2.1 Input Data

This module is composed of three main parts: reading and initial processing of data, calculating active degrees of freedom (DOF) and calculating the global force boundary condition vector.

- **Initial Processing of Data:**

This part of the module reads the data header, which includes the number of 2D/3D elements and nodes, the maximum number of iterations, the user specified tolerance limits and an identification of the analysis type, i.e., linear or nonlinear. Then the module dynamically declares the size of the arrays and matrices that depend on the number of nodes, elements and degrees of freedom. Following the declaration of arrays, this program module generates the entire finite element model data base including materials property tables, list of element types, nodal coordinates and the connectivity matrix.

Finally this module reads the kinematic boundary conditions and external loading conditions of the structure and calculates the bandwidth of the global stiffness matrix and the number of equations. The program dynamically declares the arrays and matrices that depend on the bandwidth and number of equations. The input data file structure is as follows;

# of elem	*# of nodes.*	*2-D or 3-D*	*element types*	*Max No. of Iter.*	*Tolerance*	*Nonlinear flag,*	*Number of Incr.*	
12	**8**	**3**	**2**	**200**	**1E-7**	**1**	**100**	
EA	*EI_y*	*EI_z*	*GJ*					
3172e6	**2246400**	**2246400**	**1728000**					*Material Properties for element type 1*
-1								*Joint element flag*
/joint_1.dat/								*Location of joint data file (elem. type 2)*
1 1 1 1 1 1 1 1 2 2 2 2								*Elements types array*
0 0 0 0 0 0 0 0 0 0 0 0								*Elements orientation angles array*

X	*Y*	*Z*	
0.000	**1.000**	**0.000**	*Nodal Coordinates*
0.000	**0.000**	**0.000**	
1.000	**1.000**	**0.000**	
1.000	**0.000**	**0.000**	
1.000	**0.000**	**1.000**	
1.000	**1.000**	**1.000**	
0.000	**1.000**	**1.000**	
0.000	**0.000**	**1.000**	

1 2	*Connectivity Matrix*
1 3	
3 4	
5 6	
6 7	
7 8	
3 6	
1 7	
6 8	
3 5	
1 4	
2 7	

4 *Number of restrained nodes*

Node Number	*UX*	*UY*	*UZ*	*ROTX*	*ROTY*	*ROTZ*
2	**0**	**0**	**0**	**1**	**1**	**1**
4	**0**	**0**	**0**	**1**	**1**	**1**
5	**0**	**0**	**0**	**1**	**1**	**1**
8	**0**	**0**	**0**	**1**	**1**	**1**

4 *Number of Concentrated loads*

Node Number	*FX*	*FY*	*FZ*	*MX*	*MY*	*MZ*
1	**1.0**	**-1.0**	**1.0**	**0.0**	**0.0**	**0.0**
3	**1.0**	**-1.0**	**1.0**	**0.0**	**0.0**	**0.0**
6	**1.0**	**-1.0**	**1.0**	**0.0**	**0.0**	**0.0**
7	**1.0**	**-1.0**	**1.0**	**0.0**	**0.0**	**0.0**

- **Active DOF Vector:**

This subroutine sorts and counts the global DOF for the structure nodes. During this operation, the program omits the constrained DOF and creates an array for the active DOF. If a DOF has a nonzero specified value, it is considered active and its treatment is postponed until after the assemblage of the global stiffness matrix.

- **Force Boundary Conditions:**

This subroutine, calculates the distributed load vector for the structure in three steps. In the first step, it calculates the local distributed load vector for each element using Equation (2-19). Then this local load vector is transformed to the global coordinate system using Equation (2-20). Finally, these load vectors are assembled based on the active DOF vector. After calculating the distributed load vector, the subroutine reads the external concentrated load vector from the input data file and adds it to the distributed load vector to get the total load vector.

3.2.2 Assembly of the Global Stiffness Matrix

This module calls the stiffness subroutine of each element according to its type. In the stiffness subroutine, the element geometry, cross sectional area, moment of inertia, and element length are updated and the stiffness matrix for the particular element is calculated. Also, the stiffness subroutine performs stiffness transformation from local coordinates to the global coordinate system.

Based on the active degrees of freedom vector, the global stiffness matrix is assembled. Since the global stiffness matrix is banded and symmetric, the subroutine saves only the upper triangle of the matrix in a rectangular form. The array size of the global matrix is given by:

*Array Size = number of active degrees of freedom * (half-band width + 1)* (3-1)

The collection of the array elements is illustrated in following figure. The added zeros to the left of the matrix are used to simplify the transformation from the global stiffness matrix index to the array index and vice versa.

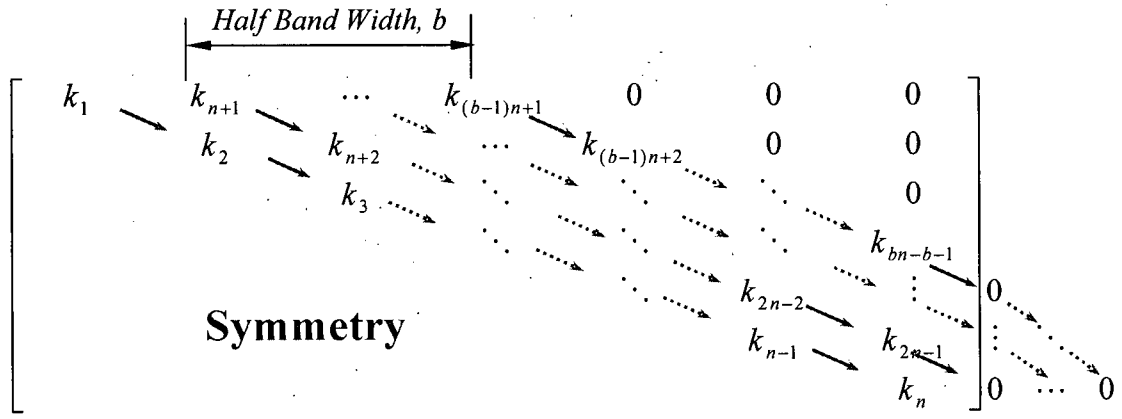

where,

K_i : is the stiffness value at the index i in the stiffness array.

n : is the number of system equations which is equal to the active degrees of freedom.

b: is the half band width.

3.2.3 Solution of the System of Equations

Once the global stiffness matrix is assembled, the program calls the Gauss elimination subroutine to solve the equation system that is followed by back substitution to obtain the incremental displacements for the given load increment. Based on these incremental displacements, the program updates the nodal coordinates and calculates an updated global stiffness matrix. The updated global stiffness is used with the residual load vector to obtain the iterative displacements for the increment. The procedure is repeated until the residual

displacement norm satisfies the user specified tolerance limits and convergence is achieved.

After the convergence criterion is achieved, the structure geometry, load and displacement vectors, stresses and internal forces are updated to the end of increment values and the program proceeds to the next load increment. If the convergence criterion could not be achieved after the allowed number of iterations, the program stops and gives a message indicating non-convergence report. Figure 3.1 shows a flow chart of the nonlinear finite element code.

In nonlinear analysis, the structure response depends on the history of load application. In the analysis of transmission towers, the external concentrated loads, the body forces as well as the distributed loads are applied in the first load step. These loads are applied incrementally according to the designated number of increments specified by the user. Any consequent displacements boundary condition, like those due to frost heave or foundation settlement, are applied in a next loading step, taking into account the deformation history of the structure. These displacements are divided by the designated number of increments to define the incremental displacements for each sub-step.

3.2.4 The FE Program Output Results

After obtaining the nodal displacements of the structure, the program calculates the final structural quantities of all tower elements and joints. The program output includes the reactions, internal loads for each member, and the final condition for each joint. The joint quantities are the slippage amount and the joint carried load. As discussed above, normally joints yield before structural members. From the input experimental results, the program predicts the yield load for each joint type. Then, it reports the status of all joints and the internal load in each joint as a percentage of its yield load. For structural members, the internal compressive loads are checked

for the possibility of buckling. If a member compressive load is more than eighty percent of its buckling load, the program flags the element in the output report. In addition, the program reports the final configuration of the deformed structure due to all applied loads.

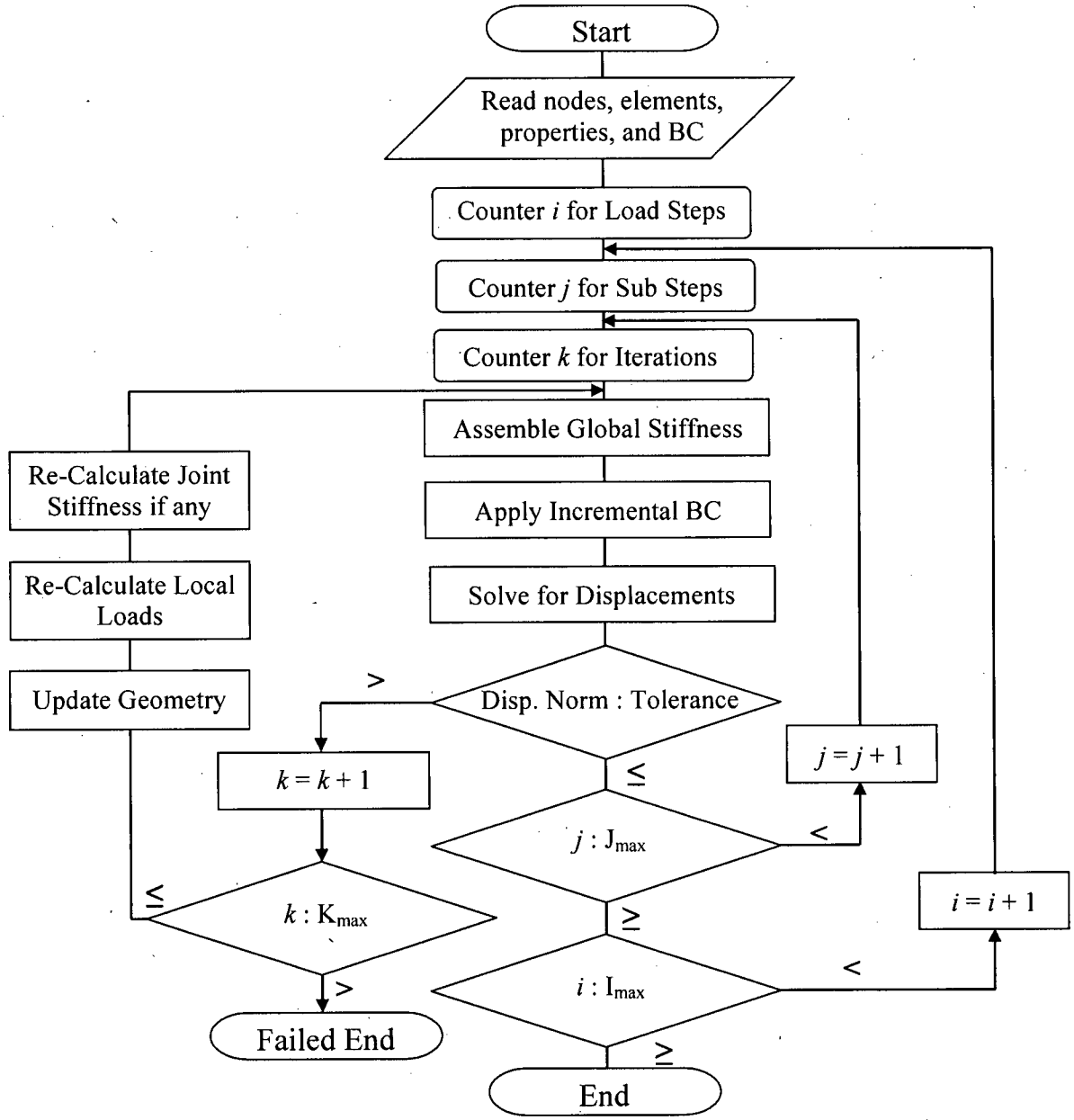

Figure 3.1: Flow chart of the nonlinear finite element code.

3.3 The User Interface

Graphical user interfaces are useful tools to process very comprehensive input data to a computer program through a few simple steps. The current FE program is incorporated with a graphical user interface (GUI) to ease the handling of the data input. This interface is a MS-Windows application written in Visual Basic Language. Microsoft Visual Basic is a production environment used to create computer applications for the Microsoft Windows family of operating systems. The interface program consists mainly of forms which are the main interactive screens with the user. These forms contains graphical objects through which, the user input the needed data for the finite element analysis. The graphical objects interact with the mouse actions through subroutines written in Basic Programming Language.

The interface consists of a starting screen and a main screen. The starting screen, as shown in Figure 3.2, shows the title of the program and facilitates different input fields. Through these input fields, a user defines the job working directory, job title and whether it is an existing or a new job. The starting screen also gives the option of choosing the tower type under study. However, this option is not enabled yet in the current version of the interface program.

The main screen has three phases, as shown in Figure 3.3, pre-processing, solution and post-processing phases. Saving and resuming the data base of the job are always available at any point by pressing the related buttons. Entering any of the three phases is done by clicking on the related tab, as shown in Figure 3.3.

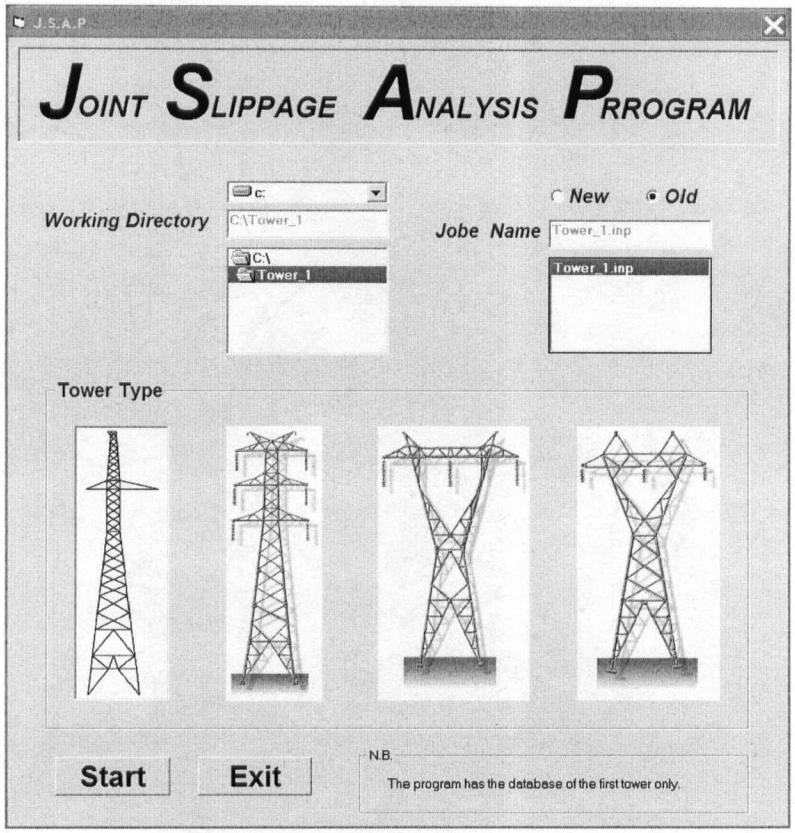

Figure 3.2: Starting screen of the user interface of the program.

3.3.1 The Pre-Processing Phase

The pre-processing phase defines the coordinates of the tower nodes, element type of each member, section properties of each member and joints properties. These data are fed to the interface program through three tabs; geometry input, meshing and elements properties tabs. A A user can select any of these tabs by clicking on the tab title, Figure 3.3.

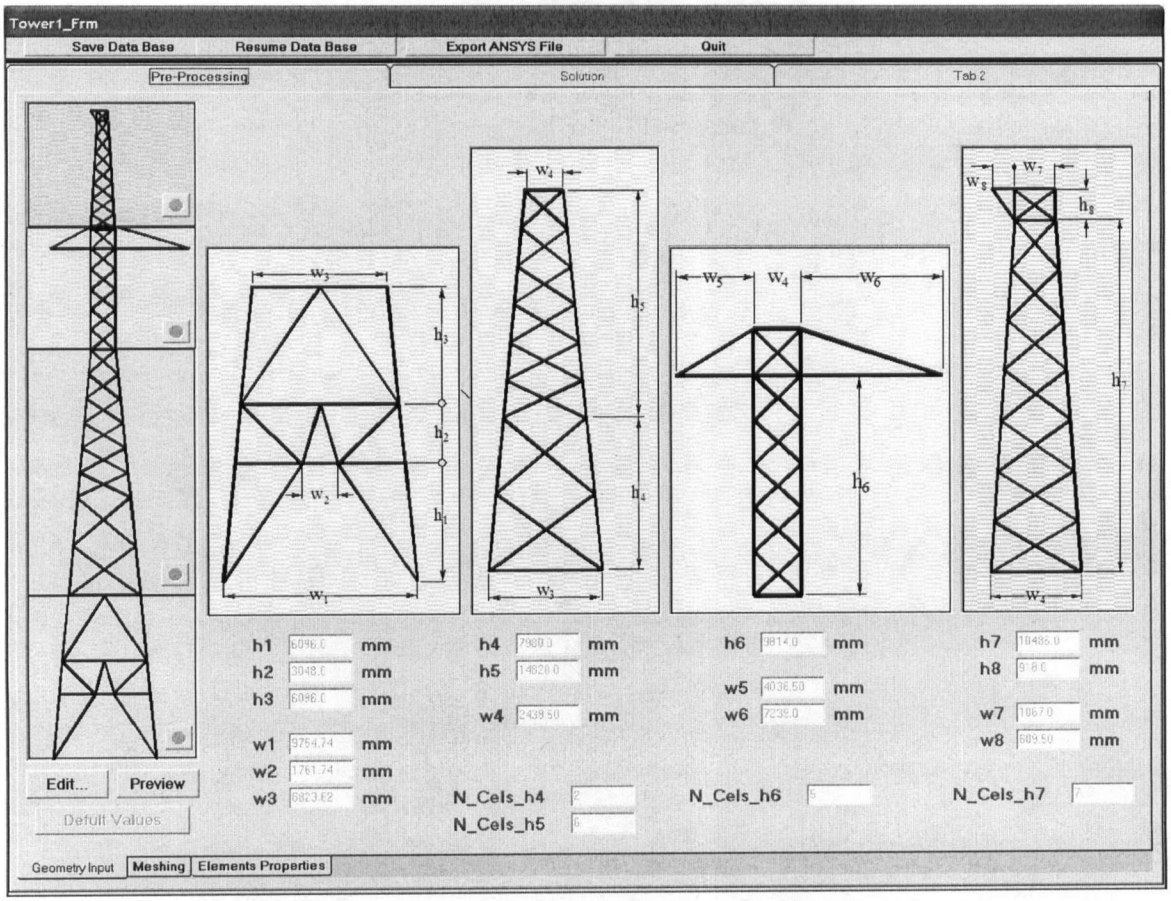

Figure 3.3: Main screen of the user interface.

In the first tab, "Geometry Input", the tower is divided into four main sections based on the geometrical relation between the members of each section. The coordinates of the members of each section can be defined by using a few parameters like the width and height of each pattern within the section. This method defines 230 coordinate points of the tower members by the knowledge of only 16 input data. The program starts with default values for these parameters. A user can change it by clicking on the "Edit" button. After defining the new values of these parameters a user clicks on the "Calc..." button to calculate the nodal coordinates of the tower based on the input parameters. Then a user can examine the tower geometry by clicking the

"Preview" button. Figure 3.4 shows the front view of a tower after clicking on "Preview" button. The other views can be shown by clicking the related buttons, see Figure 3.5 (a & b). Also, zooming on particular section of the four sections of the tower is available by clicking on the zooming button at bottom left corner of the logo of each section; see Figure 3.5 (c & d).

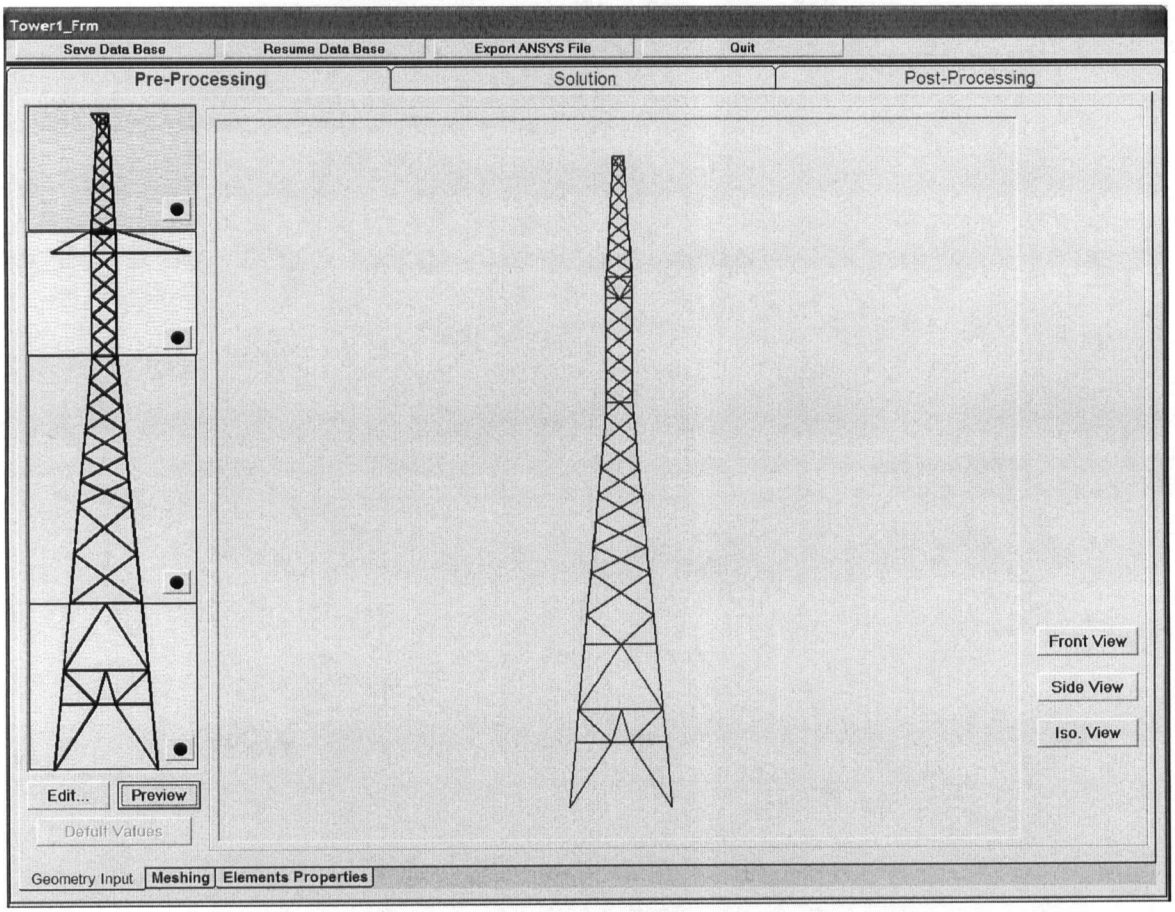

Figure 3.4: Preview of the tower front view in the geometry tab in the pre-processing phase.

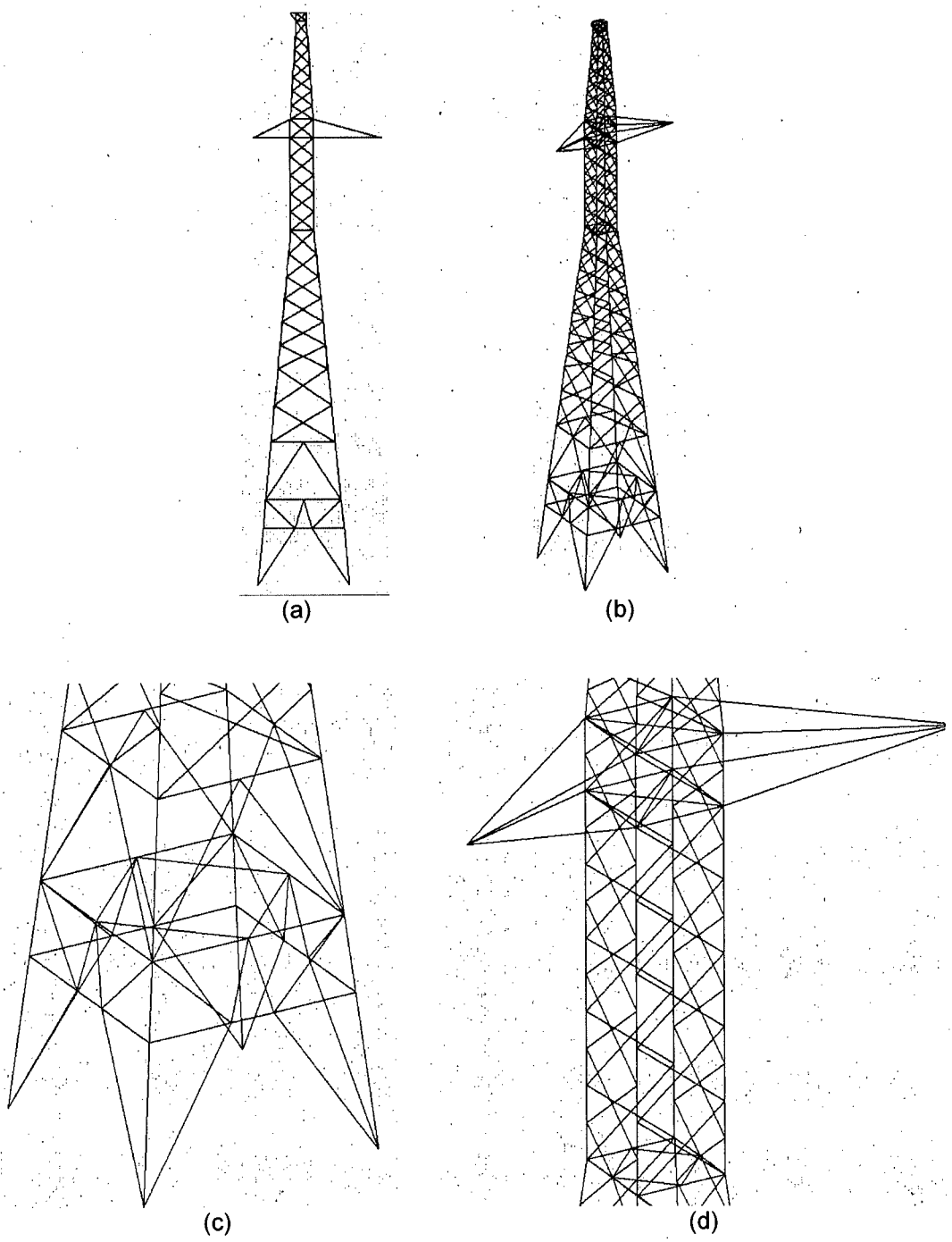

Figure 3.5: Different views and zooming of the tower sections in the pre-processing phase.
a- Side full view, b- Isometric full view
c- Isometric zooming for section -1-, c- Isometric zooming for section -3-

In the second tab, "Meshing", a user defines the element type, joint type, and section number for each member of the tower. Figure 3.6 shows the contents of the "Meshing" tab, which are; interacting fields and informative fields. The interacting fields are; scroll bar for browsing the tower members, element type and joint type checking boxes, section number spinning button. The informative fields are isometric views of the tower members, illustration view of the element cross section and information boxes for the element number, element coordinates, and section properties. The interface program starts with default values for the meshing tab, however, it allows a user to change any of these values by clicking the "Edit" button. A user can browse these default values by scrolling the element number scroll bar. The examined element is highlighted in the isometric view. A user can change the element type, joint type, and section number for each tower member. After finishing the editing of the member meshing parameters, a user saves the new data by clicking on "OK" button.

In the third tab, "Elements Properties", a user defines the main properties of the tower member cross sections which are the angle side lengths and thickness. Also a user can examine the joint stiffness by plotting the experimental load-displacement diagram and the extracted stiffness displacement diagrams for different joint types. Each diagram can be plotted by clicking the related button as shown in Figure 3.7 and Figure 3.8. The interface program starts with default values for the "Elements Properties" tab, however, it allows a user to change any of these values by clicking the "Edit" button. After finishing the data input for the section dimensions, a user saves the new data by clicking "OK" button.

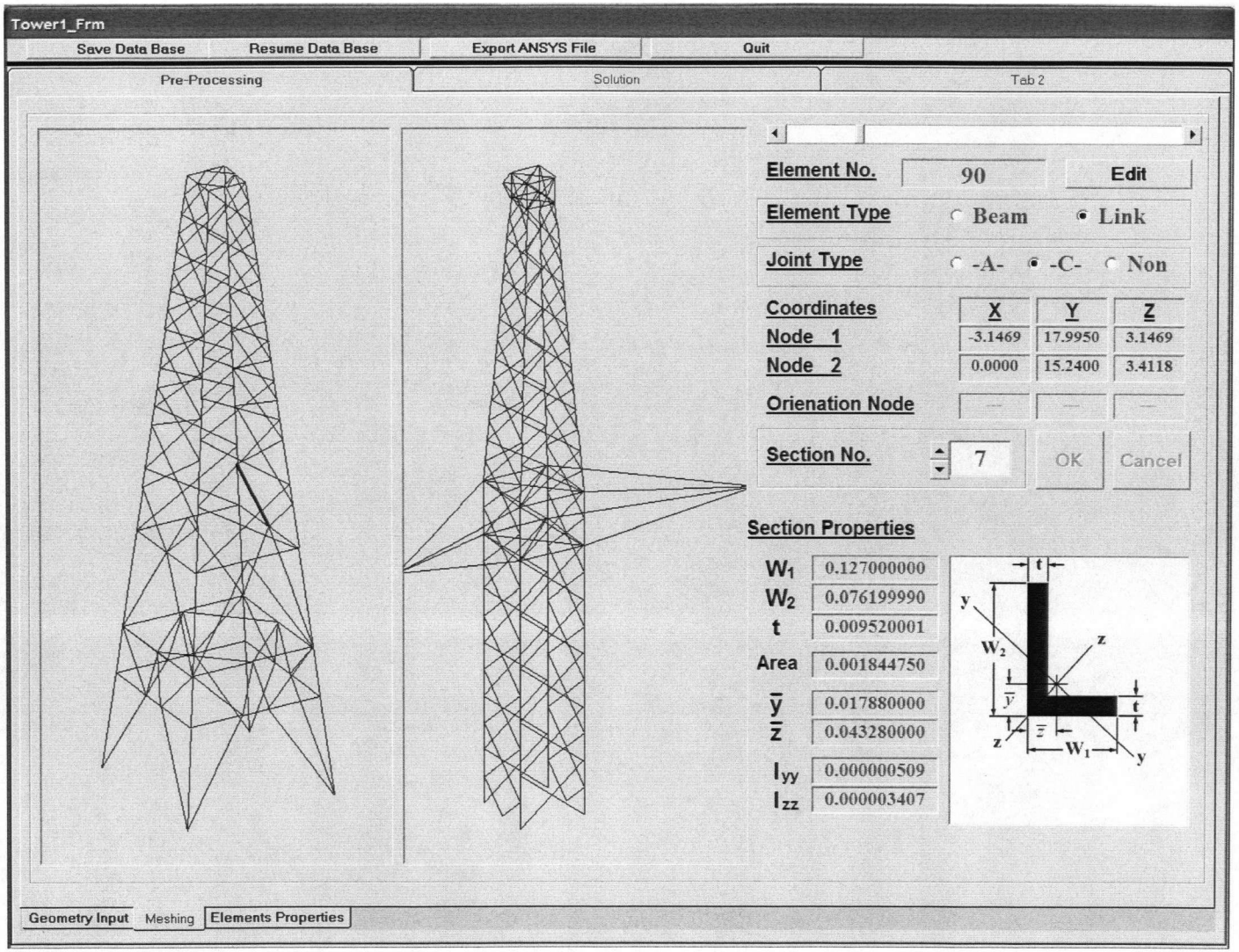

Figure 3.6: "Meshing" tab contents in the pre-processing phase.

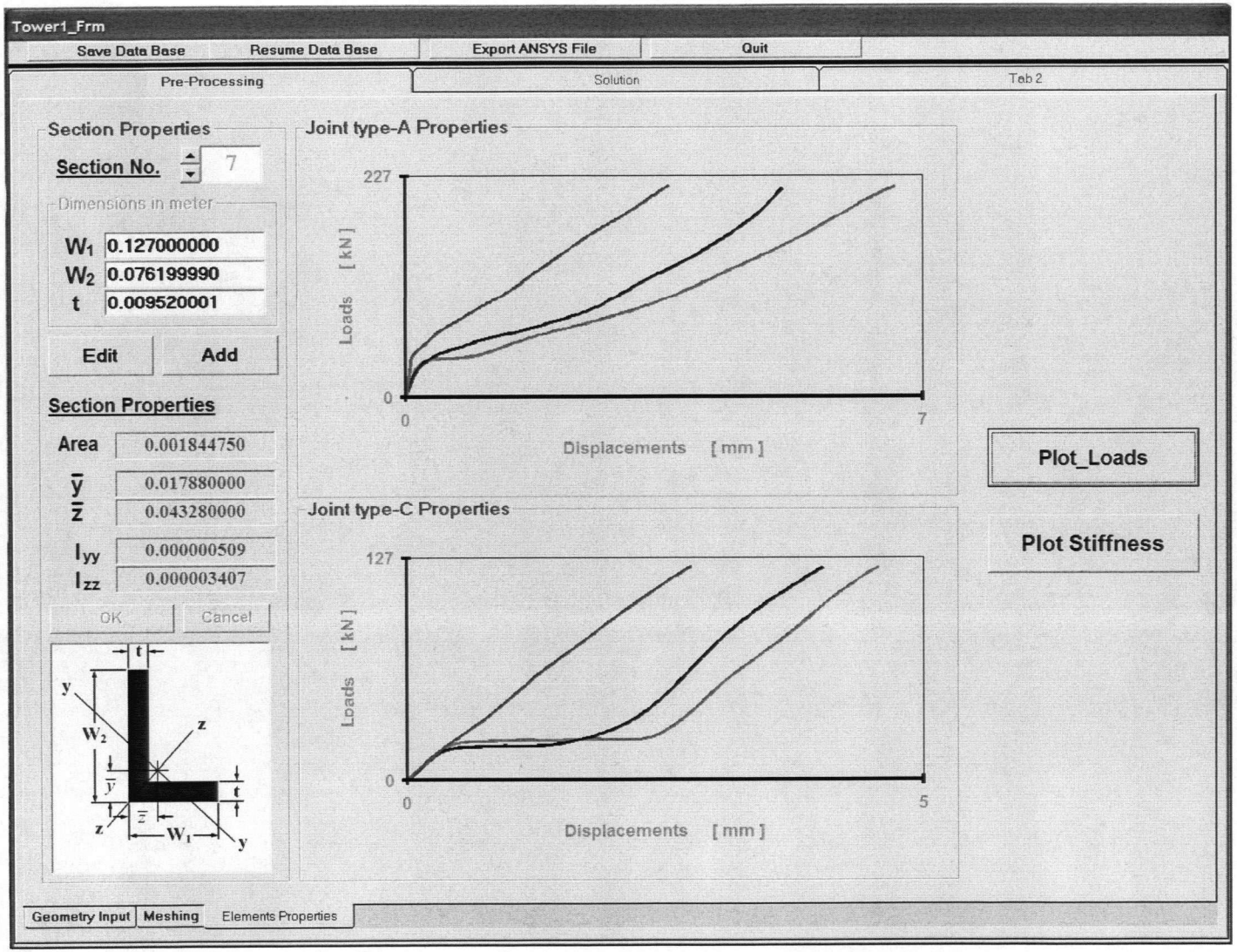

Figure 3.7: "Elements Properties" tab contents in the pre-processing phase.

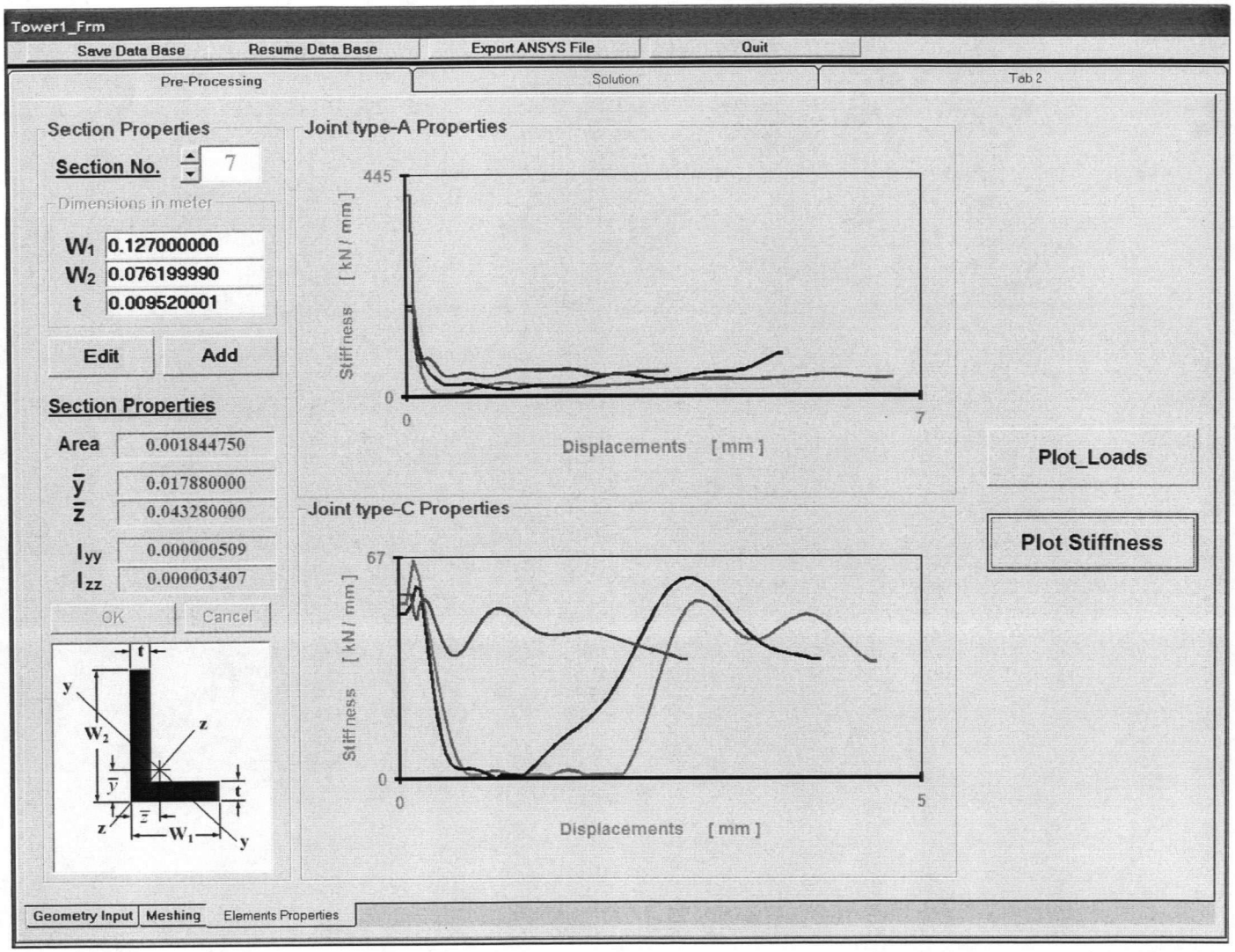

Figure 3.8: "Elements Properties" tab contents in the pre-processing phase.

3.3.2 The Solution Phase

The solution phase defines the number of load steps, boundary conditions for each load step, convergence tolerance, number of iterations, and number of sub-load steps for each load step. These data are fed to the interface program through two tabs; loads and boundary conditions, and solution parameters. A user can select any of these tabs by clicking the tab title, Figure 3.9.

In the first tab; "Loads and Boundary Conditions", the relevant nodes are shown with labels for the directions of the coordinate axes. The nodes of the four tower legs are labeled L_1, L_2, L_3 and L_4. These nodes have displacement boundary conditions in all load steps. The nodes corresponding to the cable connection points are labeled P_1, P_2 and P_3. The program starts with default values for the "Loads and Boundary Conditions" tab, however, it allows a user to change any of these values by clicking the "Edit" button. A user browses the available boundary conditions by using the load step number scroll bar. Then a user can change the forces or displacement boundary conditions for designated load step. After finishing the editing of the boundary conditions, a user saves the new data by clicking "OK" button.

In the second tab; "Solution Parameters", see Figure 3.10, a user defines the nonlinear analysis parameters. These parameters are the convergence tolerance, maximum number of iterations, and number of sub-steps for each load step. Also, a user specifies which load step should be active or inactive. After defining the solution parameters, the finite element analysis is performed by clicking "SOLVE" button.

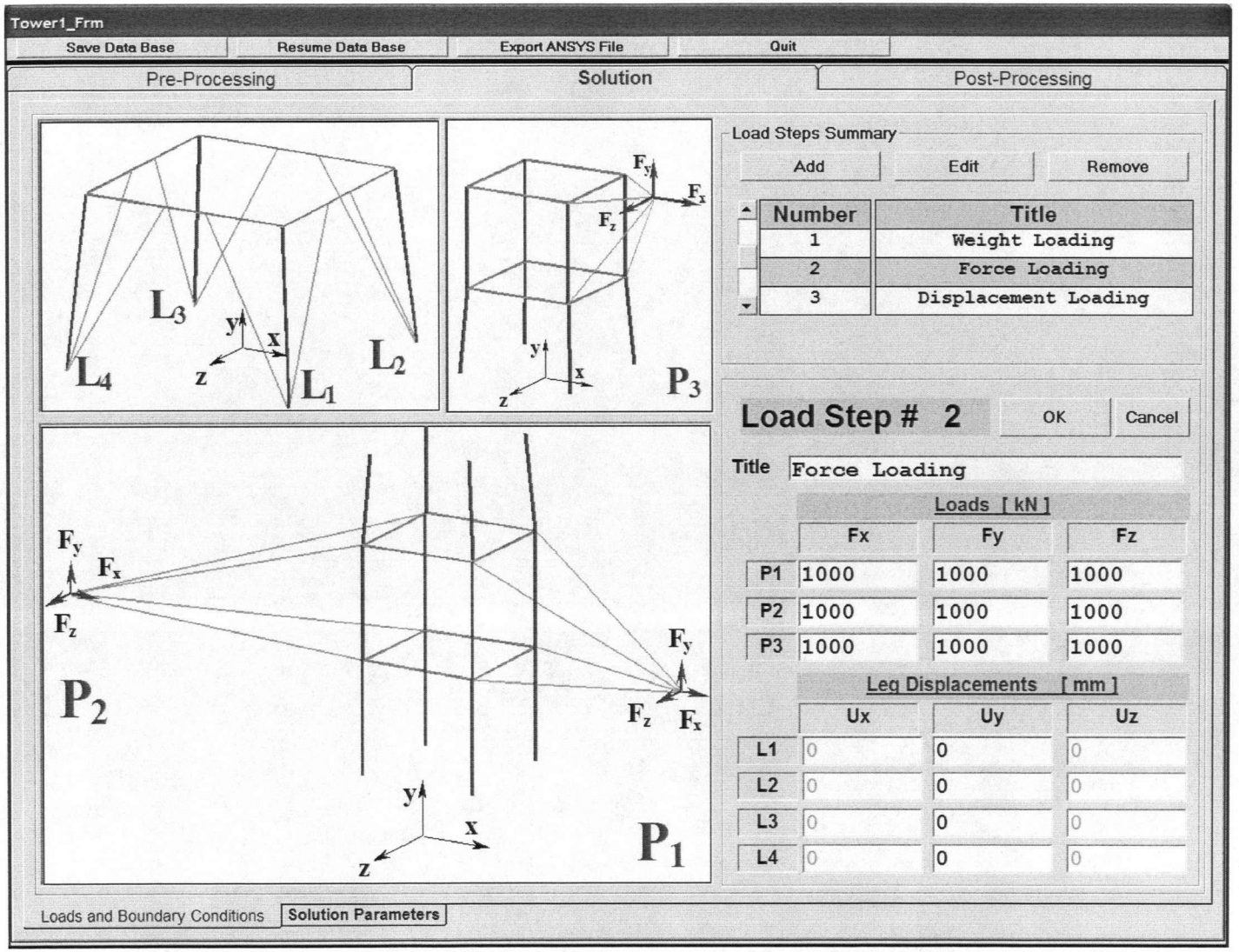

Figure 3.9: "Loads and Boundary Conditions" tab contents in the Solution phase.

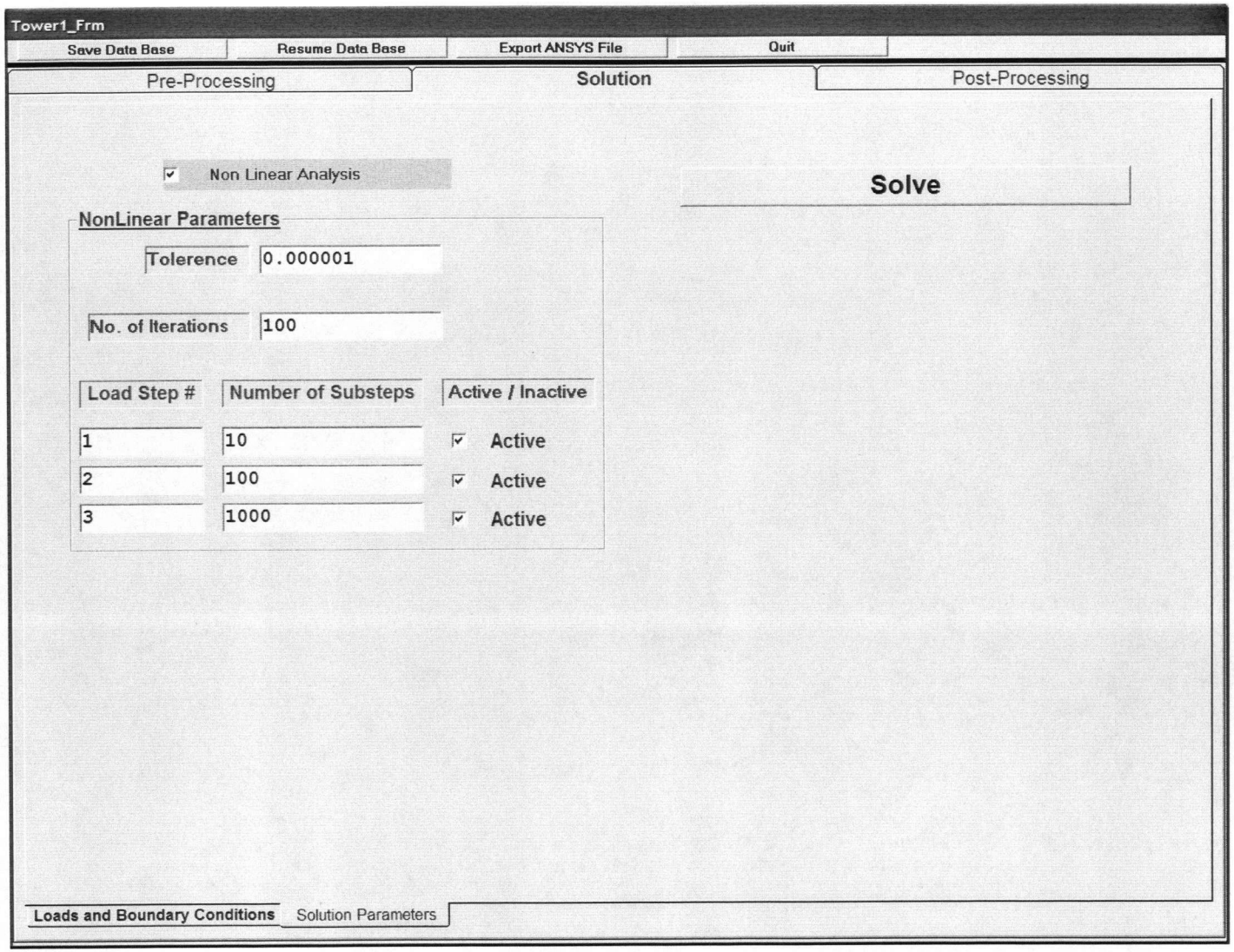

Figure 3.10: "Solution Properties" tab contents in the Solution phase.

3.3.3 The Post-Processing Phase

The post-processing phase is the final stage of the transmission tower analysis. This phase has only one tab which starts with isometric views of the tower members, a scroll bar for browsing the tower members, element type and joint type information boxes, and "Read Results" button, see Figure 3.11. After the finite element solution is completed, a user clicks on the read results button to start the post-processing phase. Also after each new analysis, a user should click on the read results button to re-read the results file and refresh the results data. If the results file is not available or the solution could not reach a converged solution, a warning message pops up with the message "Results file is not available", see Figure 3.12.

If a results file is available, a frame appears showing the axial loads, axial displacements and stresses of the first element. The results for other elements can be displayed by using the scroll bar, see Figure 3.13. The post-processing screen allows the display of results for all sub steps and load steps. A user can change the load step or sub step results by using the "Load Step No." and the "Sub-Step No" buttons. For each element, the element type, its joint type (if any), nodal displacements, axial force, axial stress, ratio between the axial stress and the member yield stress, ratio between the axial load and the Euler buckling load and axial displacement are displayed by the post-processor. If an element contains joint effects, the post-processing phase presents the amount of slippage displacement and the ratio between the axial load and the joint yield load.

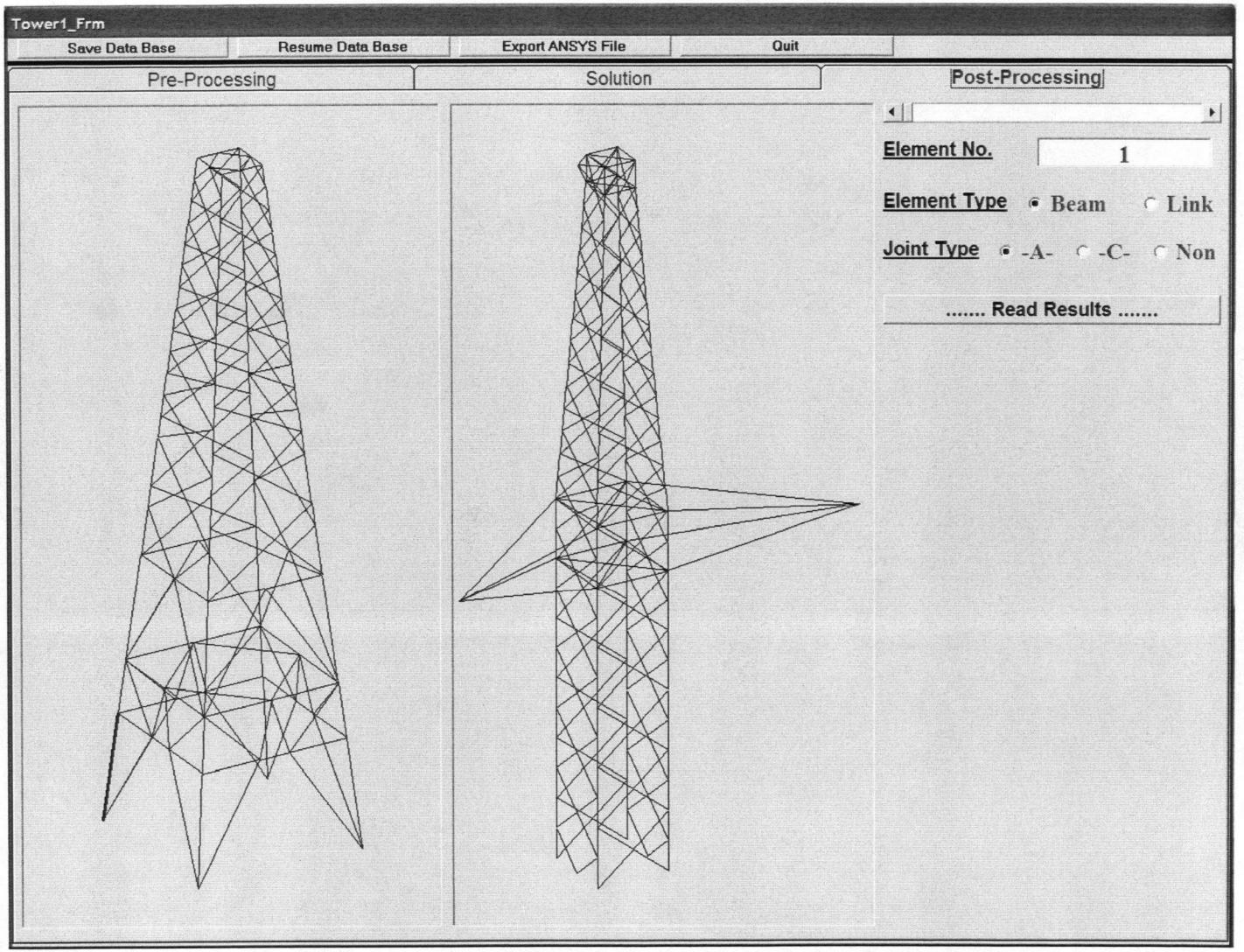

Figure 3.11: Post-Processing phase showing tower geometry.

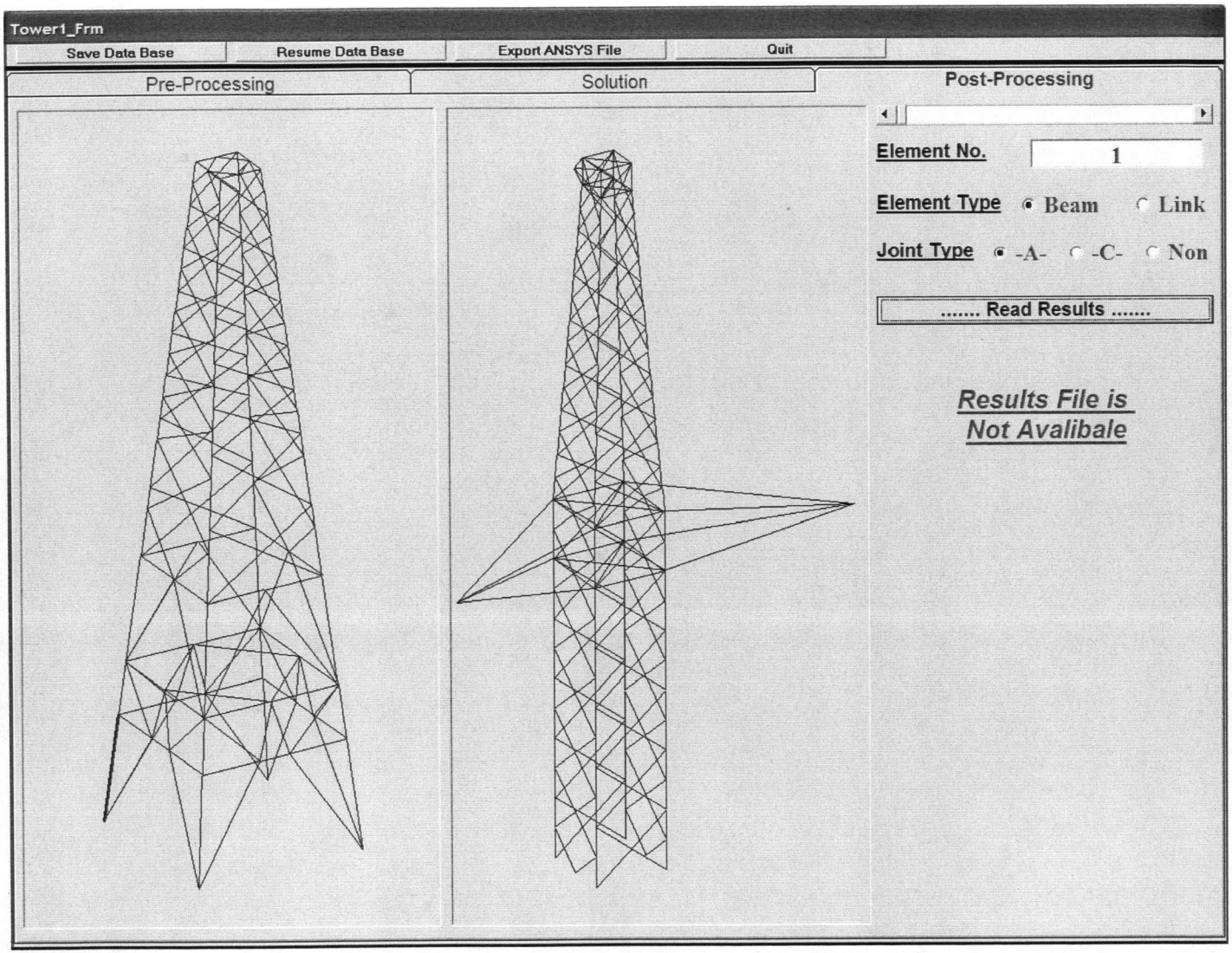

Figure 3.12: Post-Processor display if result file is not available.

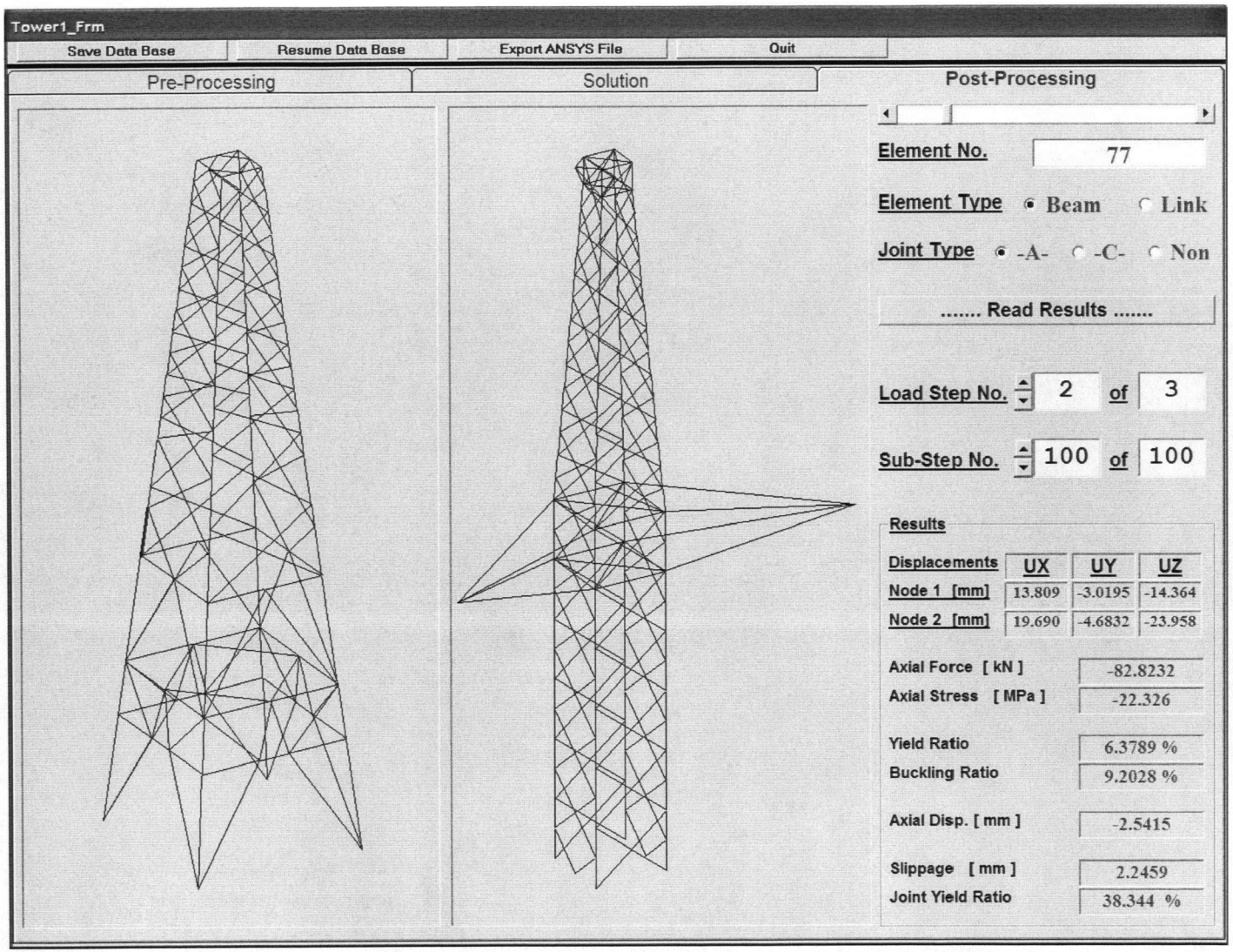

Figure 3.13: Post-Processor display showing the results for element 77 at load step number 2 and last sub-step.

Chapter 4

TRANSMISSION TOWER ANALYSIS

4.1 General

This chapter presents the numerical results from the FE program developed in this study. The FE program is first verified by using ANSYS and results reported by other researchers. Thereafter a 2-D structure is analyzed to study the influence of different joint types on the behavior of a structure. The behavior of a full-scale tower under different frost heave conditions is also analyzed by using the FE program and a discussion of the results is presented.

4.2 FE Program Verification

Several simple structures are analyzed in this section to establish the accuracy of the FE code. The code is first compared by considering the results for a simple cantilever beam obtained from the ANSYS program. Thereafter, the code is further verified by comparing with the studies done by Kitipornchai, et al (1994) and Kroeker (2000) that account for joint slippage.

4.2.1 Simple Cantilever

A 3-D cantilever beam, 1.0 m long and 12x12 mm cross-section, is analyzed by using the FE code (Figure 4.1). The beam is loaded with an axial load F_x and two lateral loads F_y and F_z each equal to (0.01 F_x). The magnitude of F_x is varied from zero to 400N. Geometric nonlinearity is assumed in the analysis. The analysis is carried out by dividing the load into 100 steps. Three different models are analyzed; the first with one finite element, second with four finite elements

and third with fifty finite elements. The results for different finite element models are shown in Figures 4.2, 4.3 and 4.4. The current FE code and ANSYS give almost identical deflections for the 4 and 50 element models. The results for the one-element model show that the current code gives results more closer to the 4- and 50- element models when compared to the corresponding results from ANSYS. It should be noted that the FE code developed in this study updates the geometry, geometric stiffness, and transformation matrix at each iteration whereas ANSYS performs these updates only at the beginning of each load step. Several other cases involving 2-D and 3-D trusses and frames were analyzed by using the current FE code and ANSYS, and the results were almost identical.

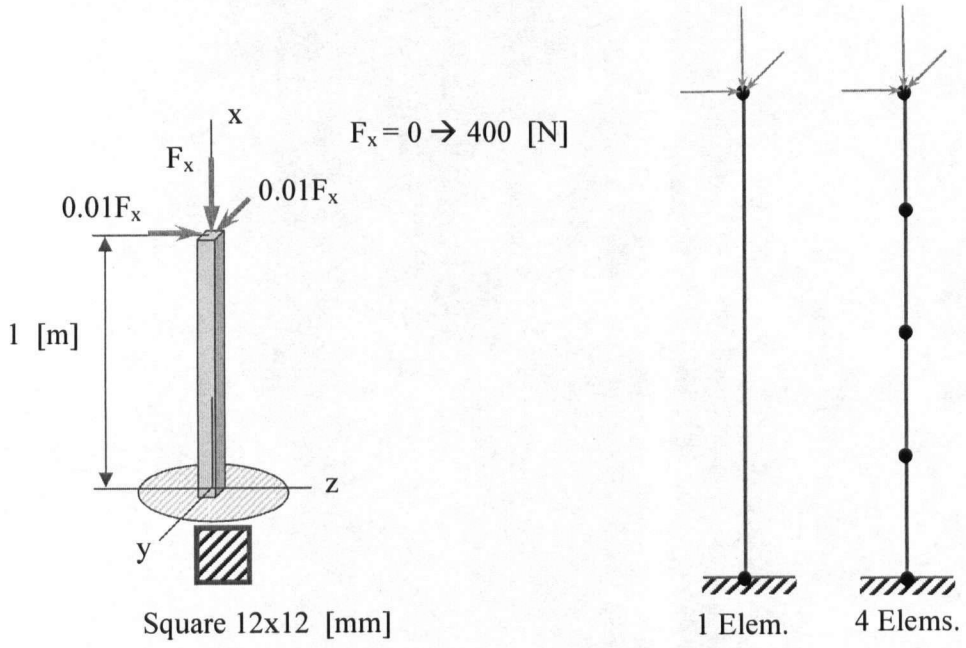

Figure 4.1: 3-D beam model used in FE code verification.

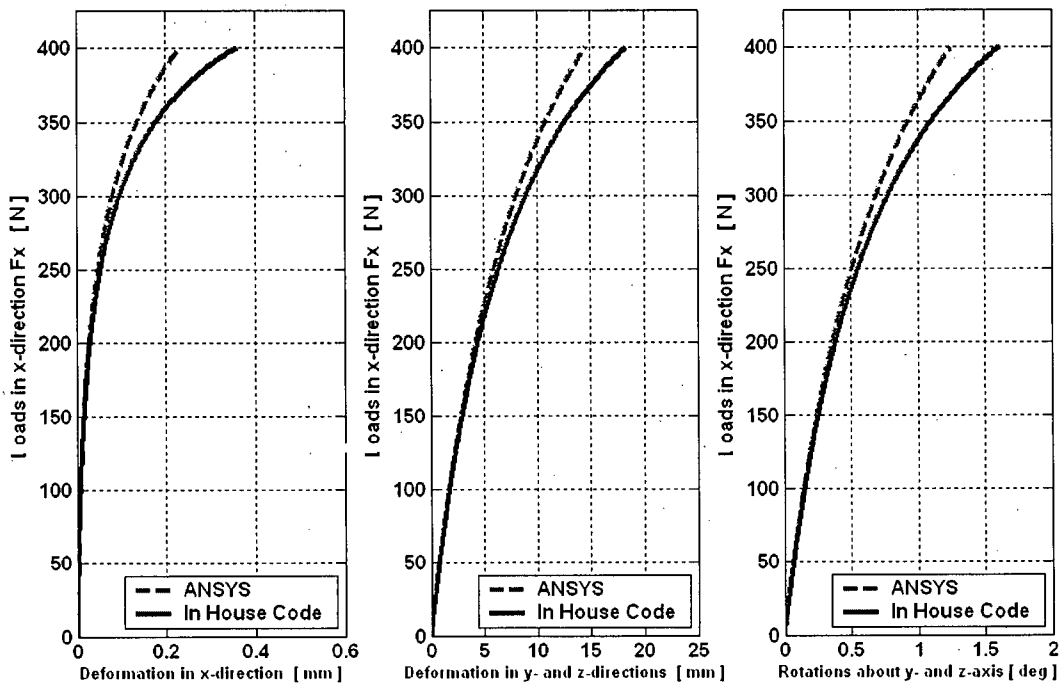

Figure 4.2: Comparison of deformations obtained from ANSYS and the current FE code for one-element model.

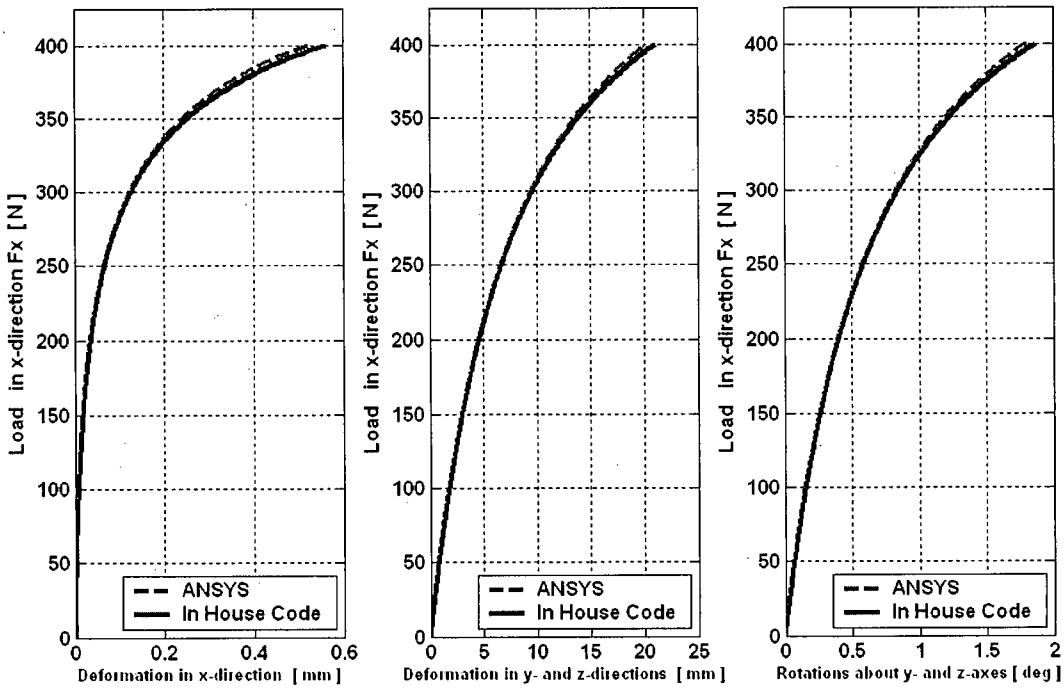

Figure 4.3: Comparison of deformations obtained from ANSYS and the current FE code for four-element model.

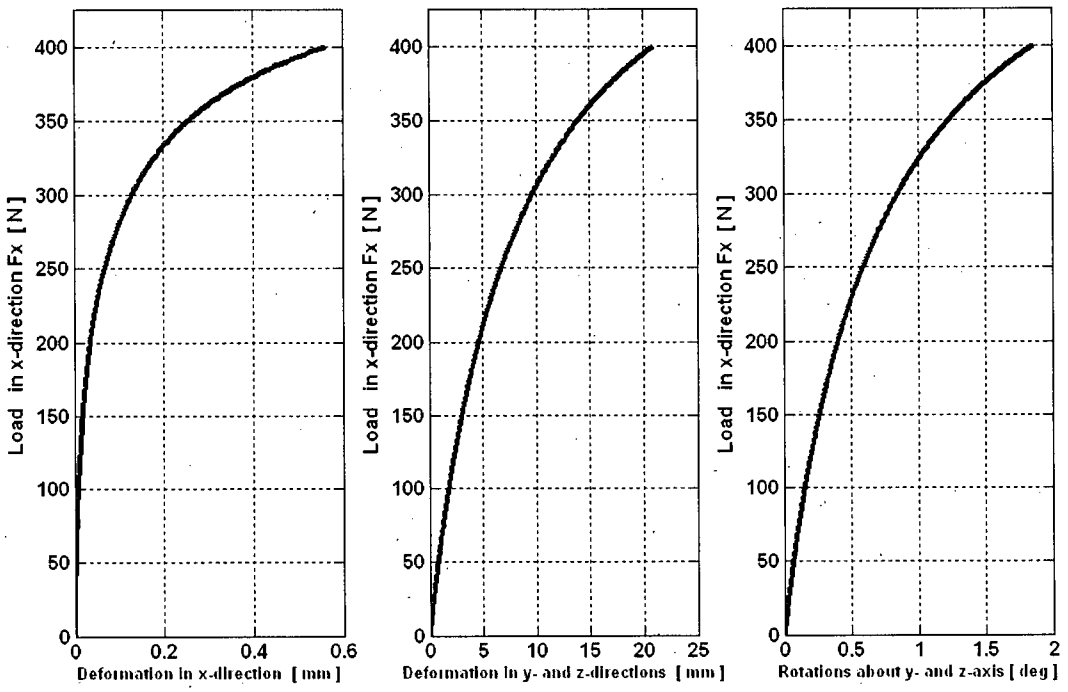

Figure 4.4: Comparison of deformations obtained from ANSYS and the current FE code for 50-element model.

4.2.2 Double Diagonal Plane Truss

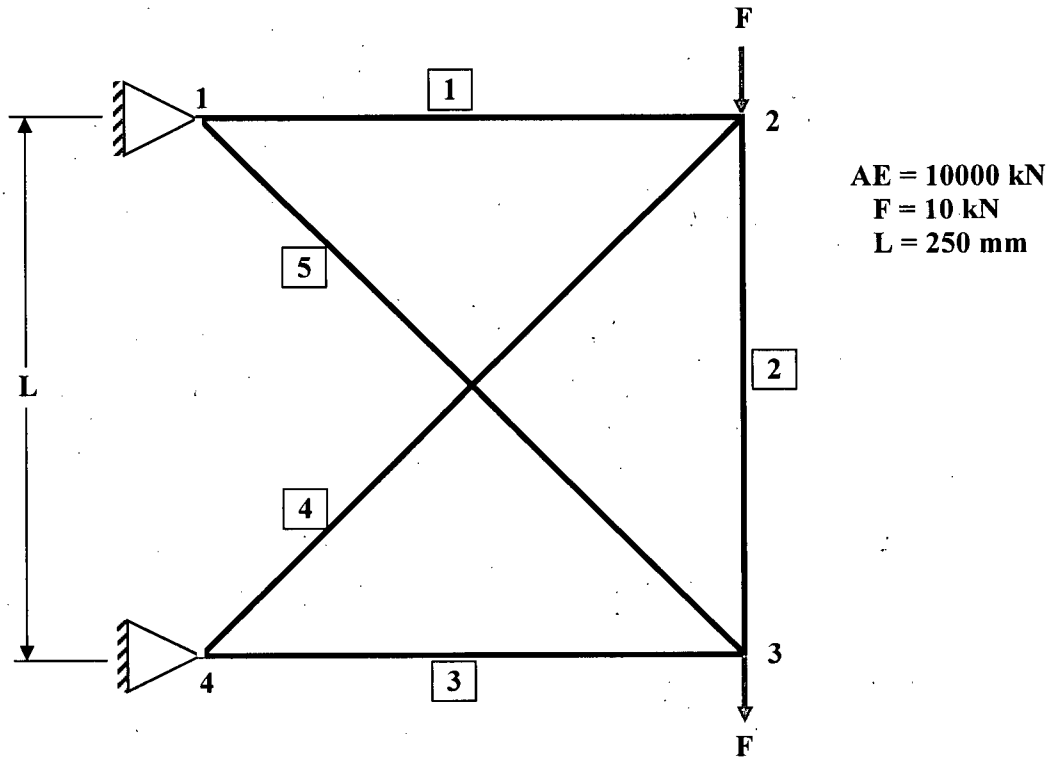

Figure 4.5: Double-diagonal plane truss.

A double diagonal plane truss, (Figure 4.5) was investigated by Kitipornchai, et al (1994) and Kroeker (2000) in their investigations of bolted joint slippage. The same truss is analyzed here to verify the FE code for a case without slippage and to compare the current slippage model, based on experiments, with the idealized slippage models used by Kitipornchai, et al (1994) and Kroeker (2000). The dimensions and material properties of the truss members are shown in Figure 4.5. The diagonal members of the truss i.e., (elements 4 and 5), are assumed to have beam-to-column joints with one bolt at the ends of each element. The stiffness of this joint is extracted from the idealized slippage curves obtained by Ungkurapinan (2000), (Figure 2.8 in

Chapter 2). Thereafter the equivalent stiffness of a diagonal element considering the effect of the two joints at its ends is calculated as;

$$K_C = K_{J_C}\left(\frac{EA}{L}\right)\Big/\left[K_{J_C} + 2\left(\frac{EA}{L}\right)\right] \tag{4-1}$$

The above value of K_C is used in equation 2-23 of Chapter 2, for elements 4 and 5 in the FE analysis. Note that the cross sectional area of the truss elements is very small, A=0.00004762 m^2, when compared to the cross sectional area of the joint members used by Ungkurapinan (2000).

Table 4-1 shows that the vertical deflection of the node 2 of the truss without considering the joint slippage is exactly same as that obtained by Kitipornchai, et al (1994) and Kroeker (2000). The deflection of node 2 is slightly greater when the joint slippage is considered for the compression diagonal rather than the tension diagonal. This behavior is similar to the results obtained by Kroeker (2000). Note that the results reported by Kitipornchai et al (1994) and Kroeker (2000) are for a continuous slippage model. Table 4-1, also shows the deflection of node 2 when joint slippage is considered at the diagonal member joints and at all joints of the truss. It is evident that as more joints are allowed to slip the deformation of node 2 increases substantially.

Table 4-1: Comparison of deflection of Node 2 (F=3.145 kN).

	Vertical Deflection of Node 2 (mm)				
	No Joint	**Slippage in**			
		Tension Diagonal member joint	**Compression Diagonal member joint**	**Both Diagonal member joints**	**All Joints**
Kitipornchai, et al (1994)	0.301	0.339	0.328	-	-
Kroeker (2000)	0.301	0.328	0.335	-	-
Current Model	0.301	0.422	0.454	0.758	0.955

4.2.3 Simple Transmission Tower

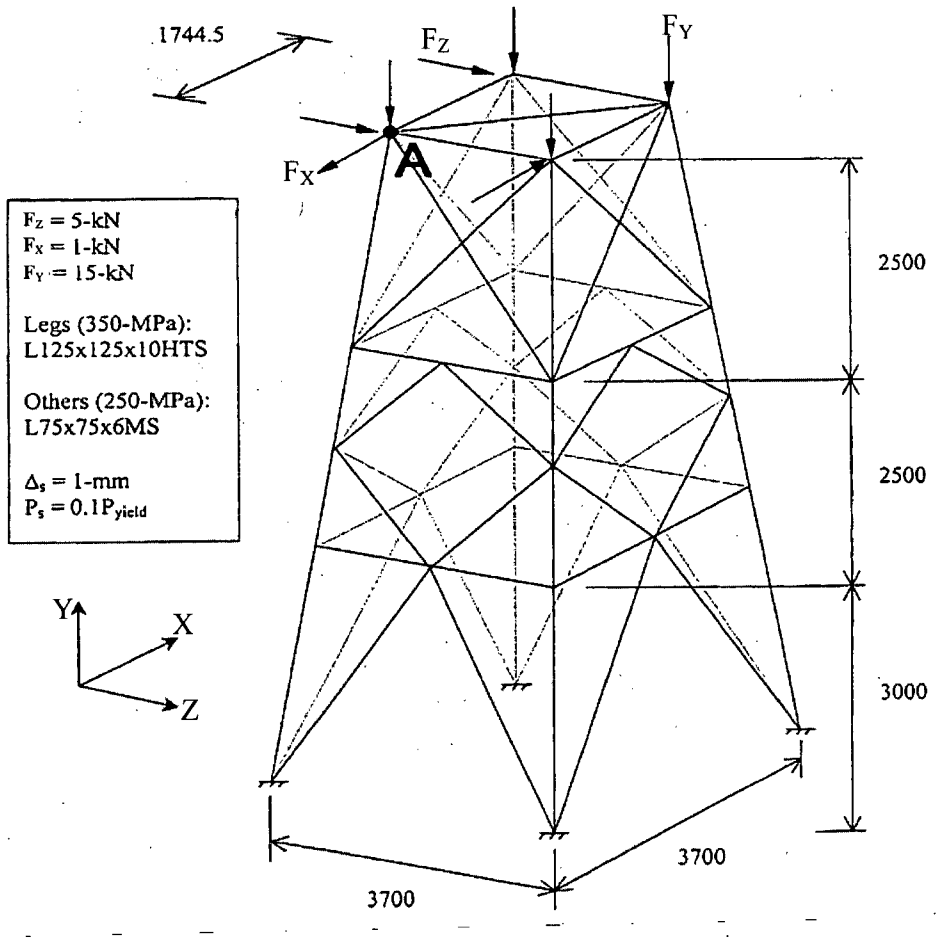

Figure 4.6: Simple transmission tower model.

A simple transmission tower with joint slippage (Figure 4.6) was analyzed by Kitipornchai, et al (1994) and Kroeker (2000). The tower member dimensions and material properties are shown in Figure 4.6. The tower legs as well as the horizontal bracings are modeled as beam elements. The cross bracings are assumed to have beam-to-column joint elements with one bolt at the ends of each element. The stiffness of this joint is extracted from the idealized curves obtained by

Ungkurapinan (2000) (see Figure 2.8 in Chapter 2). As in the previous example Equation (4-1) is used and column-to-column joints are not considered.

Table 4-2 shows that results from the current code agree very closely with the results reported in the literature for a structure without joint slippage. The results reported by Kitipornchai, et al (1994) and Kroeker (2000) are for the continuous slippage model only. It should be noted that the current slippage model allows joint to deflect more than 5 mm (Figure 2.8, Chapter 2), while the pervious models restrict the joint deflection to 1 mm. As a result, the deflection from the present analysis is higher for the cases involving joint slippage.

Table 4-2: Comparison of transverse deflection (U_Z) of point A
for (F_Z, F_Y, F_X) = 27.9 * (5, 15, 1) kN

	Deflection in (mm)	
	No Joint	**Beam-to-Column Joints**
Kitipornchai, et al (1994)	15.76	18.51
Kroeker (2000)	14.54	15.48
Current Model	14.43	41.61

The above comparisons show that the FE code developed in this study is accurate for non-linear structural analysis without joint slippage. However, due to the difference between the current slippage model based on experiments and the idealized slippage models proposed by Kitipornchai et al (1994) and Kroeker (2000), the current FE code results did not agree with previous results for structures with joint slippage. The main differences between the present and the past models are the maximum joint deflection and joint yield load limit. The previous studies restricted the joint deflection to 1 mm and ignored the joint yield limit. The current model considers the joint yield limit in defining the ultimate behavior of a structure and adopts the deflection of a joint according to the experimental results of Ungkurapinan (2000).

4.3 Effect of Slippage on the Response of Towers

4.3.1 2-D Tower Case

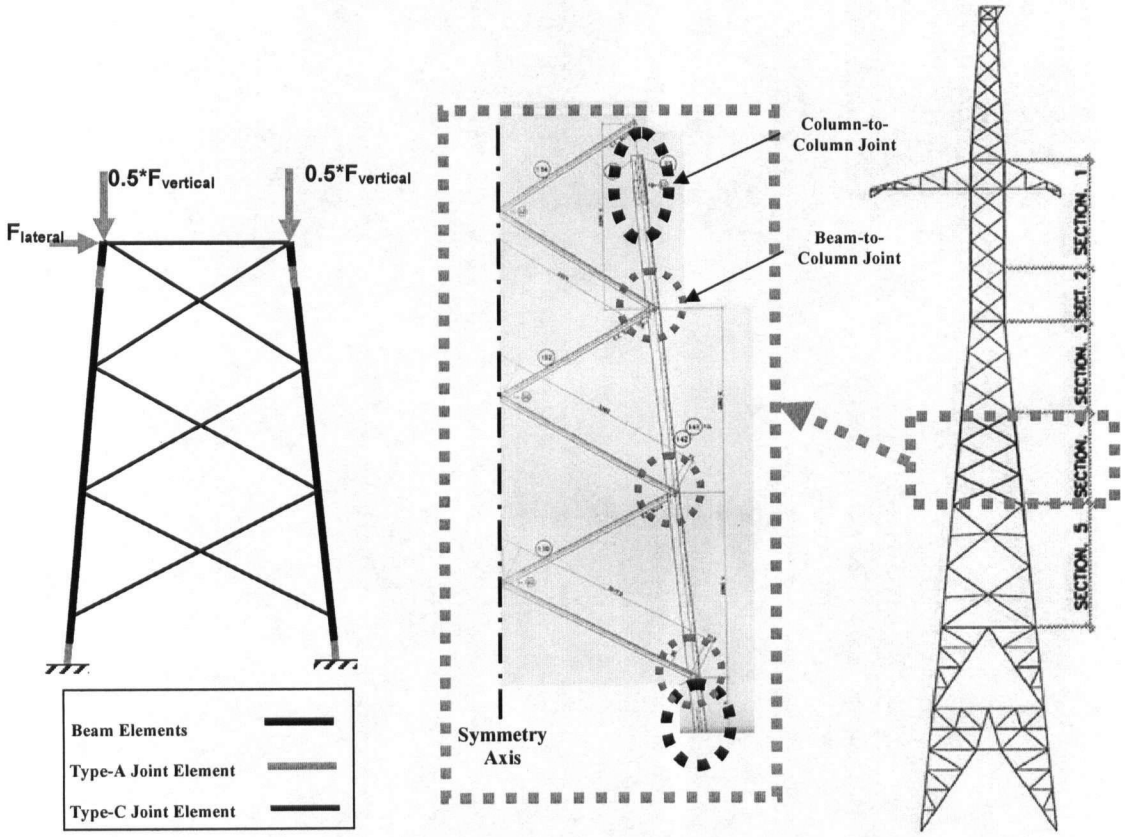

Figure 4.7: Finite element model of the transmission tower substructure.

Figure 4.7 shows a sub-assembly of a typical transmission tower used by Manitoba Hydro for the Radisson-Dorsey HVDC transmission line. This subassembly is first idealized as a 2-D structure to investigate the effect of joint nonlinearity on the load carrying capacity of the tower. Three different models are considered; first one with fully rigid joints, second one with one type of joints being nonlinear and third with both types of joints being nonlinear. Figure 4.7 shows

the finite element model with the locations and types of joints used in this subassembly. Type-A joints, column-to-column joints, are used to connect the subassembly with the rest of the tower whereas type-C joints, beam-to-column joints, are used to connect the braces and horizontal members to the main columns. The subassembly has six braces and two horizontal members. In the all-rigid joints case, these braces and horizontal members are modeled as truss elements whereas the rest of the structural members are modeled as beam elements. In the nonlinear joint models, the truss elements are replaced by equivalent link elements that represent the brace elements with two type-C joints at their ends. The gage size of the substructure members is equal to the gage size of the tested joints of Ungkurupinan (2000) which is an angle section of 4x4x0.25 inches.

The subassembly is studied with three load cases. The first load case has a lateral load that is one sixth of the vertical load [similar to a case used by Kitipornchai et al. (1994)]. In the other two load cases, the lateral load is set to one half and one twentieth of the vertical load (Figure 4.7). In all load cases and joint types, the analyses are carried out until a maximum vertical load of 1200 N is reached or until the onset of yielding (which ever occurs first).

The results of the above loading cases are summarized in Figures 4.8 and 4.9. Figure 4.8 shows that for the first load case, when the slippage of type-A joint is ignored, the slippage in the type-C joints has transferred more loads to the columns resulted in slightly decreasing the load carrying capacity. Although, the yield limit of type-C joints is very small compared to that of the column material, see (Table 4-3), the structure has failed due to yielding of the columns rather than due to yielding of the type-C joints. Figure 4.8 also shows that type-A joints has yielded at a load level less than half of the full loading capacity which has a significant impact on the load carrying capacity of the structure. It worth noting that slippage of type-A joints has a dominant

effect on the behavior of the structure. Slippage of type-C joints has more impact on the flexibility of the structure than slippage in type-A joints, as can be seen from Figure 4.9.

For the other load cases, Figure 4.8 shows that reducing the ratio of the lateral load to the vertical load decreases the effect of the slippage of the type-C joints. In a similar way, increasing this ratio would significantly decrease the load carrying capacity of the structure. On the other hand, changing the ratio of the lateral load to the vertical load has no or little effect on the behavior of the slippage of the joints.

Table 4-3: Comparison between the yield loads of the structure different members

	Rigid Structure	Column-to-Column joint	Beam-to-Column joint
Yield Load [kN]	425.0	200.0	75.0

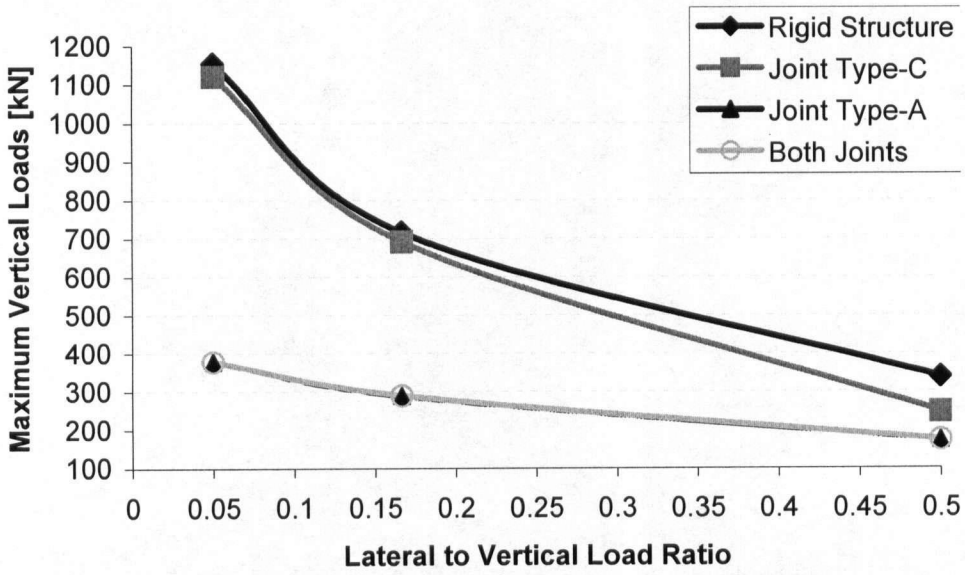

Figure 4.8: Effect of joint slippage on load carrying capacity for various load ratios and joint types.

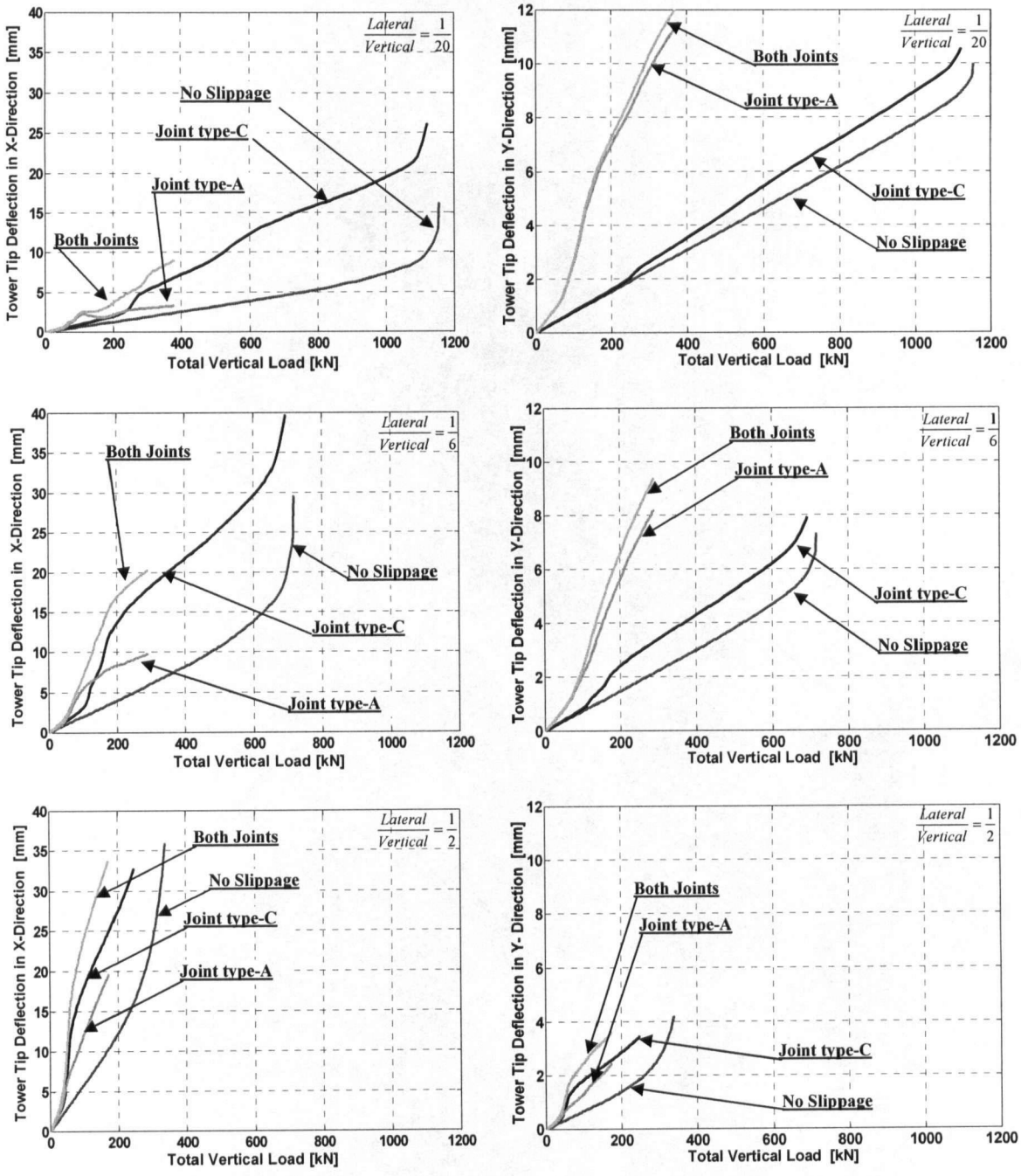

Figure 4.9: Tower tip deflections in x- and y- directions for a tower with different types of joints.

4.3.2 Full-Scale Tower

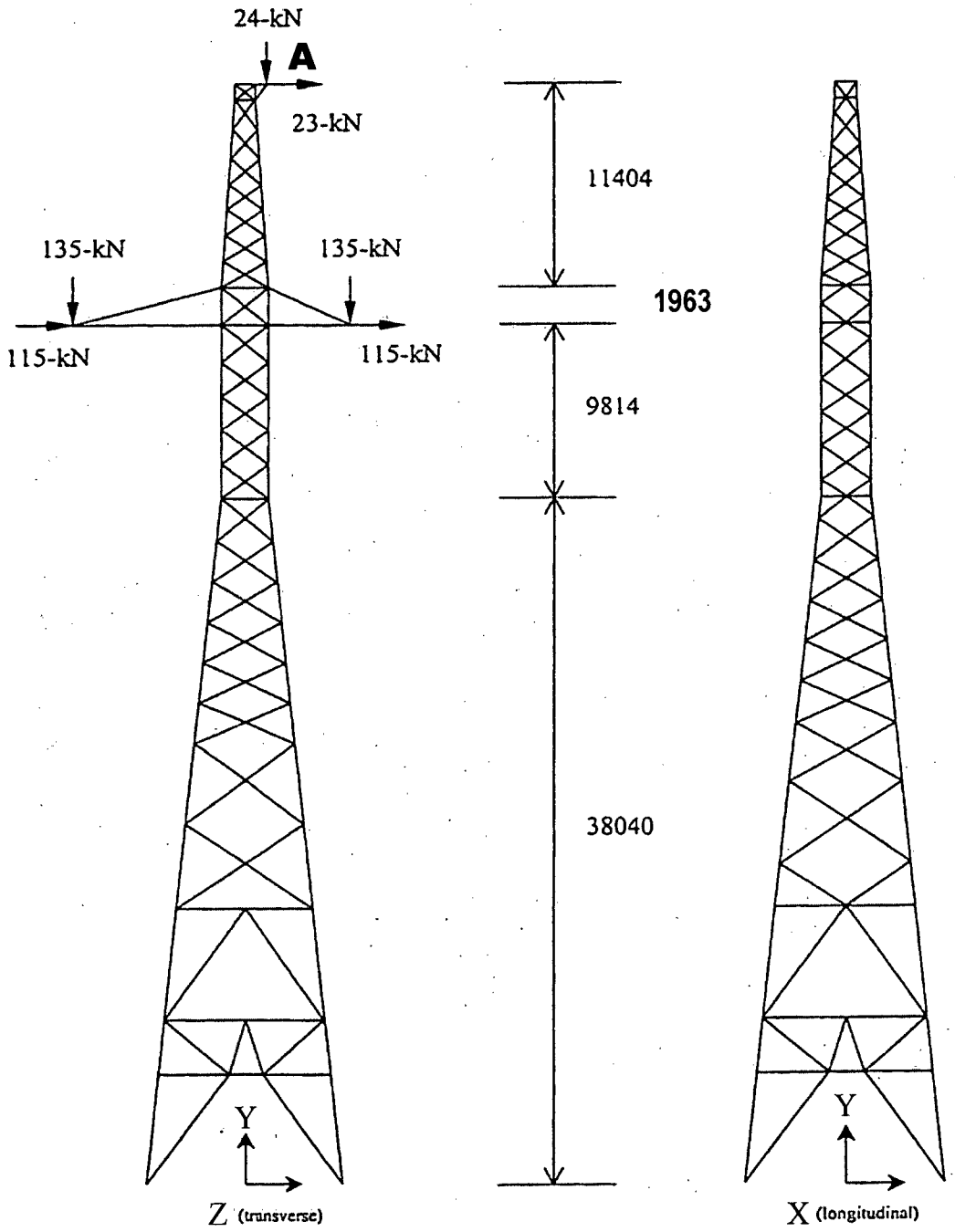

Figure 4.10: Full-scale transmission tower used by Manitoba Hydro.

The full-scale transmission tower shown in Figure 4.10 is part of Manitoba Hydro's Nelson River DC transmission system. The tower has 708 angle members with 16 different angle sizes from L51xL51x4.8 in the upper section of the tower to L152xL152x13 in the bottom section of the tower. These members are primary members supported with secondary members to reduce the un-braced length. The tower is, modeled using 500 elements and 217 nodes (Yue, 1994). The weight of the neglected secondary members is assumed to be 20% of the weight of the reduced tower structure (Yue, 1994).

The tower legs and horizontal bracing members are modeled as beam elements with bending stiffness using Equations 2-12, 2-13, and 2-14. The tower legs elements have a common third node located at the tower center line. The third nodes of the horizontal bracing elements are defined by the intersection of the tower center line and the maximum moment of inertia plane of each element. The cross-bracing members are modeled as truss elements without bending stiffness. The loading case shown in Figure 4.10, is one of the extreme load cases considered by Kroeker (2000).

Table 4-4 shows that, the deflection of node A (Figure 4.10) of the tower without considering the joint stiffness agrees closely with the results obtained by Kroeker (2000) under the tower self weight and external loading shown in Figure 4.10. Note that the height of the tower tip in the current model is 61.221 m, which is taken from Manitoba Hydro's drawings, while it was 61.392 m in Kroeker's model. This probably and the consideration of geometric stiffness in the analysis are the reasons for the minor difference between the results.

Table 4-4: Comparison of tower deflections (U_X, U_Y, and U_Z) at point A

	U_X (mm)	**U_Y (mm)**	**U_Z (mm)**
Kroeker (2000)	-0.00	-29.972	531.56
Current Model	0.20577E-14	-33.597	517.29

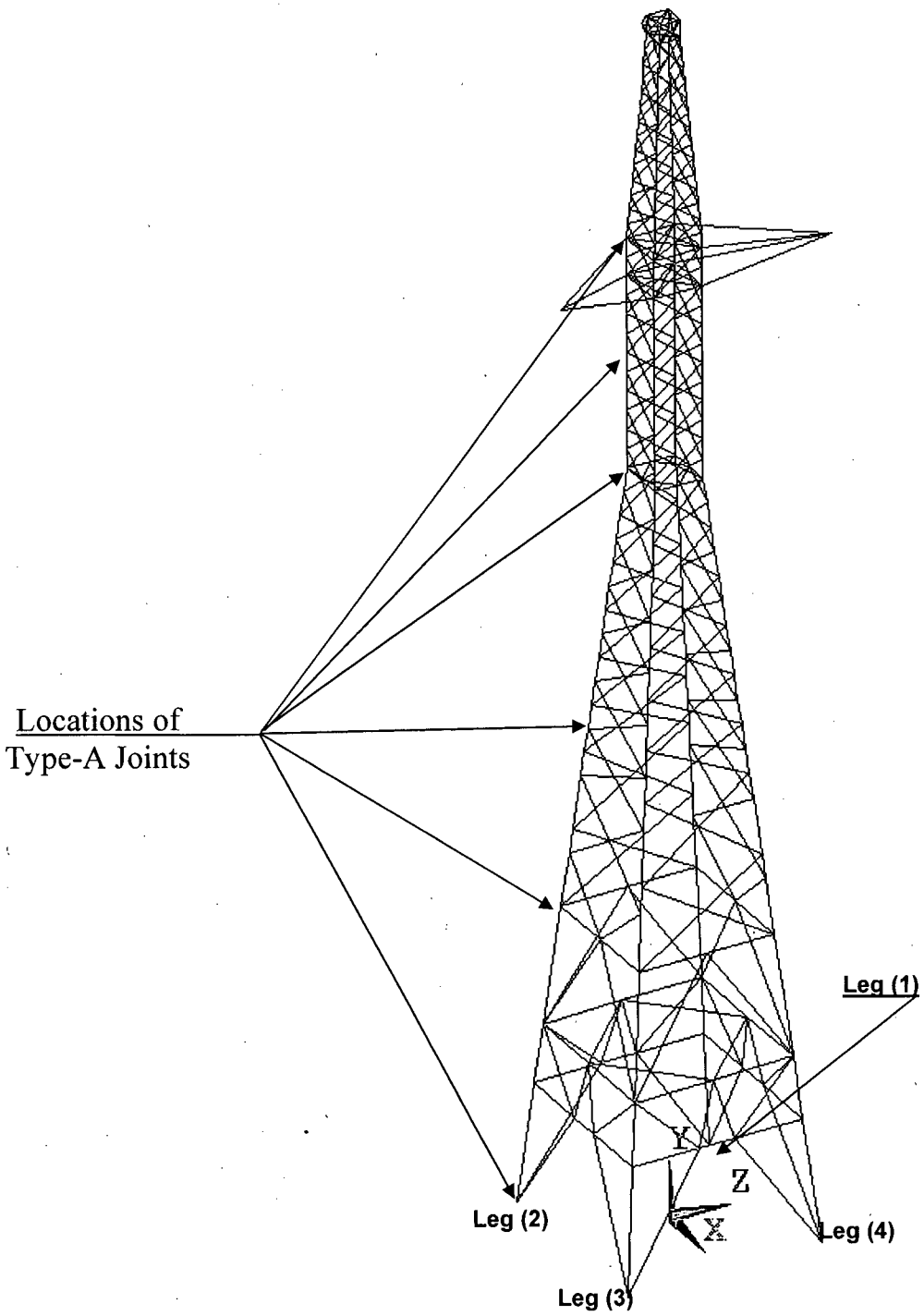

Figure 4.11: Finite element model of full-scale tower with the six locations of the type-A joints.

Figure 4.11 shows the finite element model of the full-scale transmission tower showing the locations of the column-to-column joints and the numbering of the tower legs. Note that beam-to-column joints are used at all cross bracings. The effects of column-to-column and beam-to-column joints stiffness on the response of the tower is investigated through several loading cases. The first case is for the tower under its self weight and working loads shown in Figure 4.10. The axial loads of column and beam elements at a particular height from the tower base are normalized with respect to their yield loads and the maximum absolute axial load of this group is identified. These normalized maximum axial loads at particular height are then plotted against the normalized height from the tower base for column and beam elements. Figure 4-12 shows the normalized axial loads of leg members if the joint slippage is ignored. Consideration of joint slippage in the analysis results in slightly higher axial loads in the tower legs as shown in Figure 4-13. The results for beam elements are shown in Figures 4.14 and 4.15. It is evident that the maximum axial loads in beam members are generally smaller than that in column members and a majority of beam elements have axial loads less than 30% of the yield loads.

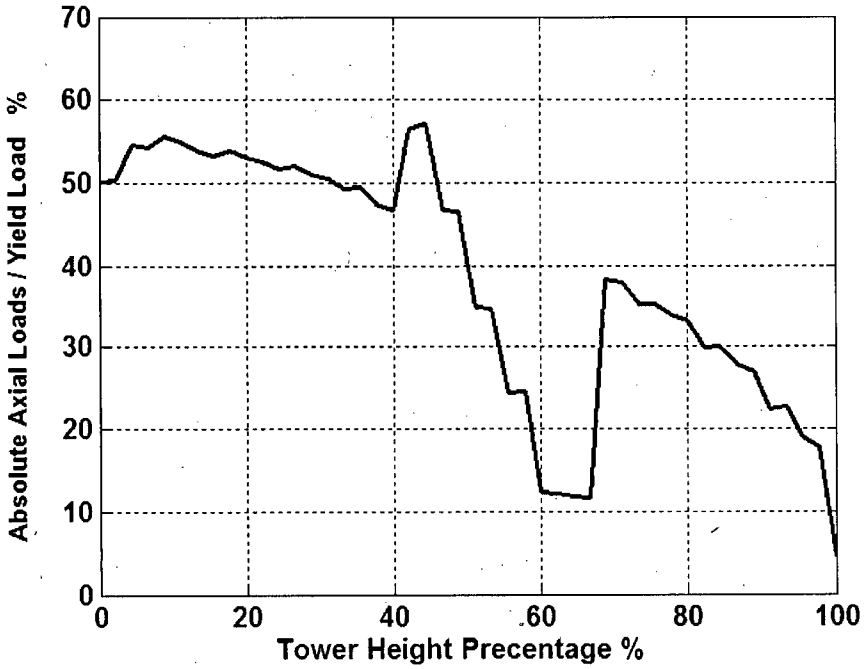

Figure 4.12: Normalized axial loads of tower columns under self weight and working loads without joint slippage.

Figure 4.13: Normalized axial loads of tower columns under self weight and working loads with joint slippage.

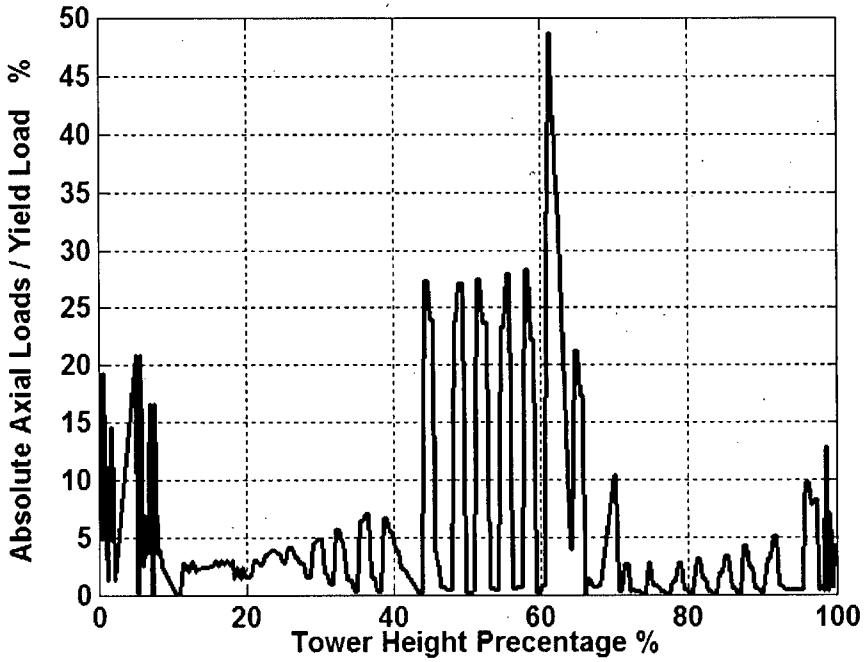

Figure 4.14: Normalized axial loads of tower beams under self weight and working loads without joint slippage.

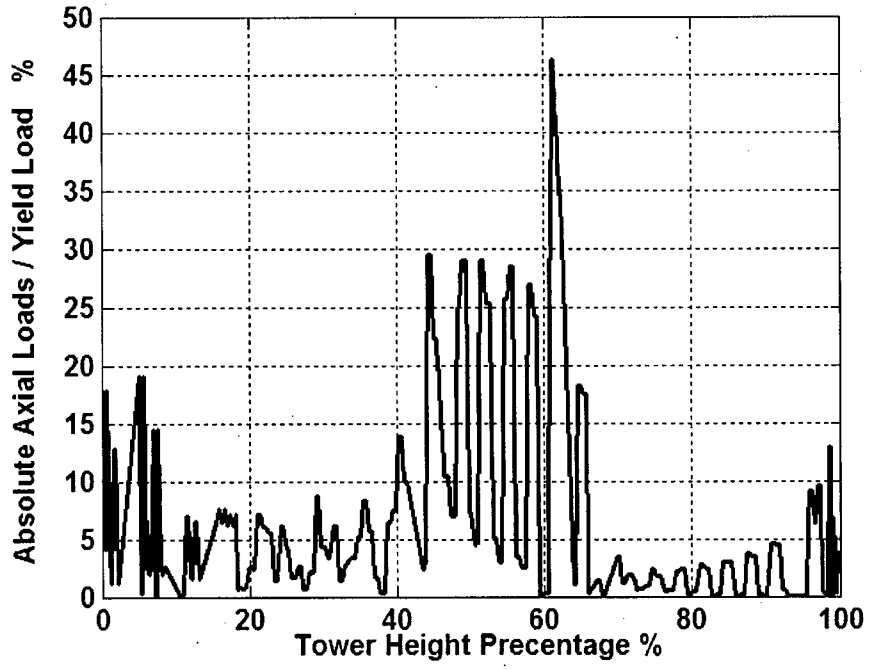

Figure 4.15: Normalized axial loads of tower beams under self weight and working loads with joint slippage.

Figure 4-16 and Figure 4-17 show the estimated normalized axial loads in the tower elements due to a frost-heave induced displacement of Leg #2 by 100 mm, without joint slippage. Ignoring joint slippage in the analysis, results in a significant increase in the member axial loads tending to failure of some members. Including the joint slippage in the analysis, however, results in only 27% increase in the axial loads. This confirms that in a real tower substructure, force redistribution takes place as a result of joint slippage when subjected to frost heave displacements at the base.

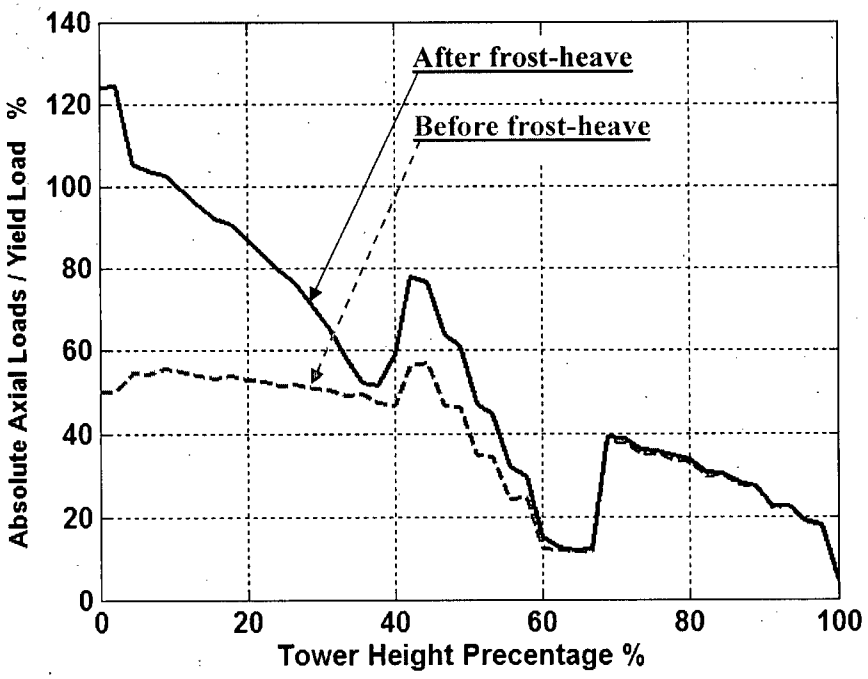

Figure 4.16: Increase of normalized axial load of tower columns due to a frost-heave displacement of 100 mm (without joint slippage).

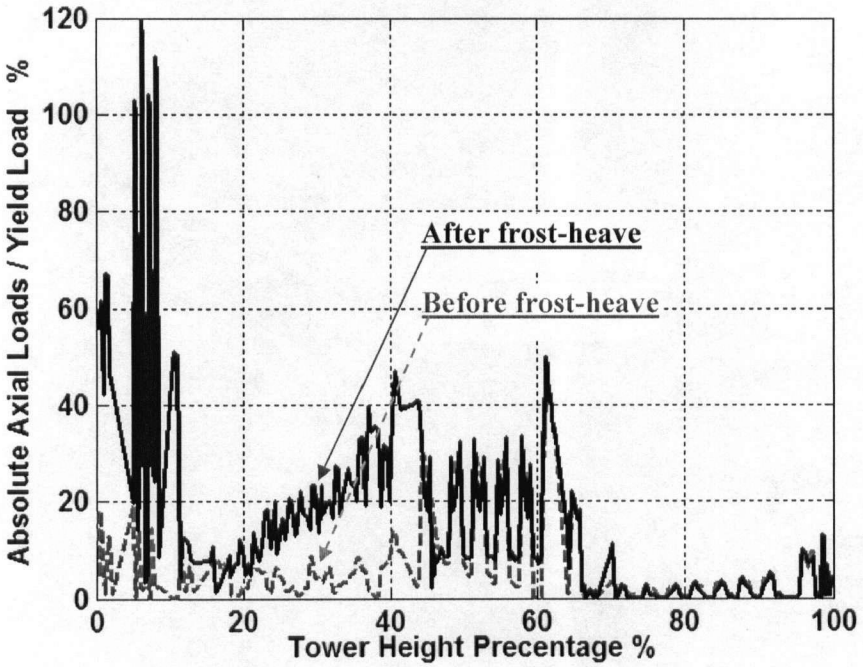

Figure 4.17: Increase of normalized axial load of tower beams due to a frost-heave displacement of 100 mm (without joint slippage).

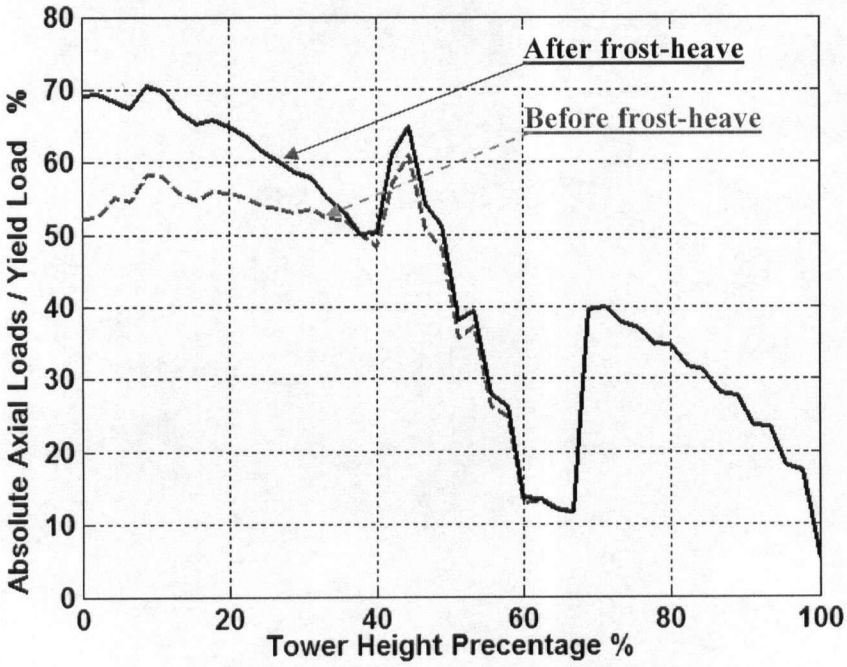

Figure 4.18: Increase of normalized axial load of tower columns due to a frost-heave displacement of 100 mm (with joint slippage).

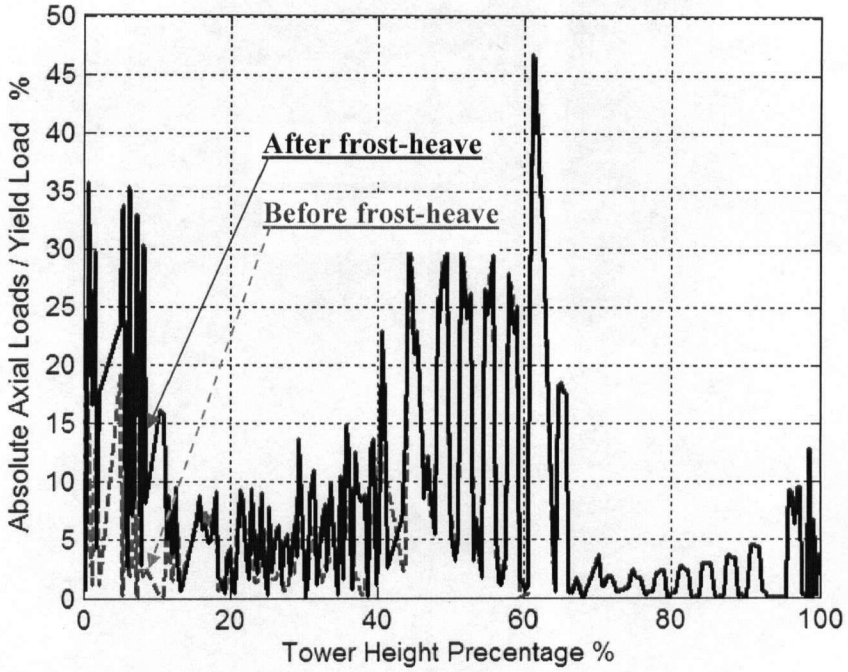

Figure 4.19: Increase of normalized axial load of tower beams due to a frost-heave displacement of 100 mm (with joint slippage).

In the third case, a displacement of 100 mm of adjacent legs, (leg #2 and leg #3), is considered. The results are shown in Figures 4-20 and 4-21. The results are similar to those shown in Figures 4.18 and 4.19 for both with and without joint slippage. It appears that the displacement of an adjacent leg reduces the force generated due to frost-heave.

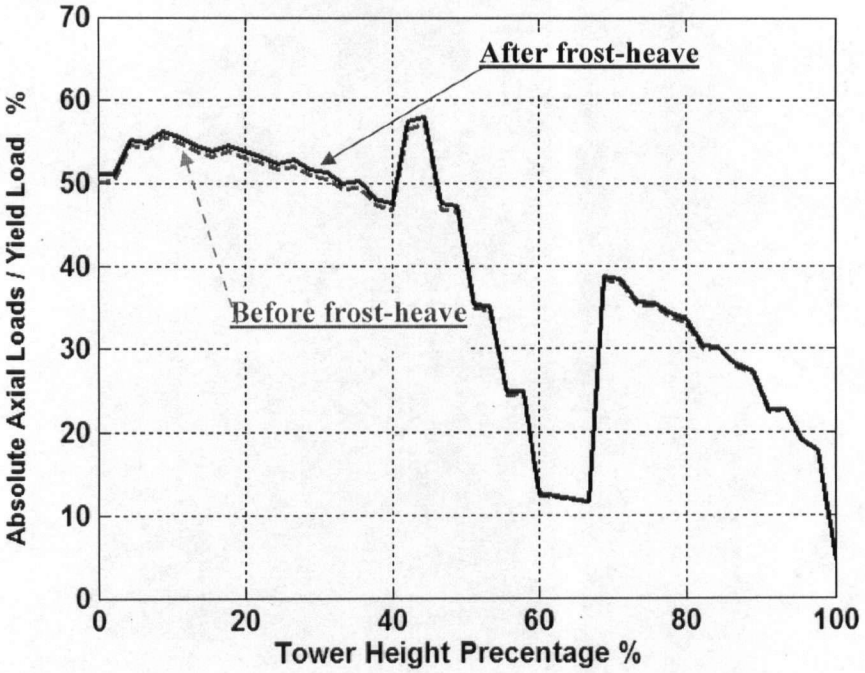

Figure 4.20: Increase of normalized axial load of tower columns due to a frost-heave displacement of 100 mm of two adjacent legs (without joint slippage).

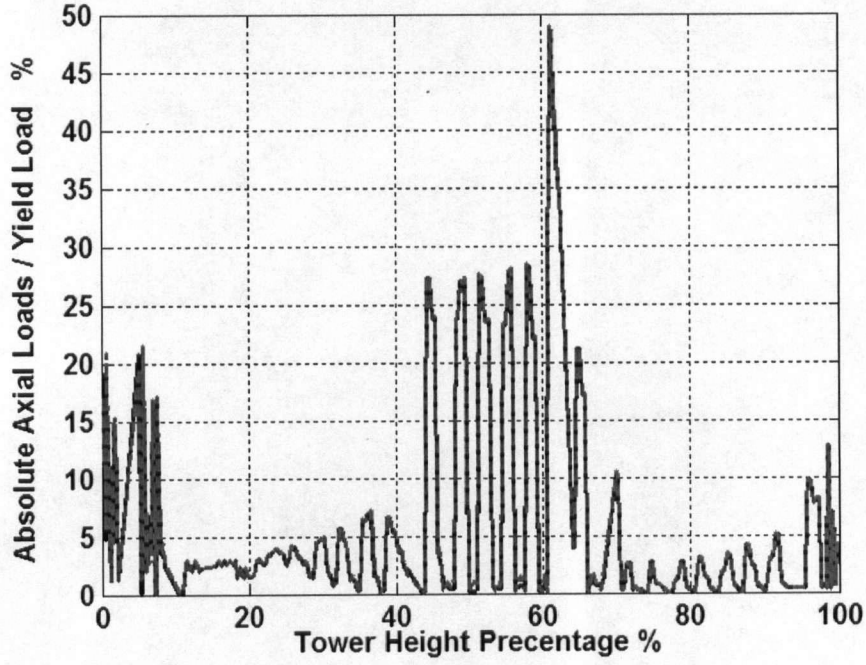

Figure 4.21: Increase of normalized axial load of tower beams due to a frost-heave displacement100 mm of two adjacent legs (without joint slippage)

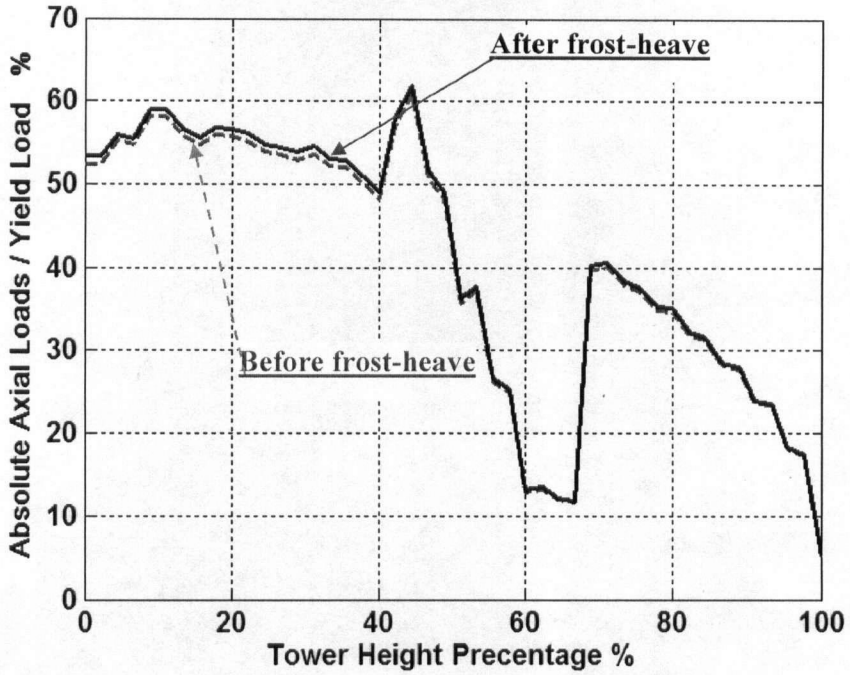

Figure 4.22: Increase of normalized axial load of tower columns due to a frost-heave displacement of 100 mm of two adjacent legs (with joint slippage).

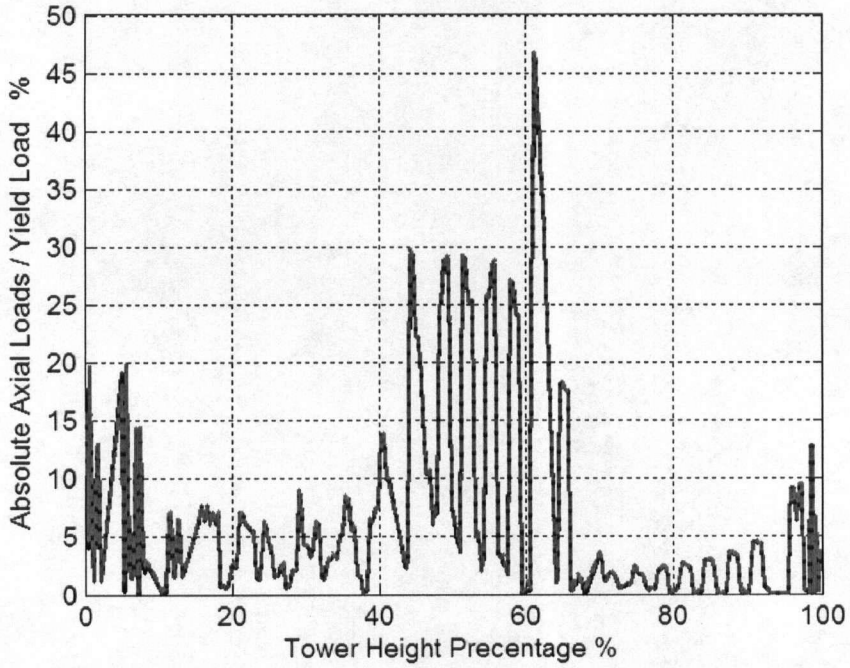

Figure 4.23: Increase of normalized axial load of tower beams due to a frost-heave displacement of 100 mm of two adjacent legs (with joint slippage).

In the forth case, a single leg is assumed to experience a frost-heave induced displacement of 300 mm, which corresponds to field conditions of some towers in Northern Manitoba. Figure 4-24 and Figure 4-25 show the normalized axial loads in the tower elements due to this large displacement when joint slippage is included in the analysis. It is evident that under these large displacements at the base, tower column members near the base experience axial loads larger than their yield loads. Some beam members near the base also have axial loads very closer to their yield loads.

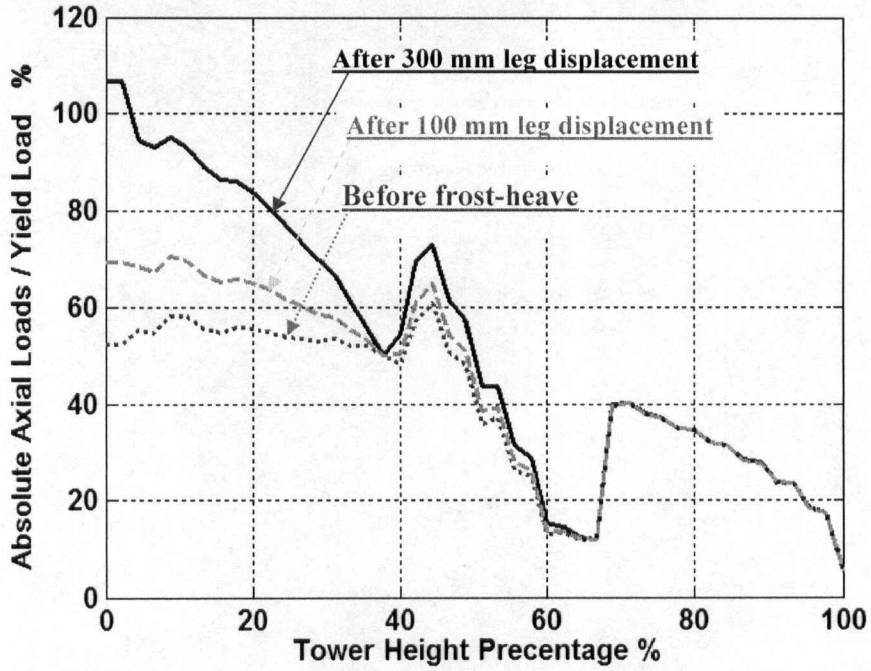

Figure 4.24: Increase of normalized axial load of tower columns due to different frost heave displacements (with joint slippage).

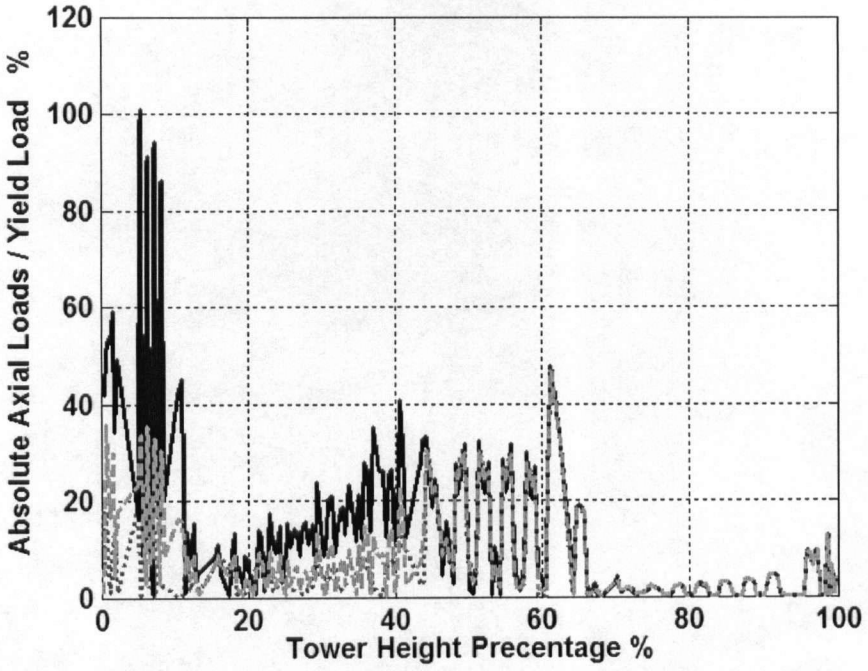

Figure 4.25: Increase of normalized axial load of tower beams due to different frost heave displacements (with joint slippage).

Chapter 5

CONCLUSIONS

5.1 Summary and Conclusions

Slippage of bolted joints has an important role in transmission tower structural behaviour. In the present study, new finite element joint models accounting for slippage are developed based on a set of experimental results for bolted joints. A column-to-column joint (Type-A joint) is treated as a conventional beam connection with an extra nonlinear spring connected in series to a beam element. A beam-to-column joint (Type-B joint) is treated as a conventional truss element with an extra nonlinear spring connected in series to a truss element. Stiffness matrices for the proposed finite elements are obtained by using the experimental results for the load-deflection response of each joint type. The proposed joint models give more realistic stiffness characteristics of a tower joint in the axial direction.

An elastic geometrically nonlinear finite element code is developed based on Fortran 90 for the analysis of transmission tower structures. The code takes into account the effect of bolted joint slippage as well as geometrically nonlinear behavior of a tower. A graphical user interface developed in Visual Basic to perform pre- and post-processing functions is also included in the finite element code.

The numerical study shows that slippage of type-C joints has a significant effect on the load carrying capacity of a transmission tower depending on the ratio of the lateral and vertical loads. The current study also shows that the effect of slippage of the type-A joints on a transmission

tower load carrying capacity is more significant than that of joint type-C. Furthermore, this effect is independent of the ratio of the lateral load to the vertical load. The yield limit of a type-A joint is the most dominant parameter controlling the ultimate load of a tower. It is also observed that slippage of type-A joints is as significant as slippage of type-C joints for lateral deformations. Slippage is also the most dominant parameter affecting vertical displacements.

The behavior of a 3-D full-scale tower under its dead and selected working loads is investigated with and without joint slippage. The results show that joint slippage has a minor influence on tower member force distribution under dead and external loads. Thereafter, the response of a tower under different frost heave induced displacements is investigated. The results show that upward displacement of a single leg induces large axial forces in the tower members if joint slippage is neglected. However, further frost heave induced displacement of an adjacent leg causes minor changes in the tower member axial forces. The numerical results show that ignoring the joint slippage in the analysis results in tower leg axial forces that are almost twice the forces corresponding to a case with joint slippage. In the case of bracing elements, the axial forces could be as high as six times of the slippage case. These findings provide a scientific basis for the assessment of structural integrity of transmission towers in Northern Manitoba under frost heave induced displacements.

5.2 Future Work

Following future work is proposed based on the findings of the present study:

1. Experimental investigation of 3-D stiffness characteristics of tower joints is recommended to understand the behaviour under 3-D loading. The tests should be

done for a wide range of bolts sizes and arrangements, and member cross-sections.

2. Development of a finite element model for tower joints considering friction and contact conditions.

3. Consideration of dynamic loads in finite element analysis.

REFERENCES

Alam, M.J., and Santhakumar, A.R., "Reliability Analysis and Full-Scale Testing of Transmission Tower" *Journal of Structural Engineering*, 122(3), 338-344, (1996)

Al-Bermani, F.G.A., and Kitipornchai, S., "Nonlinear Analysis of Thin-Walled Structures Using Least Element/Member", *Journal of Structural Engineering*, 116(1),215-234, (1990)

Al-Bermani, F.G.A., and Kitipornchai, S., "Elasto-Plastic Large Deformation Analysis of Thin-Walled Structures", *Engineering Structures*, 12(1), 28-36, (1990)

Al-Bermani, F.G.A., and Kitipornchai, S., "Nonlinear Analysis of Transmission Towers", *Engineering Structures*, 14(3), 139-151, (1992A)

Al-Bermani, F.G.A., Kitipornchai, S., and Chan, S.L., "Formex Formulation of Transmission Tower Structures", *International Journal of Space Structures*, 7(1), 1-10, (1992)

Al-Bermani, F.G.A., and Kitipornchai, S., "Elasto-Plastic Nonlinear Analysis of Flexibly Jointed Space Frames", *Journal of Structural Engineering*, 118(1), 108-127, (1992)

ASCE, "Guide for Design of Steel Transmission Towers", *ASCE Manual 52, 2nd edition, New York*, (1988)

ASCE, "Guidelines for Electrical Transmission line Structural Loading", *ASCE Manual 74, New York*, (1988)

Beck, C.F., "Computer's Role in Transmission Line Design", *Journal of the Structural Division, ASCE*, 97(1), 63-79, (1971)

Bergstrom, R.N., Arena, J.R., and Kramer, J.M., "Design of Self Supported Steel Transmission Towers", *Journal of the Power Division, ASCE*, 86(3), 55-88 (1960)

Chen, W., and Lui, E., "Effects of Joint Flexibility on the Behavior of Steel Frames", *Computers and Structures*, 26(5), 719-732, (1987)

Compaq, "Language Reference Manual", *Compaq Computer Corporation, Houston, Texas*, (2001)

Corpuz, R.F., Erickson, P., and Lindsey, K.E., "Recent Experience Restoring Damaged Transmission Lines by National Power Corporation of the Philippines", *Power Delivery Asia, New Delhi, India,* (1998)

Delvecchio, J.N., and Soom, A., "Tolerances and Available Relative Motion in Bolted Connections", Advances in Design Automation, ASME, 2, 177-183, (1991)

Dutson, J.D., and Folkman, S.L., "A Nonlinear Finite Element Model of Truss Using Pinned Joints", *American Institute of Aeronautics and Astronautics Journal*, 793-803, (1996)

Federal Highway Administration (FHWA), "Friction-Type Bolted Connections with A588 Weathering Steel", *Report No. FHWA/RD-81/147, Offices of Research & Development, Structures and Applied Mechanics Division, Washington D.C.*, (1981)

Ghali, A., and Neville, A.M., "Structural Analysis – A Unified Classical and Matrix Approach", *Chapman and Hall London*, (1978)

Gilchrist, R.T., and Chong, K.P., "Thin Light-Gage Bolted connections without Washers", *Journal of the Structural Division, ASCE*, 105(1), 175-183 (1979)

Kemp, A.R., and Behncke, R.H., "Behavior of Cross-Bracing in Latticed Towers", *Journal of Structural Engineering*, Vol. 124, No. 4, pp. 360-367 (1998)

Kitipornchai, S., and Al-Bermani, F.G.A., "Nonlinear Analysis of Lattice Structures", *Journal of Constructional Steel Research*, 23, 209-225, (1992)

Kitipornchai, S., Al-Bermani, F.G.A., and Peyrot, A.H. "Effect of Bolt Slippage on Ultimate Behavior of Lattice Structures", *Journal of Structural Engineering, ASCE*, 120(8), 2281-2287, (1994)

Kitipornchai, S., Zhu, K., Xiang, Y., and, Al-Bermani, F.G.A., A.H. "Single-Equation Yield Surfaces for Mono-symmetric and Asymmetric Sections", *Engineering Structures*, 13(10), 366-370, (1991)

Kitipornchai, S., and Chan, S.L., "Nonlinear Finite Element Analysis of Angle and Tee Beam-Columns", *Journal of Structural Engineering*, 113(4), 721-739, (1987)

Knight, G.M.S., and Santhakumar, A.R., "Joints Effects on Behavior of Transmission Towers", *Journal of Structural Engineering*, 119(3), 698-712, (1993)

Krishnamoorthy, C.S., "Finite Element – Theory and Programming", *2nd edition, Tata McGraw-Hill Publishing Company Limited, New Delhi*, (1996)

Kroeker, D., "Structural Analysis of Lattice Towers with Joint Slippage", *M.Sc. Thesis presented to the University of Manitoba, Winnipeg*, (2000)

Lo, D.L., Morcos, A., and Goel, S.K., "Use of Computers in Transmission Tower Design", *Journal of Structural Division, ASCE*, 101(7), 1443-1453 (1975)

Lobb, V., and Stoller, F., "Bolted Joints under Sustained Loading", *Journal of Structural Division, ASCE*, 97(3), 905-933 (1971)

Marjerrision, M., "Electric Transmission Tower Design", *Journal of the Power Division, ASCE*, 94(1), 1-23, (1968)

Marthaller D.A., *Tips & News*, Vol. 3, No. 1, January 1997

Mercadal, M., and Vander Velde, W.E., "Analysis of Limit Cycle in Control Systems for Joint-Dominated Structures", *Journal of Guidance*, 12(3), 388-395 (1989)

Natarajan, K., and Santhakumar, A.R., "Reliability-Based Optimization of Transmission Line Towers", *Computers and Structures*, Vol. 55, No. 3, pp. 387-403 (1995)

Onada, J., Sano, T., and Minesugi, K., "Passive Damping of Truss Vibration Using Pre-loaded Joint Backlash", *American Institute of Aeronautics and Astronautics Journal*, 33(7), 1335-1341 (1994)

Owen, D.R.J., and Hinton, J., "Finite Element in Plasticity", *Pineridge Press Limited, UK*, (1980)

Petersen, W., "Design of EHV Steel Tower Transmission Lines", *Journal of the Power Division, ASCE*, 88(1), 39-65, (1962)

Pai, N.G., and Hess, D.P., "Three-Dimensional Finite Element Analysis of Threaded Fastener Loosening Due to Dynamic Shear Load", *Engineering Failure Analysis*, 9, 383-402, (2002)

Rossow, E.C., Lo, D.L.C., and Chu, S., "Efficient Design-Analysis of Physically Nonlinear Trusses", *Journal of Structural Division, ASCE,* 101(4), 839-853 (1975)

Roy, S., Fang, S., and Rossow, E.C., "Secondary Stresses on Transmission Tower Structures", *Journal of Energy Engineering,* 110(2), 157-173 (1984)

Russell, D.L., and White, L.W., "An Elementary Nonlinear Beam Theory with Finite Buckling Deformation Properties", *SIAM, Journal of Applied Mathematics,* Vol. 62, No. 4, pp. 1394-1413 (2002)

Savory, E., Park, G.A.R., Zeinoddini, M., Toy, N., and Disney, P., "Modeling of Tornado and Microburst-Induced Wind Loading and Failure of a Lattice Transmission Tower", *Engineering Structures,* 23, 365-375 (2001)

Shi, G., and Atluri, S.N., "Nonlinear Dynamic Response of Frame-Type Structures with Hysteretic Damping at the Joints", *American Institute of Aeronautics and Astronautics Journal,* 30(1), 234-240 (1991)

Ungkurapinan, N., "A Study of Joint Slip in Galvanized Bolted Angle Connections", *M.Sc. Thesis presented to the University of Manitoba, Winnipeg*, (2000)

Ungkurapinan, N., Chandrakeerthi, R., Rajapakse, R.K.N.D., and Yue, B., "Joint Slip in Electrical Transmission Towers", *Engineering Structures, Vol., pp.,* (2003)

Williams, D.C.J., and Brightwell, I.W., "Stochastic Method of Assessing the Effect of Joint Deformation on Bolted Lattice Towers", *Probabilistic Methods Applied to Electric Power Systems, Proceedings of the First International Symposium*, 365-373 (1987)

Winants, V., and Riez, M., "Conductor Galloping on Overhead Lines" *CIGRE SC22, Paper 06, Paris*, August, (1970).

Winter, G., "Tests on Bolted Connections in Light Gage Steel", *Journal of Structural Division, ASCE,* 82(2), paper 920, 1-25 (1956)

Yue, B., "Tower Design and Analysis Program User Manual", *Manitoba Hydro-Transmission and Civil Design Department,* (1994)

Zienkewicz, O.C., and Taylor, R.L., "The Finite Element Method", *4th edition, McGraw-Hill Book Company, London*, (1989)